Electronic Fuel Injection
Techniques for Hydrogen Fueled
I. C. Engines

C. A. MacCarley M. S. Thesis

UNIVERSITY OF CALIFORNIA

Los Angeles

Electronic Fuel Injection Techniques for Hydrogen Fueled Internal Combustion Engines

A thesis submitted in partial satisfaction of the requirements for the degree of Master of Science in Engineering

by

Carl Arthur MacCarley

1978

The thesis of Carl A. MacCarley is approved.

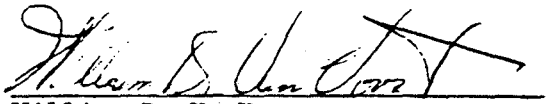

William D. VanVorst

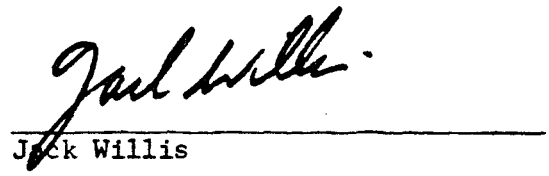

Jack Willis

Alan Z. Ullman, Committee Chairman

University of California, Los Angeles

1978

TABLE OF CONTENTS

ACKNOWLEDGMENTS

I wish to gratefully acknowledge the assistance of my colleagues at UCLA, and the support of the U.S. Postal Service in providing funding for this work. I also wish to thank the following manufacturers for their donations:

Yamaha International Corporation

American Motors Corporation

Beech Aircraft Corporation

Autolite, Division of General Motors Corporation

NGK Spark Plugs, U.S. Operations

POSA Inc.

Impco Carburation Inc.

ABSTRACT OF THE THESIS

Electronic Fuel Injection Techniques for Hydrogen Fueled Internal Combustion Engines

by

Carl Arthur MacCarley
Master of Science in Engineering
University of California, Los Angeles, 1978
Professor A. Z. Ullman, Chairman

Numerous studies have demonstrated the advantages of hydrogen as a fuel for Otto Cycle engines due to high thermal efficiency and low exhaust pollutant levels. Characteristic of hydrogen engine operation using pre-mixed intake charge formation is a problem of pre-ignition resulting in an intake manifold "backfire." Additional problems include high NO_x production when using certain equivalence ratios and power output degradation due to low fuel energy/volume density.

Techniques for direct and manifold fuel injection are discussed as means for overcoming these problems. Emphasis is placed on the need for total engine control, integrating control of fuel injection, ignition timing, intake air throttling, and vehicle subsystems within a central electronic unit. An electronically actuated fuel injection valve and a prototype electronic control system are developed. These are applied in manifold and direct injection system geometries, and evaluated in engine testing. System effectiveness and feasibility are discussed.

1. INTRODUCTION

The distinctive combustion characteristics of a hydrogen-air mixture present both advantages and disadvantages in I.C. engine applications. Wide limits of flammability allow the use of quality governing techniques in which the fuel-air ratio is varied for engine control. However, low required ignition energy, wide variability in flame velocity and peak temperature, and low fuel energy volume density create problems of undesired pre-ignition, possible high NO_x generation, and low power output. These and other features of hydrogen combustion indicate the need for engine aspiration and control schemes more complex than those descendent from existing gaseous fuel technology.

Methods for direct hydrogen injection have been demonstrated under experimental conditions by several researchers. A manifold injection method, geometrically similar to that in use on gasoline fueled engines is developed by the author. The separation of the fuel and air charges that all these systems allow has proven to be advantageous to premixed charge formation techniques. Integrated engine control employing one of these aspiration methods and dynamic control of ignition timing, manifold vacuum and fuel supply system operation would allow for optimized engine overall performance, and a total vehicle package more acceptable in actual use than single parameter engine control methods.

2. HYDROGEN COMBUSTION CHARACTERISTICS

Effective utilization of hydrogen fuel in an I.C. engine normally associated with the use of gasoline must consider several distinctive features of hydrogen combustion.

An air-hydrogen mixture will successfully detonate over a wide range of stoichiometry. At conditions of 17°C, 1 atm, downward flame propagation in a 1.6 x 30 cm closed firing end tube will take place between limits of 7.7 molar per cent hydrogen and 72.6% [1]. Corresponding equivalence ratios (ϕ) are 0.20 and 6.31 fractions of the stoichiometric reaction ratio of 29.6 molar per cent hydrogen. These limits vary with charge temperature and pressure, presence of non-reacting gases, and geometry of reaction vessel.

The lower flammability limit is somewhat reduced by increasing temperature. This limit increases with increasing pressure to a peak at 20 atm and falls at pressures above this. Figures (1) and (2) depict the data of Coward and Jones [2] on variation of hydrogen flammability limits with temperature and pressure. Under conditions most similar to those encountered at the point of ignition in a typical reciprocating engine, limits of approximately 8.7 and 75 molar per cent hydrogen are estimated ($.23 < \phi < 7.34$) [2,3].

The wide range allows the possibility of a "quality governing" control scheme in which a powerplant may be controlled by varying the air-fuel ratio rather than intake manifold vacuum. As a constant manifold pressure near atmospheric may now be maintained, pumping losses of the powerplant, significant under partial throttle conditions, are

reduced. Thermal efficiency under partial load increases.

Detonation velocity for the hydrogen-air mixture is significantly a function of equivalence ratio (ϕ). Figure 3 correlates the data of Breton [4] and Wendlandt [5] on laminar and unstable flame front propagation respectively. Experiments were conducted using downward flame propagation in a glass tube at atmospheric pressure in both cases. An abrupt transition occurs at $\phi = .53$ as flame propagation changes from laminar for $\phi > .53$ to unstable for $\phi < .53$. Unstable flame propagation is characterized by decreasing flame front velocity with travel distance. For $\phi < .26$ the flame front will self-extinguish after a certain propagation distance which is variable with charge consistency and type of ignition source. For equivalence ratios approaching the lower limit at $\phi = .20$, combustion is often incomplete, the degree of completion effected by combustion vessel geometry and charge consistency [2]. An upper regime of unstable detonation occurs for $\phi > 3.41$ [6].

Although combustion conditions are significantly different in a reciprocation S.I. engine, it is anticipated that the sharp velocity transition is still encountered. Figures 1 and 2 indicate only minor variation of flammability limits with pressure and temperature. It may be inferred from this that the transition occurs under engine combustion conditions at a ϕ value close to that observed in the laboratory cases. Experimental data on engine performance verifies this as an abrupt change in ignition timing is required with variation of ϕ from .4 to .6. The data of Finegold and VanVorst [7] are shown in Figure 5. For one case represented, the timing position must be advanced from 60°

BTDC for ϕ = .4 to 20° BTDC for ϕ = .6, with timing at TDC for ϕ = 1.0.

The degradation of combustion stability for ϕ < .53 creates problems for engines operated with these mixtures. Application of quality governing requires the use of these low ϕ mixtures under light loads and engine idling conditions. Long combustion durations and the onset of incomplete combustion determine a practical lower limit on usable equivalence ratio. The rapid flame velocities encountered with rich mixtures (ϕ approaching 1.0) require ignition timing positions at or after TDC to yield satisfactory cylinder pressure distributions over the combustion stroke.

NO_x formation in the hydrogen-air engine is fundamentally dependent on factors of reaction temperature and residence time. These are in turn functions of equivalence ratio, compression ratio, and engine geometry. According to deBoer et al. [8], for mixtures leaner than ϕ = 0.8, the NO reaction is limited by thermal quenching during the formation processes, while for mixtures richer than this, the net NO emissions are determined by quenching of NO decomposition reactions during the expansion stroke. The data of McLean et al. [9] relating NO_x emission in gm/HP-hour to ϕ is depicted in Figure 6. Of significance to this discussion is the existence of a high NO_x region between ϕ = .65 and ϕ = .95, with a peak at ϕ = .8. Operation of an engine within this range of equivalence ratios results in high NO_x emissions relative to power output, a considerable blemish to the otherwise clean exhaust, primarily water vapor and nitrogen. Production of hydrogen peroxide has also been observed [10], but its significance as a pollutant is unresolved.

The energy required for ignition of a hydrogen-air mixture is significantly lower than that required for other common fuels. Its functionality with ϕ is given in Figure 4 [11]. This property is seen to be the root of the pre-ignition problem associated with hydrogen engines. Undesired auto ignition may occur from a number of possible sources. Pre-ignition during the engine intake stroke results in an intake manifold "backfire." In an engine aspirated with a premixed charge, the backfire involves detonation of not only the in-cylinder fuel charge, but the contents of the intake manifold as well. The results of this can range from simply engine stall to destruction of the carburetion system and fuel system fire. Potential pre-ignition sources include combustion chamber hot spots, residual hot or still burning (in the case of low ϕ mixtures) exhaust products, suspended oil, carbon, or dust particles serving as combustion nuclei, and spark plug discharge due to electromagnetic cross induction between plug leads [12,13,8]. Additionally, King noted the properties of certain non-catalytic surfaces as conducive to auto-ignition [14]. Pre-ignition may occur at the porcelin tip of a spark plug at a lower temperature than at a cast iron surface of the cylinder head. Many methods of dealing with the backfire tendency have been applied. A reasonable degree of success has been achieved using combustion modifiers, notably water or water vapor. Water induction has additionally been shown to reduce NO_x emissions [15].

The low ignition energy of hydrogen eases the task of achieving successful spark ignition. Conventional spark plugs are usually gapped at a narrow setting, taking advantage of the low minimum quenching

distance of hydrogen, approximately 0.6 mm at $\phi = 1.0$. However, unsuccessful ignition has been observed in conditions of heterogeneous fuel-air charge composition. It is hypothesized that false ignition occurs due to the presence of local fuel-air mixtures in the vicinity of the igniter which are beyond the ignition limits, either too lean or too rich. Thus, gas ionization may occur without ignition.

The problem of inadequate fuel-air mixing has been observed by several researchers using direct cylinder injection methods [16,8]. Additionally, Woolley et al. [15] has reported variations in cylinder to cylinder AF ratios using premixed charge formation. In a study by Yu [17] using a multi-cylinder engine powered by propane, significant variations in AF ratio, $\Delta AF = 7.4$, were noted between cylinders, and only with induction through a manifold consisting of a 5 foot hose, swirl chamber and venturi was this reduced to a more ideal $\Delta AF = 0.3$. A reported figure for typical gasoline-air mixtures is $\Delta AF = 2.4$ [17]. While the wide flammability limits of hydrogen are tolerant of these variations in premixed charge induction, systems employing in-cylinder or near-cylinder charge formation must be designed to insure adequate mixing to avoid heterogeneous charge formation and associated problems of false ignition, incomplete combustion resulting in poor thermal efficiency, and erratic NO_x formation characteristics.

Under stoichiometric conditions, 29.6% volume of the fuel-air charge is occupied by hydrogen. Comparatively, 2% volume of a gasoline-air mixture is assigned to gasoline. Thus a power output limitation is imposed on hydrogen engines aspirated at atmospheric pressure, approximately 15% below equivalent gasoline performance [9].

This is termed a form of volumetric efficiency loss. Methods of supercharging or direct cylinder injection allow recovery of this loss by charge pressurization, either during intake in the first case or during the compression stroke in the latter. A summary of hydrogen combustion properties appears in Figure 7.

3. FUEL INJECTION TECHNIQUES FOR HYDROGEN

3.1 MANIFOLD INJECTION

Manifold injection will refer here to a timed hydrogen injection technique in which fuel is delivered under pressure to individual cylinders at positions in the intake manifold near, but upstream of the intake valves.

The key features of such a system are: (1) the ability of the system to initiate fuel delivery at a timing position some time after the beginning of the intake stroke. (2) Fuel metering is independent of air flow or pressure conditions. (3) The intake manifold contains no combustible fuel-air mixture.

The primary advantage indicated with this system is control of the backfire problem. In a carbureted engine, valve overlap between the exhaust and intake stroke can bring the incoming fuel-air charge in contact with the residual hot or still burning gases (in very lean mixtures or in isolated areas of an incompletely mixed charge) of the preceding exhaust stroke. This effect becomes pronounced under low RPM, high load conditions where backflow into the intake manifold is tolerated due to a valve timing design trade-off to insure optimum flow under high RPM, peak power conditions.

Delayed delivery of hydrogen insures against possible pre-ignition due to this effect. Additionally, a certain "pre-cooling" effect of the air inducted prior to the onset of fuel delivery is realized. This may reduce the effect of surface related pre-ignition sources and provide for a dilution or quench of any residual hot combustion products

present in the compression space near TDC. If water induction or injection is employed, it will have an enhanced effect as a precooling medium.

Due to the lack of a combustible mixture in the intake manifold, should pre-ignition occur during the intake stroke, its effect will be a partial-charge single cylinder backfire, far less consequential than that encountered when the entire charge in the intake manifold detonates in multi-cylinder carbureted engines.

Swain and Adt have demonstrated a related "Hydrogen Induction Technique" in which fuel flows through holes in the seat of the intake valve. Their reports based on the performance of a Toyota 1600 powerplant verify the effectiveness of use of a separate fuel delivery point over premixed charge carburetion in minimization of the ramifications of pre-ignition during the intake stroke [18].

Fuel delivery in the injection system is not strictly dictated by intake air flow. Thus, a separate functional relationship between fuel and air may be defined based upon selected engine parameters. This allows for careful tailoring of the control function to avoid known backfire conditions and minimize NO_x formation (through precise control of ϕ or a technique described later). This feature is optimally utilized in quality governing, or combined quality-throttle control schemes.

3.2 DIRECT CYLINDER INJECTION

Direct injection will here imply a timed hydrogen injection technique employing direct delivery of fuel individually to each cylinder.

An early example of a direct injection scheme was demonstrated by Erren in his work from 1923-1939 in which a third valve was used as a

pressurized hydrogen inlet [19,20]. More recent works by Saga and Furuhama [16], Murray and Schoeppel [21], McLean et al. [9], and Oehmichen [22] have demonstrated timed high pressure mechanical injection techniques on test engines.

Direct injection shares the same fuel metering and late injection onset characteristics as outlined for manifold injection, but additionally allows for fuel delivery after the closure of the intake valve, during the compression stroke. Due to the pseudo-exponential nature of the isentropic (ideal case) compression, it is calculated that only moderate injection pressure (30 psig) is sufficient to overcome cylinder pressure as late as 90° after bottom dead center. Figure 8 illustrates an ideal 180° compression stroke. Also illustrated is a condition of no pressurization until the intake valve is completely closed as an approximation for intake flow at low RPM. Both are based on the geometry of a 326 cc per cylinder air-cooled, high speed test engine to be discussed later.

If the duration of injection occurs entirely in the compression stroke, it is possible to recover the volumetric efficiency loss previously discussed. A power output improvement of 42% (in the theoretical limit) is possible. Partial overlap of injection into the intake stroke proportionally reduces this advantage.

A problem exists if injection takes place in the vicinity of BDC due to late closure of the intake valve. It is possible that backflow of hydrogen out the intake manifold may occur in the period between BDC and the point where the intake valve is fully shut. This can only occur to a significant degree at lower engine speeds (compared to the

RPM of maximum power), due to gas inertia in the intake manifold. The consequence of this is a small residual amount of hydrogen upstream of the intake valve. While this would make the system non-ideal, it is not anticipated to significantly alter the argument for backfire suppression.

Saga and Furuhama [16] and others have noted problems with adequate fuel-air mixing for injection timing positions late in the compression stroke. The heterogeneous fuel-air charge resulting after late injection can cause problems of erratic ignition and incomplete combustion. Stratified charge formation may be valuable for very low overall ϕ mixtures as a means of achieving complete detonation. It is undesirable for mixtures approaching $\phi = 1$. Optimum injector discharge direction and in-cylinder turbulence are required for higher pressure injection with timing closer to TDC.

System control in direct injection schemes is similar to the manifold injection case.

3.3 MECHANICAL INJECTION DEVELOPMENT

Prior to concentration of effort on electronic injection control techniques, several mechanical approaches were investigated. A full scale experimental mechanical injection system was developed using the geometry of a multi-port rotary type valve. Referring to Figure 9, its operation may be described as follows: A cylindrical shaft, driven at one-half of the engine speed, rotates in intimate contact with the sealing surface of the valve housing. A flat slot across the axis of the shaft connects adjacent pairs of ports in the valve housing. Three ports, denoted A, B, and C are provided, connected to the engine

combustion chamber, a buffer chamber, and the hydrogen supply respectively. As the shaft rotates, ports A and B are first connected; then ports B and C; finally, all ports are closed.

The cycle begins with port B and C connected. At this point the calibrated volume chamber is charged to the pressure of the incoming hydrogen entering port C. The shaft rotates clockwise until first port B, then port C is blocked. The shaft continues to rotate until ports A and B are briefly connected. The pressurized hydrogen stored in the volume chamber is discharged from port B to A into the combusion chamber of the engine.

Fuel metering is accomplished by variation of the hydrogen feed pressure of the system. This injection principle may be applied in implementation of either manifold or direct injection, but was specifically intended in this system for direct injection.

Problems encountered in the practical development of this system are sealing of the shaft against the valve housing while rotating, and adequate port flow characteristics over the entire operational range of the engine. The shaft sealing problem was approached by using solid bearing materials in conjunction with a water-pressurized valve containment jacket. Bearing materials investigated included several TFE compounds such as Rulon® and Turkite®, and an experimental silver-stainless steel bearing/seal system. The interface of 18-8 stainless steel and pure silver as a low friction, wear resistant, but non-lubricated bearing combination was suggested by data of the Hughes Aircraft Corporation on non-lubricated bearing surfaces for satellite and spacecraft applications.

It was the lack of a satisfactory solution to the sealing problem that eventually led to abandonment of the rotary valve injection concept. Indeed, related applications of rotary valves for liquid or gas distribution have historically been plagued with sealing difficulties. An additional disadvantage of this or any mechanical injection system is a lack of control flexibility due to the mechanical complexity required to implement a multi-dimensional control function based upon pressure and temperature parameters.

A photograph of the experimental rotary valve mechanism fabricated for the AMC 6-cylinder engine appears in Figure 10.

3.4 ELECTRONICALLY CONTROLLED FUEL INJECTION

Application of electronic control to hydrogen engine aspiration shows advantage in permitting a complex, many parameter control scheme with only minor increase in system complexity. Implementation of such a system requires:

(1) Development of hardware for engine control and fuel delivery.

(2) Generation of a multi-dimensional engine parameter map applicable to the entire operational range of a particular powerplant. Function parameters include:

Engine RPM
Accelerator pedal position
Ignition timing
Injection timing and cycle duration
Air throttle position
NO_x production characteristics
Backfire conditions
Ambient air pressure and temperature
Fuel pressure and temperature (important with cryogenic H_2 storage)

Flow response of injectors
Inertial response to load or speed transients.

Auto industry progress with manifold injection systems for gasoline has demonstrated both mechanical and electrical design approaches. Mechanical injection systems have appeared for many years in racing vehicles and in O.E.M. applications. The earliest successful commercial offering of electronic fuel injection appeared in the 1958-59 Chrysler 300 sedan, a Bendix designed system [23]. In 1967, a system produced by Robert Bosch appeared in the Volkswagen Variant model, primarily designed to reduce emissions in the face of 1968 U.S. pollution control regulations. This system offered "computerized" control and successfully reduced exhaust emissions and improved fuel economy significantly compared to the non-injected model [24]. Systems similar to this now appear in current model vehicles manufactured by Volkswagen-Porsche, Datsun, Volvo, General Motors, Chrysler, Citroen and others [25].

The flexibility of control offered by the electronic system permits features of fuel shutoff during deceleration, precise fuel metering and cylinder distribution, cold start enrichment, compensation for absolute air pressure (altitude compensation), enrichment for acceleration and full load, overspeed cut-off, and protection from flooding. Automated production processes are now available for rapid individual system calibration [26]. The significant recent popularity of these systems is due to public and governmental demands for improved fuel economy and reduced emissions. It may be assessed from the commercial success of these systems that design sophistication and economics of

production favor the electronic injection system over mechanical offerings. With this observation, and the added control problems associated with backfire suppression in hydrogen fueled engines in mind, it appears that an electronic system approach is best suited to the task.

With the advent of advanced, low cost digital electronic technology, the implementation of even a very complex control function is often reduced to a problem of appropriate programming of a microprocessor. Hybrid and integrated circuits are recently finding a rapidly expanding field of application in automotive engine control. Delco division of General Motors offers the MISAR microprocessor based ignition control system on several 1978 model cars [27]. Programmed storage of an experimentally generated engine parameter map could provide data necessary for optimal total engine control; injection, ignition, fuel system and vehicle accessories.

In our developmental work, a hardwired analog and digital approach is used in compatibility with the particular requirements of the intended test vehicle.

4. SYSTEM REQUIREMENTS

4.1 CONTROL SYSTEM

Desired features for injection of hydrogen under electronic control may be summarized as follows:

1. Determination of an injector "on" pulse duration and timing position. Available mechanisms for governing the engine are the injection pulse duration, pressure to the injection valves, and throttle plate position (manifold vacuum control). Pulse duration is determined as a function of:

Throttle position

Fuel pressure at injectors

Engine RPM.

Limits on maximum fuel delivery for establishment of the full power, $\phi = 1.0$ condition are established by:

Maximum available fuel pressure

Fuel temperature

Ambient air pressure and temperature

Injector flow vs. pulse duration characteristics.

The engine idling condition is defined by minimum fuel delivery. In a quality governing scheme, a practical minimum equivalence ratio is established slightly above, but near the $\phi = .23$ lean flammability limit. deBoer et al. [8] recommend a minimum practical limit of $\phi = .30$. Experimental engine performance has shown the need for a certain amount of manifold vacuum to establish an acceptable idle. As a quality governed engine incurs minimal pumping losses, only frictional,

compression and engine accessory loads establish the idle condition. Operation with very lean ϕ values presents problems due to inconsistent detonation and long combustion times. Fuel energy is wasted due to incomplete combustion, and a potential backfire condition is created due to residual combustion at time of intake. Reduction of the fuel-air charge energy content below the equivalence ratio of minimum acceptable combustion requires reduction of the air pressure in addition to the fuel fraction, or the use of a charge dilutant such as recirculated exhaust gas. Air pressure reduction is most easily attained and implies the need for some degree of throttling. The manifold vacuum created, as a pumping loss factor, also assists in maintaining a stable idle speed. A pure quality governed engine behaves much like a two cycle engine in its very gradual deceleration when unloaded.

Definition of the minimum fuel delivery condition is based on:

Manifold vacuum

Minimum regulated fuel pressure

Fuel temperature

Ambient air pressure and temperature.

2. Deceleration fuel cut-off. As an efficiency improving feature, and to avoid the problem of residual combustion on deceleration due to low combustion speeds at low ϕ values, but high engine speeds, it is desired that fuel flow be withheld during deceleration transients. A condition of engine RPM greater than the idle value while the governor is in idle position (foot off the pedal) is identified by the electronics as a deceleration condition, and fuel flow is withheld until the idle speed is attained.

3. NO_x control. McLean et al. have shown that NO_x production per power output appears to reach a peak at $\phi = 0.8$ and decline to a value at $\phi = 1.0$ approximately equal to that at $\phi = 0.6$ [9]. A zone of high NO_x production exists between the ϕ values of 6.5 and 9.5. For full power it is desirable to have available a $\phi = 1.0$ mixture. In the case of a multi-cylinder engine, it is possible to "jump through" this zone one cylinder at a time, or in pairs of opposing cylinders, as the governor is advanced through positions corresponding from 2/3 power to full power. Thus the entire condition of high NO_x production is avoided with a tolerable degree of acceleration "surge" incurred near full power.

4. Ignition timing. Optimum ignition timing in a hydrogen engine is both a function of engine speed and AF ratio. The variation of ϕ when using quality governing requires ignition timing variability of up to 60° (Fig. 5). An abrupt timing change is required in the vicinity of $\phi = .5$ due to combustion transition from unstable to stable with a concomitant change in combustion completion time. Integrated injection and ignition control would allow for ignition timing responsive to ϕ and engine RPM, and other immediate operating conditions of the powerplant.

5. Interactive control of a water injection system, if applied. Water delivery may be tailored to the requirements of the powerplant for backfire suppression or NO_x reduction only as actually required. Practically, water injection might be applied so as to track hydrogen flow proportionally or be applied only under conditions of high ϕ and high load.

6. Engine overspeed protection. Fuel delivery may be reduced if engine speed exceeds a predetermined value.

7. Fuel supply control. Master fuel valve shut-off is desirable in conditions of engine stall, on-board fire, or vehicle rollover. Detection of a minimum acceptable engine speed, with over-ride during starting, identifies the engine stall condition. Fire or rollover require suitable sensors.

8. Interactive control of a cryogenic, metal hydride, or chemical hydride fuel storage system. A heating cycle is used for gas withdrawal from a liquid hydrogen vessel. This is made to respond to engine fuel demands either via line pressure data or in a linear control scheme in which heat admitted to the LH_2 loop is made to track fuel mass flow requirements. A similar control scheme is used in metal hydride storage in which engine exhaust or coolant heat is used for hydrogen release from a hydride bed.

In a chemical hydride storage system such as the sodium borohydride system, parameters of reaction temperature, solution pH, and catalytic surface area contact are available for control of the hydrogen release reaction. An optimized control scheme for hydrogen supply in sync with engine demand may be implemented through the engine control electronics [28] (See Figure 11).

4.2 INJECTION VALVE

Required is an electronically actuated valve (injector) capable of very fast reaction times and high flow rates. Time allowed for injection decreases with increasing RPM or decreasing radial duration of the

injection cycle. Thus, for a high speed engine using a narrow radial duration, severe requirements are placed on the injector.

For direct injection systems, it is additionally required that the injector be capable of blocking and withstanding the full pressure and temperature of combustion. Adiabatic heating alone imposes severe materials requirements.

5. SYSTEM DEVELOPMENT

As a basis for evaluation, an experimental system which may be configured for either manifold or direct injection was developed and tested. Additionally, comparative data was taken using carbureted aspiration and on baseline engine performance with gasoline.

Experimental work centered on system installations on a two cylinder 653 cc air cooled test engine (1974 Yamaha TX-650). Characteristic of this powerplant is a slightly over-square bore/stroke (75 x 74 mm), 8.7-1 compression ratio, and a valve geometry and timing designed for high speed, high performance operation.

This work is directed towards the development of an optimized system for use in a prototype mail delivery vehicle for the U.S. Postal Service. The stock 232 C.I.D. powerplant of a 1974 AMC Jeep is to be modified for hydrogen operation in conjunction with a cryogenic fuel storage system. This vehicle also will incorporate an exhaust water condensation system designed to supply water injection requirements using a water/hydrogen mass ratio of up to 5.0. Gaseous hydrogen available to the engine may vary widely in temperature depending on vehicle operating conditions. The injection system must be designed to accommodate fuel over a temperature range of -50° to $+50^{\circ}C$, and a pressure range of 40 to 100 psig. Final design requirements for the injection system are defined to be compatible with this vehicle package.

Basic components of the injection system in either a manifold or direct configuration are shown in Figure 12.

5.1 CONTROL SYSTEM

5.1.1 General Description

The control electronics constitute the heart of the injection system, providing for fuel metering and general system control responsive to designated engine and environmental parameters. Circuitry for the AMC 6-cylinder vehicle is represented diagramatically in Figure 13. This system provides integrated hydrogen and water injection control and features dynamic injection timing as well as pulse duration modulation. It is compatible in either manifold or direct cylinder injection applications. At the time of writing the final AMC vehicle system has not been completed. Verification of circuit performance was determined from experimental work with breadboarded circuit subsystems and dynamic computer simulation using the SPICE (Simulation Program with Integrated Circuit Emphasis) routine of the UCLA OAC facility. Complete schematics appear in Figures 14 through 19. The modular nature of the control system is emphasized in Figure 14, the mainframe wiring diagram.

A similar 2-cylinder version of this system has been constructed for the 653 cc test engine and fully tested in actual engine operation over a broad range of control conditions. This simpler system employed static injection timing in compatibility with the experimental nature of the engine use. Essentially, it consists of 2 channels of the 6 channel AMC system described in detail here, less the circuitry for dynamic injection timing. A photo of the installed system is shown in Figure 20.

5.1.2 Injection Triggering

An optical sensing system employing six LED-phototransistor pairs is built into the engine distributor, modified to accommodate this assembly. A slotted disc rotates with the distributor rotor, providing a trigger signal when a beam is completed between each of the six optical switch pairs. Figure 21 is a photograph of the disassembled distributor/injection trigger assembly.

A significant problem with any automotive electronic system employing integrated circuitry is interference from electrostatic noise generated by the engine ignition system. Substantial design effort has been made to make the triggering and information processing circuits of the injection control unit intrinsically noise-immune, in addition to externally shielding all transducer interface cables and locating the control unit as far as possible from ignition system components.

A current sensing rather than voltage sensing trigger interface circuit is used. Six individual current sinking amplifiers are built into the distributor assembly providing a low impedance connection to the main control unit. These appear to the left in Figure 15 as the D1, Q1 and Q2 group, one group for each channel. A Schmitt trigger buffered interface bus containing comparitors A1 through A6 provides a degree of hysteresis in current sensing, further enhancing the noise immunity of the trigger circuit.

5.1.3 Control Inputs

An analog control voltage is used to define maximum and minimum pulse durations for both hydrogen and water injection. It is generated by an analog computer calculating the function:

$$V_{control} = \frac{(P_{air,absolute})(T_{H_2,absolute})}{T_{air,absolute}} \times V_{C_O}$$

V_{C_O} is an adjustable reference control voltage level set to define the maximum equivalence ratio. Hydrogen supply pressure is varied by the driver's accelerator pedal which is also coupled to an air throttling butterfly valve. Air throttle actuation is non-linear with pedal position. Only with pedal positions of less than 1/4 of maximum travel is significant manifold vacuum created. This control method provides throttling for an acceptable idle condition, but quality governing under all other engine operation conditions (see Fig. 22).

Circuitry for the analog computation appears in Figure 15 on the right. Hydrogen fuel temperature and ambient air temperature are monitored by thermistors RTH and RTA, respectively. RPA is a variable resistance absolute pressure transducer used to monitor air pressure (partial vacuum) inside the intake manifold. Accelerator pedal position is indicated by $R_{Throttle}$ and used to determine a control voltage VCW for use in control of the pulse duration of the water injection subsystem. Low resistance values, nominally 1K, are specified in all transducer elements, resulting in high quiescent current flow. This is done to improve noise immunity in the sensing circuitry. Operational amplifiers A7 and A8 implement the analog multiplication and division of the sensed signals resulting in VCH, the injection pulse duration control voltage. R50 through R56 provide for trimming of the transducer resistance signals to allow final injection system tuning. .01 MF capacitors appear across the inputs of all op amps in the system. These are

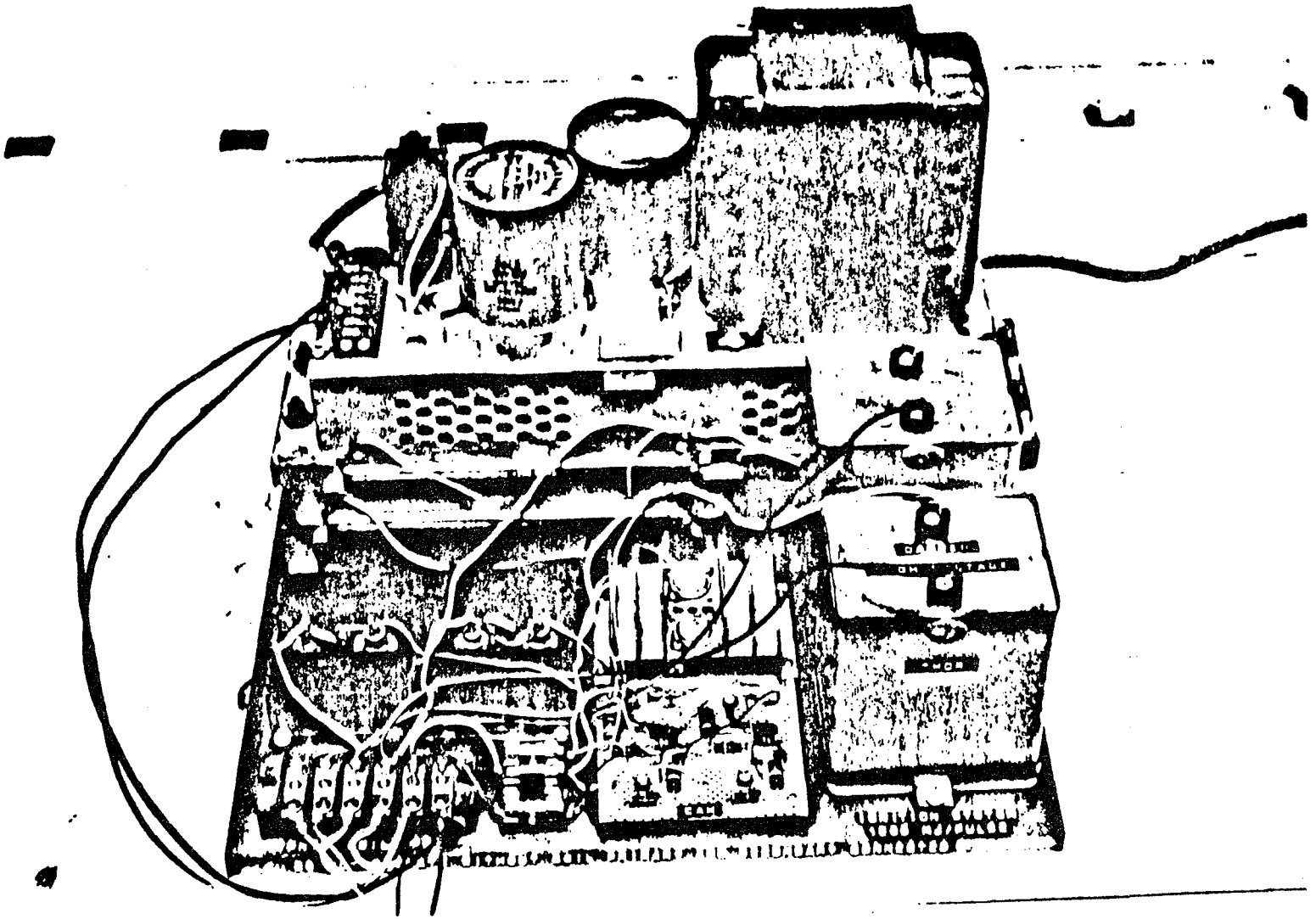

Figure 44. "Thor" High Power Ignition System Used for Pre-Combustion Chamber Injection Experiments

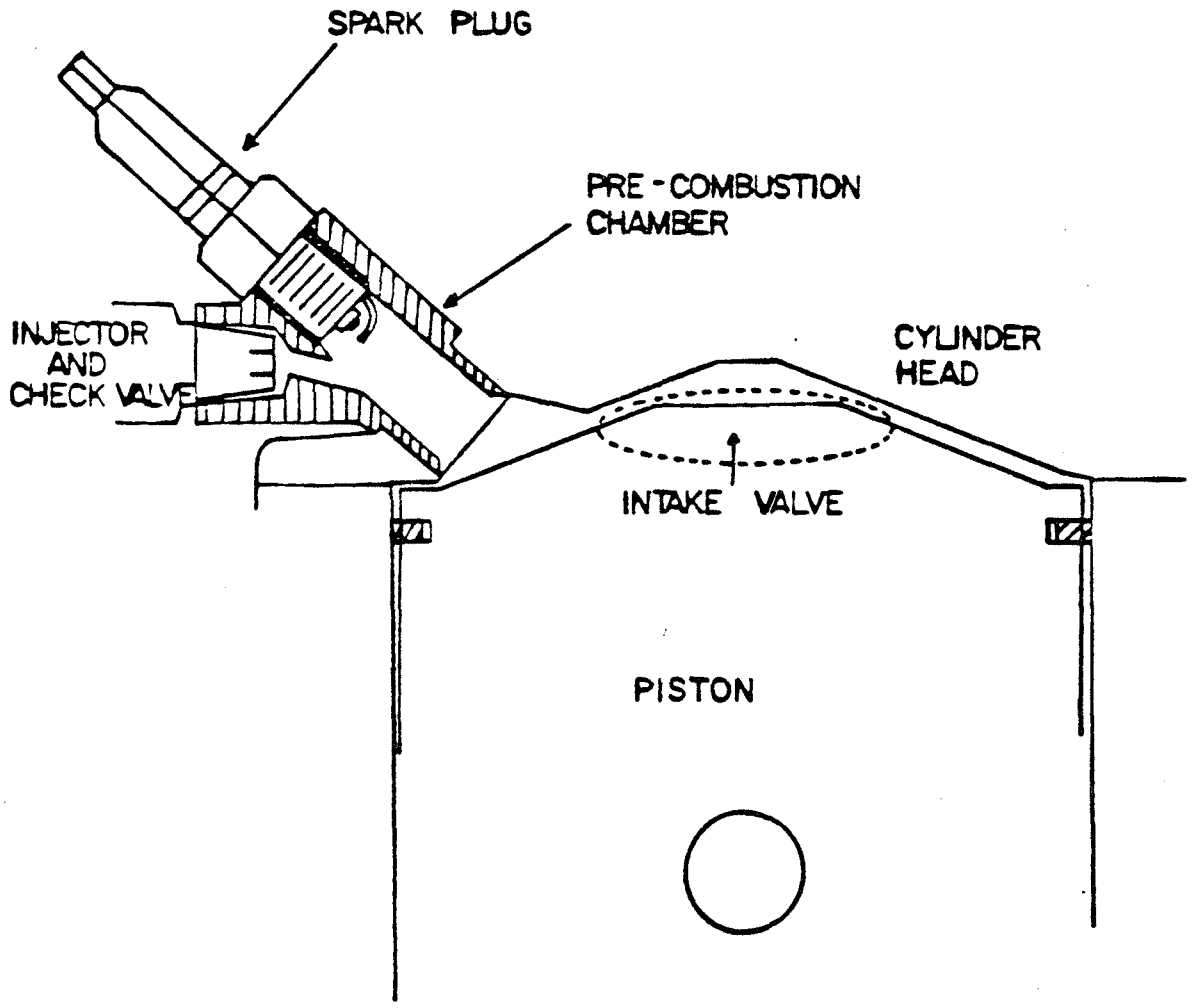

Figure 43. PRE-COMBUSTION CHAMBER CROSS SECTION

physically located in very close proximity of the integrated circuit packages, actually soldered directly to the IC pins. This fabrication method has been determined experimentally to be most effective for electrostatic noise immunity of the op amps.

5.1.4 Pulse Generation

Delivered fuel quantity is determined by both the injection pulse duration and the hydrogen secondary pressure. This control system utilizes secondary pressure variation over the control range, but restricts the maximum equivalence ratio (for full power), and minimum equivalence ratio (for idle) via the pulse duration.

A monostable multivibrator is used to generate a pulse of the desired duration, variable with VCH, the control voltage. Figure 16 shows the circuitry of one of the six identical pusle computer modules used in the system. The pulse generation circuit centers around the MC1555 voltage-controlled timer IC appearing at the bottom left of this schematic. Variations in injector flow characteristics between units may be compensated by adjustment of R26, the RC time constant determining resistor, which trims the pulse duration of each channel. The timer output is positive logic and drives the injector driver circuit through emitter follower Q5.

5.1.5 Dynamic Injection Timing

The injection pulse occupies a finite completion time but requires a variable duration in crankshaft degrees, functional with engine RPM. As will be later explained, it is desirable to time the injection cycle

such that it always ends at a constant radial position. For direct injection, cycle termination at 90° BTDC in the compression stroke is optimum; for manifold injection, 140° ATDC in the intake stroke is optimum (see Figure 23). This requires determination of a cycle initiation position based upon instantaneous RPM such that the required pulse duration is fitted into the allowed radial duration so that it terminates at a position constant with RPM.

The cycle begins with injection triggering at 60° ATDC in the intake stroke. A time delay is generated so as to initiate the injection pulse at some time after this position, but prior to the 90° BTDC cycle termination point. This time delay is determined from stored information on the duration of the trigger signal from the previous cylinder's injection cycle. Thus, RPM information is determined over 60° of a crankshaft rotation only 60° prior to its use in generation of the appropriate timing position. Maximum timing error for the fastest engine speed transient expected is less than 1%. The appropriate time delay functional with RPM is given by:

$$t_d = \left[\frac{35}{RPM} - 0.010 \right] \text{ sec} \qquad RPM < 3500$$

or $$= 0 \text{ sec} \qquad RPM \geq 3500$$

and is graphically represented in Figure 24.

This function is dynamically implemented by the circuitry of the pulse computer module of Figure 16. Engine RPM information is stored as a voltage V_1 on capacitor C_1 representative of the charging time allowed during the previous injection trigger cycle. V_1 varies as a non-linear inverse function of RPM since increasing RPM allows decreased

charging time via R1. Figure 25 gives the functional relationship. Charging of a second capacitor C_2 is initiated upon triggering of the present injection cycle. On triggering, the RS flip-flop consisting of high threshold logic (HTL) NAND gates N_1 and N_2 is set and drives Q4 into conduction, charging C_2 through R2. At the point when V_2, the voltage on C_2, exceeds V_1, the MLM111 comparitor switches initiating the present injection pulse by triggering the MC1555 timer. Figure 26 represents graphically the time delay generated during the period when C_2 is charging but $V_2 < V_1$, parametric with V_1 values resulting from various engine speeds (from 500 to 3500 RPM). Component values, charging times, and quiescent capacitor voltages (prior to charging) are tailored so as to precisely generate the desired delay function of Figure 24. Thus, initiation of the injection pulse occurs at a position in the engine timing circle, between 60^{o} ATDC and 90^{o} BTDC, appropriate for the instantaneous engine rotational speed. A plot of dynamic circuit voltages vs. radial time appears in Figure 27. Computer generated plots from SPICE simulation of the timing circuitry are shown in Figure 28 depicting the generation of appropriate time delays for several engine speeds.

5.1.6 Water Injection

A single electronically actuated water injector is used, located just after the air throttle in the intake manifold. Water injection is triggered upon the firing of each cylinder, insuring an even dispersion of water in the intake air charge. A constant water pressure of 60 psig is maintained at the injector, and metering is by pulse duration alone. Although future work may indicate a superior water injection control

function, this system provides a reasonably constant water-to-hydrogen mass flow ratio according to:

$$\text{Water flow} \sim (\text{RPM}) \times (\text{pedal position})$$

Water flow linearly tracks ϕ except at engine idle during which the water flow to ϕ ratio decreases due to manifold air throttling.

The circuit for water injection pulse generation is shown in the upper half of Figure 17. Diodes D1 through D6 perform a negative logic wired AND function, triggering the MC1555 monostable multivibrator with each fuel injection trigger signal. The water injector drive circuit shown in Figure 18 is driven by the positive logic output of the monostable through emitter follower Q4. Variation of the R12 pot allows pulse duration range adjustment by altering the R12-C12 time constant of the timing circuit.

5.1.7 Ignition Timing

Ignition advance is mechanically coupled with accelerator pedal position. A non-linear actuation scheme is used, similar to the air throttle linkage, to provide significant ignition advance at the idle position, rapidly decreasing to approximately the 1/2 pedal travel position and only gradually decreasing beyond this to the minimum advance position at full power. This provides an ignition advance function with ϕ which crudely approximates that shown in Figure 5. A centrifugal advance mechanism is retained to provide a smaller degree of advance, parametric with engine RPM.

5.1.8 Fuel Supply Control

Circuitry is provided for the sensing of a minimum RPM level, below which the hydrogen supply is cut off at the main shutoff valve. This insures that fuel flow is terminated in the event of engine stall. The threshold RPM is set below the engine cranking speed to allow fuel flow during starting.

This circuit is schematized at the bottom of Figure 17. Essentially, it is a low speed tachometer. C18 is charged via Q2 such that its voltage roughly tracks engine RPM. When it exceeds a threshold voltage set by R23, the MLM111 comparitor switches driving the hydrogen solenoid valve "on" through emitter follower Q3. Positive feedback through R24 insures that the comparitor switches abruptly and provides an improved electrostatic noise margin for the circuit.

5.1.9 Instrumentation

An instrument interface is provided for control and monitoring of the vehicle injection, ignition, and cryogenic fuel storage systems. It is necessarily kept simple and straightforward in consideration of the intended use of the vehicle in fleet operation. Figure 29 is the vehicle wiring diagram showing the dashboard instrumentation. Warning lights are provided for indication of key system states. A fuel flow meter indicates approximate fuel consumption rate via:

$$H_2 \text{ (mass flow)} \simeq \text{RPM} \times \text{Equivalence ratio}$$

A voltage corresponding to fuel flow is available at the water injector intermediate drive output (terminal FM in Figure 17) using the integrating capability of the D'Arsonval meter movement.

5.2 INJECTION VALVE

Development of a suitable high speed electronically actuated injection valve (or injector) has proven to be a significant obstacle in system implementation. Indeed, certain design limitations of either the manifold or direct injection system are dictated by the actuation speed and flow capabilities of the injectors.

Two figures of merit apply to injector performance: the steady state flow coefficient C_v and the total actuation time τ_{act}. C_v is defined by the Fluid Controls Institute (USA) as:

$$C_v = Q \frac{SG \times T}{13.61 \times P_1} \quad \text{for } P_1 > 2P_2$$

Q = Flow in SCFM

SG = Specific gravity of gas referenced to air (H_2 @ 70°F, 1 atm = .0695)

T = temp, °K

P_1 = inlet absolute pressure, PSIA

P_2 = outlet absolute pressure, PSIA

τ_{act} is defined as the total opening time plus the total closing time of the valve. Thus τ_{act} is a measure of the idealness of valve transient response, lower values corresponding to more ideal performance. C_v is an indicator of expected mass or volume flow through the valve under steady state conditions at a specified differential pressure, upstream pressure and temperature.

Conventionally available solenoid valves are supplied with C_v values compatible with injector design requirements, but actuation times for even the fastest control valves are far too slow to be usable,

typically 100 ms. An electronic fuel injector developed by Robert Bosch Ltd. (W. Germany) for gasoline EFI systems was tested for flow characteristics using hydrogen. Using a 12 volt pulse actuation signal a τ_{act} value of 3.3 ms was observed using an upstream pressure of 75 psig and atmospheric downstream. Opening time accounted for 1.5 ms, the closing time 2.0 ms. These times are acceptable for gasoline injection applications using typical maximum actuation pulse durations of 8.0 ms. C_v for this valve, even when modified for improved flow by removal of the metering tip and internal filter, was far too low with hydrogen to be usable. Lynch [29] previously evaluated this injector with concurrent results.

It was experimentally determined that allowing for a 3.75 ms pulse duration and assuming opening and closing times to be equal, a circular orifice of .178 cm^2 cross-sectional area is capable of flowing 200 cc (STP) per injection cycle using an upstream pressure of 30 psig. This is an acceptable flow rate for injection application to the AMC 232 engine which has a displaced cylinder volume of 634 cc and requires 190 cc hydrogen delivery for a stoichiometric fuel-air ratio. Fuel delivery required for the TX-650 is 98 cc for $\phi = 1$, approximately half of the AMC 232 requirements. Fuel requirements for the TX-650 are given by:

$$y = \frac{137\ \phi}{1 + \frac{\phi}{2.38}}\ cm^3 \text{ per injection}$$

y = hydrogen volume (@ 68°F, 1 atm)

Total fuel flow required is plotted in Figure 30 v.s. RPM, parametric with ϕ.

Two prototype injectors were designed for use with the TX-650 manifold injection system. These utilized poppet valves driven by electromagnets taken from Bosch gasoline injectors. Orifice area was .08 cm^2. Injection delivery was measured at 66 cc using a 40 psig upstream pressure and 5.0 ms pulse duration. Pressures above 45 psig could not be used due to insufficient electromagnetic force available to lift the poppet off its seat. Minimum usable pulse duration for use in manifold injection engine testing was 2.0 ms. This injector is designated Type 1.

Further development was directed toward improvements in maximum injection delivery, and improved actuation times to achieve a wider range of usable pulse durations. Several injector configurations were tested, all retaining the basic poppet valve structure but utilizing various electromagnetic actuation geometries. It was reocgnized that a significant portion of the delay time for valve opening or closing is due to the rise and fall time of the magnetic field in the actuator electromagnet. High speed actuation was found to depend on:

reduction of the coil inductance

reduction of coil resistance for high current operation

concentration of field flux at gap between actuator slug and magnet core

high magnetic permeability of core, field containment shroud, and slug

light weight moving parts to minimize inertial delays.

However, practical restraints exist on supply current and acceptable injector heat dissipation. Additionally, several parameters are

contradictory, i.e., low inductance demands low core permeability, thus lower magnetic field concentration.

These injector test prototypes, designated Type II, employed various combinations of the above parameters for optimized performance. Fastest actuation times were achieved with low inductance structures at the sacrifice of applied force. Thus, maximum orifice size and inlet pressure were limited and flow rate was reduced. Conversely, higher flow rate was achieved with sacrificed actuation speed. Concurrently, a modified version of a low inductance prototype was tested for use as a water injector, to be applied in an integrated water injection-hydrogen injection system. Both flow rate and actuation times using water were more than adequate for this application. Using a 5.0 ms pulse duration and injector actuation with every cylinder firing, a continuous water flow condition would be reached at the 4000 RPM maximum speed of the 6 cylinder engine using a single common water injector to feed all cylinders. Thus, almost linear tracking of hydrogen mass flow may be achieved over the entire range of engine speed and fuel flow. Modifications included provisions for corrosion immunity of internal injector parts.

Problems recognized in work with the Type II injector indicated the need for a more sophisticated valve actuation scheme than use of direct electromagnetic force. A two stage valve concept was developed utilizing the principle of fluid amplification (see Figure 31). A small flow rate, high speed electromagnetic injector is used for primary fluid flow with actuates a larger valve surface providing high flow rate. The valve geometry is such that it is capable of

withstanding very high reverse pressure differentials without significant backflow. This feature makes it compatible with direct injection requirements wherein the injection valve must be capable of blocking combustion peak pressures. Tests on a prototype of this valve (designated Fluidamp injector) demonstrated more than adequate hydrogen flow rate. Actuation time, however, is sacrificed due to the two stage valve geometry. The valve opens following the opening of the primary valve and pressurization of the piston-valve disc assembly (or poppet). Valve closure requires both primary valve closure and depressurization of the displaced volume between the poppet face and the nose of the primary injector. Long valve closure times are the result of this depressurization period. Total injection cycles ranging from 7 ms to 13 ms are observed using drive pulse durations of 1 ms to 5 ms respectively and a secondary pressure of 30 psig. A period of large scale flow exists from approximately 3 ms after cycle initiation to 5 ms before cycle termination. Figure 32 demonstrates a typical flow cycle.

The long valve closure time of the Fluidamp injector need not present a problem in direct injection applications if the injection cycle is timed to terminate late in the compression stroke of the engine. Thus, cylinder compression may be used to effectively cut off hydrogen injection at the point where the cylinder pressure exceeds the secondary injection pressure. Dynamic injection timing functional with RPM and pulse duration such that this termination occurs at the correct piston position is a feature of the control electronics.

A finalized version of the Fluidamp injector for use in both the vehicle system and direct injection experiments on the test engine

incorporated an enlarged poppet primary surface to reduce primary pressure requirements, and the addition of water cooling passages to prevent material fatigue at combustion temperatures.

Injector flow characteristics were evaluated experimentally for all prototypes. Delivery volume was measured by displacement of a graduated water column. Dynamic flow response was determined by recording instantaneous pressure in an accumulator which supplied hydrogen to the injector under test (see Figure 33). Injection flow depressurizes the accumulator. Pressure traces were generated by oscilloscope displays of signals from a piezo-electric fast-response pressure transducer. Flow rate is inferred by graphical differentiation of scope photographs. In this case,

$$Q \sim \frac{-dP}{dt}$$

where Q = instantaneous flow rate and P = instantaneous pressure in the accumulator. Pressure drops in the accumulator were small over each injection cycle, thus final accumulator pressure deviated only slightly ($\Delta P < 3$ psi) from reported pressure data points. Photographs of Type I and II, and the Fluidamp Injector prototypes appear in Figure 34. Summary data on all injectors is outlined in Figure 35.

5.3 ELECTRONIC TECHNIQUE FOR HIGH SPEED ELECTROMAGNETIC VALVE ACTUATION

As previously mentioned, a major portion of the time delay in electromagnetic valve actuation is due to the rise and fall time of the magnetic field in the actuation coil. Magnetic field intensity is linearly related to coil current in simple electromagnets by the expression:

$$|H| \sim NI$$

(for core materials below the saturation point) where $|H|$ = magnitude of magnetic field, N = number of turns, and I = current. However, coil inductance, L, increases with N^2. The coil may be electrically modeled as

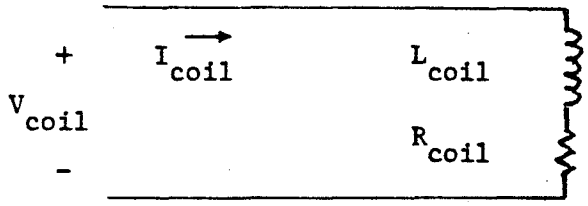

Presented with a voltage step function, coil current will rise according to the expression

$$I = \frac{V}{R_{coil}} (1 - e^{-(R_{coil}/L_{coil})t})$$

Magnetic force will rise proportionally with this function. Valve actuation will not occur until a certain threshold field force has been reached.

For actuation of a poppet valve of the type used in the hydrogen injector, maximum electromagnetic force is required at the moment of cycle initiation to overcome both the return spring force and the gas pressure forcing the valve shut. A delay time elapses from the point of voltage rise to the point where the threshold current, and thus magnetic field force is exceeded. This period can account for substantial opening time lags in valves using high inductance coils. Reduction of the coil inductance results in poor magnetic efficiency and equivalent field strengths can only be obtained with increased current.

An effective reduction in the L/R ratio is achieved by use of an increased supply voltage and a resistor placed in series with the coil. A faster current rise time results, but substantial power is dissipated in the series resistor, and high magnetic force is still applied when it is least needed late in the cycle. Total power dissipation is given by

$$P = IV = \frac{V^2}{R_{coil}+R_{series}}$$

If steady state current is held constant by appropriate series resistor variation, total power dissipation is found to linearly increase with the supply voltage. Figure 36(a) depicts the desired magnetic force function. In Figure 36(b), actual data on electromagnetic delay times for valve opening and closing are related with coil current.

A circuit which generates a current response function closely approximating the ideal case is shown in Figure ~~16~~ 2. A capacitor is charged through a ~~resistor or~~ constant current source to a voltage much higher than would be used for step function actuation. On cycle initiation, the capacitor is discharged through the electromagnetic coil. Current rises abruptly, then decays. ~~Electromagnetic~~ Inductive delay time is substantially reduced. The high force available at the beginning of the cycle (several times the allowable steady state value) significantly reduces inertial delay. After the initial decay, a low steady state "hold-in" current level is established ~~either by the capacitor charging current if an underdampled response is possible with the required component values, or by~~ via a diode connected to a low voltage supply.

At cycle end, current to the coil is cut off. Due to coil inductance, a reverse voltage spike is generated according to

$$V_{inductor} = L(di/dt)$$

For a rapid current cut-off, di/dt becomes a large negative number, thus $V_{inductor}$ can be dangerously large. Typically, switching transistors are protected from this effect by installation of a protection diode across the coil terminals such that it is reverse biased during normal operation. However, the discharge path provided by this diode leads to long current decay times, thus long valve closure delays ~~as depicted in Figure 36(b)~~. This problem ~~may be~~ is overcome ~~using~~ in the capacitor discharge driver circuit by connection of the protection diode so as to be forward biased from the collector of the transistor to the high voltage supply. Reverse coil voltage up to the level of the high voltage supply, but not exceeding it, are allowed. Transistor protection is provided while still allowing for large, but not infinite -di/dt transients. Additional advantage comes from the very low steady state current flowing at the cycle end. Almost instantaneous current cut-off and field collapse results. Valve cut-off time then depends only on moving part inertia. Although high coil current flows at the beginning of the cycle, its duration is brief, ~~less than one ms in tests with the Bosch injector.~~ Power dissipation integrated over the entire cycle is less than when using step function drive except in very short cycle durations.

Figure 3a is an oscilloscope photograph showing actual coil current in the Type III injector during actuation with a 5 ms pulse. Figure 3b indicates the response of the injector poppet valve to this current pulse. The valve opens completely within 1.2 ms after actuation, and closes completely within 1.3 ms after the end of the pulse. Hydrogen pressure was 50 psig for this case.

Tests on the Bosch injector using 75 psig hydrogen indicated flow development in 0.2 ms and flow cutoff in 0.5 ms using this system. Using step function actuation these values were 1.5 ms and 2.0 ms

respectively. The Bosch injector will not operate above 90 psig using step function actuation, but will operate at greater than 150 psig (limit of testing) using the C-D driver circuit. Figure 36(c) depicts actual coil current response using this circuit with the Bosch injector.

Optimized circuit component values were determined with the aid of computer simulation using SPICE. Simulated coil current responses of the optimized fuel injector and water injector systems are shown in the computer generated plots of Figures 37 and 38, respectively. Response of the fuel injector to conventional step function actuation is shown for comparison in Figure 39. Coil inductance values used in simulation were determined under actual operational conditions, since the "active" inductance of a coil with the slug in motion differs significantly from its static value. This driver circuit was employed in later testing of the Fluidamp injector and included in the final vehicle circuit design. A significant improvement in both valve opening and closing time resulted. Comparative Fluidamp responses with conventional and C-D electronics are shown in Figure 32.

5.4 HYDROGEN FLOW CIRCUIT

Hydrogen is supplied from the cryogenic storage system described in Figure 40. Both primary and secondary hydrogen flow circuits are required for the Fluidamp injectors. Primary flow is required at 60 psig, but at a very low flow rate. A peak pressure maintenance technique is used to insure the 60 psig required even during periods of lower line pressure. Tank pressure varies cyclically between the control limits of 40 psig and 100 psig defined by the pressure switch trip point and the dewar pressure relief valve respectively. When line pressure exceeds

the pressure in the primary accumulator, a check valve admits gas into the accumulator. This has sufficient volume to supply primary flow to the injectors during periods when line pressure is below the minimum limit of about 65 psig. The primary regulator maintains 60 psig at the injector primaries.

Hydrogen is supplied to the Fluidamp secondary inlets at between 5 and 30 psig determined by the secondary regulator. Fuel is distributed to the individual injectors through the secondary fuel gallery. An electronically actuated valve at the inlet of the fuel gallery allows master fuel cutoff by the injection control unit under previously described conditions.

6. SYSTEM TESTING

Engine tests were conducted using both direct and manifold injection system configurations. A premixed induction system was also evaluated, and baseline engine performance data using gasoline was taken. This work was directed towards testing and optimization of the experimental system hardware in actual application, and also provided a basis for evaluation of comparative system effectiveness in achieving the desired engine operational characteristics. Data presented here were generated using the Yamaha TX-650 test engine previously described. At the time of writing, work remains in progress on completion of the postal vehicle system, and test data are not yet available.

6.1 BASELINE DATA SETUP

For comparative performance evaluation, the TX-650 test engine was originally set up for operation on gasoline fuel, tuned to original factory specifications. At time of testing, the engine already had 5000 miles of actual operation logged. The power plant is normally fitted with dual constant velocity Mikuni - SU carburetors. Original exhaust equipment was retained.

A hydrogen carburetion (actually, gas-mixing) system was fabricated using two Impco type CA-50 propane carburetors modified for use of hydrogen. Modification was primarily aimed at achieving as rich a fuel-air mixture as could be delivered with these units. Practically, an equivalence ratio of 0.55 was used during testing. A water induction system was fabricated using two POSA injection carburetors

modified for variable water flow. These also served as the throttle bodies for air and fuel flow control. A separate system was used for each cylinder, but pressure equalization between intake ports was provided (see Figure 41).

The stock ignition system of the TX-650 was retained. Static timing positions were used in most tests. Conventional spark plugs of a cold heat range were used, gapped to 1.5 mm. It was necessary to locate the two ignition coils far apart from each other to avoid electromagnetic cross induction observed early in testing.

6.2 MANIFOLD INJECTION SETUP

An experimental electronically controlled manifold injection system was fabricated. This employed Type I injectors and a two cylinder version of the previously described electronics. Pressure to the injectors was maintained constant (40 psig for most tests) and pulse duration alone used to meter hydrogen delivery per injection. Maximum and minimum pulse durations (and thus ϕ) were manually set to match the test conditions.

Although basically a quality governed system, air throttling was available to establish an acceptable idling condition.

Injection valves were located in positions adjacent to each intake port. The outlet nozzles terminated approximately one centimeter behind each intake valve to provide a clear spray path into the cylinder when the intake valve was open (see Figure 42).

Water induction was available using the same system described for carbureted operation.

Triggering of injection cycle initiation was accomplished using a phototransistor - LED pair sensing system. Static injection timing was used, manually adjustable.

The ignition system used in the carbureted hydrogen tests was retained.

6.3 DIRECT INJECTION SETUP

The installation for direct injection employed predominantly the same hardware described for manifold injection tests.

Injection into a pre-combustion chamber containing the spark plug was tested in several different configurations (Figure 43). The concept behind this was to induce stratified charge formation in the cylinder which would allow the use of very low overall charge equivalence ratios to establish an engine idle condition without the need for air throttling. Thus, high efficiency at light loads, and very low fuel consumption at idle would be possible due to elimination of intake vacuum pumping losses. Problems of erratic or lack of ignition were encountered with spark plug placement at the rear of the chamber. This was presumed to be the fault of insufficient air convection into the narrow throat chamber. A different igniter geometry was attempted, using a modified aircraft heater starter. The protruding tip of this igniter extended through the center of the chamber and the electrode was exposed in the chamber throat area. Conventional ignition systems were incapable of ionizing the 4 mm electrode to wall gap under engine compression pressure. A high power, 1000 mJ per pulse ignition system was designed and fabricated to fire this igniter system (see Figure 44). Problems of insufficient ignition were eliminated, but radical

pre-ignition would occur after several seconds of engine operation. Clearly, the poor heat transfer properties of the extended electrode made it a high temperature site for pre-ignition. These problems forced abandonment of the pre-combustion chamber concept and an injection entry point approximately 2 cm from the normal spark plug position at an angle of 30^{o} from horizontal was used in subsequent engine testing (Figures 45 and 46).

These tests utilized the Fluidamp injector which is capable of withstanding combustion pressure. An additional check valve at the point of injection into the cylinder was employed later in testing to avoid a problem of metal fatigue in the poppet retaining springs of the Fluidamp injectors, due to the high gas temperatures present.

Polar gap spark plugs in conjunction with a high output Kettering ignition system were used. The spark plugs contained an internal air gap within the insulator shaft. This has been suggested as a means for improving the abruptness of discharge onset when using inductive ignition systems [30].

The injection control electronics used for manifold injection were retained, but modified by the addition of C-D driver circuitry to improve the actuation speed of the Fluidamp injectors.

6.4 TEST APPARATUS

A General Electric type TLC-50 dynamometer was employed, chain driven from the engine primary sprocket. Tests were performed in fifth (top) gear. Emissions were analyzed for total NO_x using a Thermoelectron model 10A chemiluminescense analyzer. Exhaust oxygen was monitored with a Beckman F3M31A3B magnetic deflection type oxygen analyzer.

A Beckman model 109 flame ionization detector was used to check for exhaust hydrocarbons from the engine lubricant. Exhaust port temperatures were recorded using Omega direct reading analog pyrometers. A Miriam model 50 MC2-4S laminar flow element was used to measure intake air flow rate. Hydrogen flow rate was inferred from pressure drop in a K type cylinder. Water induction rate was determined from burette water level drop. Figure 47 depicts the actual experimental setup.

6.5 EXPERIMENTAL RESULTS AND DISCUSSION

The results of full throttle, variable RPM tests on the four systems evaluated are illustrated in Figure 48. All hydrogen aspiration systems were tested using approximately the same low RPM equivalence ratio. However, equivalence ratio was found to decrease significantly with RPM in the carbureted and direct injected systems. It is deduced that a flow starvation condition for both H_2 and air causes the observed roll-off of the carbureted system about 6000 RPM. The manifold injection system, which employs an unrestricted air intake path, maintained a zero manifold vacuum, ideal flow condition through 7500 RPM, the maximum engine speed.

It was necessary to use water induction for suppression of random backfire over the entire RPM range with the carbureted system. At 3500 RPM, the water to hydrogen mass flow rate required was 4.9. This approximately followed air flow, but was found to decrease at higher RPM, a characteristic of the induction apparatus used. Engine operation above 6500 RPM was quite rough, with sporadic intake detonation occurring regardless of water induction rate.

A 5 ms injection pulse duration was used in full power manifold injection tests. An injection initiation position of 45° ATDC during intake was found to be optimum for backfire suppression. Advance of this timing position to earlier than TDC resulted in severe single charge backfiring at low RPM for any equivalence ratio. Under these conditions, an over-rich charge formed by accumulation of hydrogen behind the intake valve is inducted at the very beginning of the intake stroke. Pre-ignition due to combustion chamber surface effects and residual combustion products appears guaranteed. Substantial oil leakage into the combustion chamber was evident from significant exhaust hydrocarbon figures indicating a plentiful source of potential combustion nuclei was available. It may also be possible that the accumulated hydrogen charge behind the valve was igniting by combustion product leakage past the closed valve. Injection initiation positions later than 30° ATDC resulted in pre-ignition-free performance up to 5000 RPM. This appears to verify the effectiveness of late fuel delivery in eliminating intake pre-ignition. The 5 ms injection duration used begins to overlap its allowed duration in the intake stroke above 4500 RPM. Residual fuel may be accumulated behind the intake valve at engine speeds above this. Roughness of engine operation above 5000 RPM was observed, assumed due to this effect. For the full power tests, water induction was employed above 5000 RPM to circumvent this problem. The required water/hydrogen mass ratio at 6000 RPM was 10.8.

Full power tests on the direct injection system demonstrated the engine speed limitations imposed by longer injector actuation times. Injection cycle initiation at 90° ATDC was used for these tests to

maximize allowable injection duration. The Fluidamp injectors require 10 ms per injection cycle when driven by a 5 ms pulse duration. This is acceptable for the intended vehicle system. Flow limitation begins above 3000 RPM for the 30 psig fuel pressure used. Power appears to reach a peak between 3000 and 4000 RPM. No backfire condition was observed.

Comparisons of equivalence ratio, NO_x emissions and exhaust temperature with pulse duration were generated in constant RPM testing of both injection geometries. The manifold injection tests yielded the data of Figure 49. Flow limitations of the Type I injectors prevented operation richer than $\phi = .60$. NO_x emissions follow prediction with trivial NO_x below $\phi = .55$ and an exponential rise beginning at about $\phi = .60$.

A significant discrepancy between ϕ figures, determined from measurement of intake air and hydrogen vs. ϕ determined from analysis of exhaust oxygen content was observed for the direct injection system. Figure 50 indicates this difference plotted vs. injection pulse duration. $\phi_{effective}$ is a pseudo-equivalence ratio determined with an assumption of complete combustion from the exhaust oxygen content. Unusually high NO_x production was observed and was seen to exponentially follow ϕ_{intake}, determined from intake product flow measurements. These observations indicated that incomplete combustion was occurring. High NO_x figures may be the result of stratified charge formation and combustion occurring in local high ϕ regions. Injection initiation occurred at BDC for these tests. A retarding of the ignition timing was required for pulse durations greater than 5.0 ms to avoid combustion knock and unstable torque.

The relationship between combustion completeness and engine RPM is illustrated in Figure 51. Turbulence inducing swirl fins were installed in the engine intake ports. The engine was operated on one cylinder, the motoring loss of the other cylinder providing a light load, linear with RPM. Injection initiation at 120° ATDC was used for this test, which results in the majority of fuel delivery between BDC and 90° BTDC at 4000 RPM. Completeness of combustion was seen to improve with RPM from a low of about 55% at 1500 RPM to 97% at 4150 RPM. This appears to underscore the need for a high degree of in-cylinder turbulence to achieve adequate combustion completeness in direct cylinder charge formation.

Highest thermal efficiency (η_t) was achieved with the manifold injection system, 40% at low RPM, decreasing with increasing RPM (Figure 48). The lower η_t values of the direct injection system were explained by the incomplete combustion observed. Efficiency of the premixed charge system was 27% at 3500 RPM. A comparison figure for gasoline was 21%.

A persistent problem of undesired injection triggering due to ignition system electrostatic noise was encountered due to the close proximity of the trigger unit to the right cylinder spark plug. This required extensive shielding of the trigger unit, interface cable and the injection control unit itself.

Failure of the Fluidamp injector-check valve assembly occurred due to heat effects on the check valve moving part and the poppet retainer spring of the injector. Design refinement for improved heat transfer from these parts is indicated.

A simulated life cycle test performed on a Type I injector over 25 million cycles indicated most probable failure due to wear of moving part surfaces. This is enhanced by heat effects in direct injection applications. The use of high temperature abrasion resistant coatings may be desirable for moving part mating surfaces in a production design.

7. CONCLUSIONS

- Delayed fuel delivery possible using a timed injection technique, either at the intake port or directly to the combustion chamber, is effective in circumventing intake manifold backfire.

- Electronic control of fuel injection is feasible and may easily provide the control flexibility necessary for optimum overall engine performance.

- An electronically actuated injection valve with sufficient flow rate and actuation speed can be fabricated and applied in either manifold or direct cylinder hydrogen injection systems.

- Direct cylinder injection is susceptible to incomplete combustion and high NO_x emissions due to heterogeneous charge formation. Mixing improves with RPM due to improved turbulence. Possible improvements in volumetric efficiency by compression stroke injection are offset by thermal efficiency loss due to incomplete combustion.

- Manifold injection requires less sophisticated injection valves and avoids the problems associated with incomplete mixing in direct injection. At the present level of development, manifold injection appears more feasible.

REFERENCES

1. La Fleur, A., Ternary and Quaternary Explosion Regions and La Chatelier's Formula. Rec. travoux chim. Pays Bas, Vol. 56, 1937, pp. 442-473.

2. Coward, H.F. and Jones, G.W., Limits of Flammability of Gases and Vapors. Bulletin 503, U.S. Bureau of Mines, 1952, pp. 15-24.

3. Eitner, P., Explosion Limits of Flammable Gases and Vapors. Habilitations-Schriff, München, 1902; Jour. Gasbel., Vol. 45, 1902.

4. Breton, J., Ann. Office Natl. Combustibles Liquides, 11,487, Theses Faculte des Sciences, Univ. Nancy, 1936. (As noted in [6].)

5. Wendlandt, Z., Physik Chem. 110, 637, 1924. (As noted in [6].)

6. Lewis, B. and von Elbe, G., Combustion, Flames and Explosions of Gases. Academic Press, New York, 1961.

7. Finegold, J.G. and Van Vorst, W.D., Hydrogen Engine Technology, Proc. XV^{e} Congres International F.I.S.I.T.A., Societe des Ingeuieurs de l'Automobile, Paris, France, May 1974.

8. de Boer, P.C.T., McLean, W.J., and Homan, H.S., Performance and Emissions of Hydrogen Fuel Internal Combustion Engines, presented at Hydrogen Fundamentals Symposium, Miami, Florida, 1975.

9. McLean, W.J., de Boer, P.C.T., Homan, H.S., and Fagelson, J.J., Hydrogen as a Reciprocating Engine Fuel, Proc. Future Automotive Fuels Symposium, October 5-6, 1975.

10. Griffith, E.J., Hydrogen Fuel, Nature 248, 458, 1974. (As noted in [9].)

11. Van Vorst, W.D. and Finegold, J.G., Automotive Hydrogen Engines, and Onboard Storage Methods, Proc. Hydrogen Energy Fundamentals Symposium, Miami Beach, Florida, March 1975.

12. King, R.O., The Explosion of Mixtures of Combustible Gases with Air by Nuclear Drops of Water and Other Nuclei and by X-Rays, I. Canadian Air Ministry Official Report, 1950.

13. Sokolik, A.S., Self-Ignition, Flame and Detonation in Gases (translated by N. Kaner, 1963), Akademiya Nauk SSSR, Institut Khimicheskoi Fiziki, Izdatel' stvo Akademii Nauk SSSR, Moskva, 1960, Ch. VII.

14. King, R.O., Durand, I.J., Wood, B.D., and Allan, A.B., The Oxidation, Ignition, and Detonation of Fuel Vapors and Gases, XIV. Canadian Journal of Research, Vol. 28, Sec. F., 1950.

15. Woolley, R.L. and Henriksen, D.L., Water Induction in Hydrogen Powered I.C. Engines, International Journal of Hydrogen Energy, Vol. 1: 401-412, 1976/77.

16. Saga, K. and Furuhama, S., Performance and Emission Control in Stratified Charge Hydrogen Fueled Engines, Musashi Institute of Technology, Tokyo, Japan, 1976.

17. Yu, H., Fuel Distribution Studies, SAE Trans., Vol. 71, pp. 596-613, 1963. (As noted in [3]).

18. Swain, M.R. and Adt, R.R., The Hydrogen-Air Fueled Automobile, Proc. Intersociety Energy Conversion Engineering Conference (IECEC), San Diego, California, 1972.

19. Erren, R.A. and Campbell, W.H., Hydrogen: A Commercial Fuel for Internal Combustion Engines and Other Purposes, Jour. Inst. Fuel 6: 277-290, 1933.

20. Heinze, E.P.A., The Erren Hydrogen Engine, Engineering pp. 607-608, November 1932.

21. Murray, R.G., Schoeppel, R.J., and Gray, C.L., The Hydrogen Engine in Perspective, SAE 729216, Proc. 7th Int. Energy Conv. Engr. Conf. (IECEC), Chem-Soc., Washington, D.C., 1972.

22. Oehmichen, M., Wasserstoff als Motortveibmittel, Verein Deutsche Insenieur, Deutsche Kraftfahrtforshung, Heft 68, 1942. (As noted in [8]).

23. Winkler, A. and Sutton, R., Bendix Electronic Fuel-Injection System, SAE Trans., Vol. 65, 1957.

24. Baumann, G., Bosch Electronically Controlled Gasoline Injection System for Spark Ignited Engines, Robert Bosch G.m.b.H., Stuttgart, Germany, 1967.

25. Tractor and Mechanical Publications, The Petrol Fuel Injection Book for Automobiles, P.I. 1972, Interauto Book Co., Ltd., Middlesex, England, 1972.

26. Schlag, J.H., Automatic Computor Controlled Calibration of EFI Control Units, SAE Trans., 760243, 1976.

27. Society of Automotive Engineers, First Digital Microprocessor Goes to Toronado, Automotive Engineering, Vol. 84, No. 10, p. 49, October 1976.

28. MacCarley, C.A., Development of a Sodium Borohydride Hydrogen Fuel Storage System for Automotive Applications, Proc. Symposium on Alternative Fuels, AIAA, Santa Maria, California, 1976.

29. Lynch, F.E., Denver Research Institute, Personal correspondence, September 1977.

30. Drexl, Klaus W., Holzt, Hans-Peter, and Gutmann, Manfred, Characteristics of a Single Cylinder Hydrogen-Fueled I.C. Engine Using Various Mixture Formation Methods, Daimler-Benz AG, Central Research, 7 Stuttgart 60, W. Germany, 1976.

31. Obert, E.F., Internal Combustion Engines, International Textbook Co., Scranton, Pennsylvania, 1968.

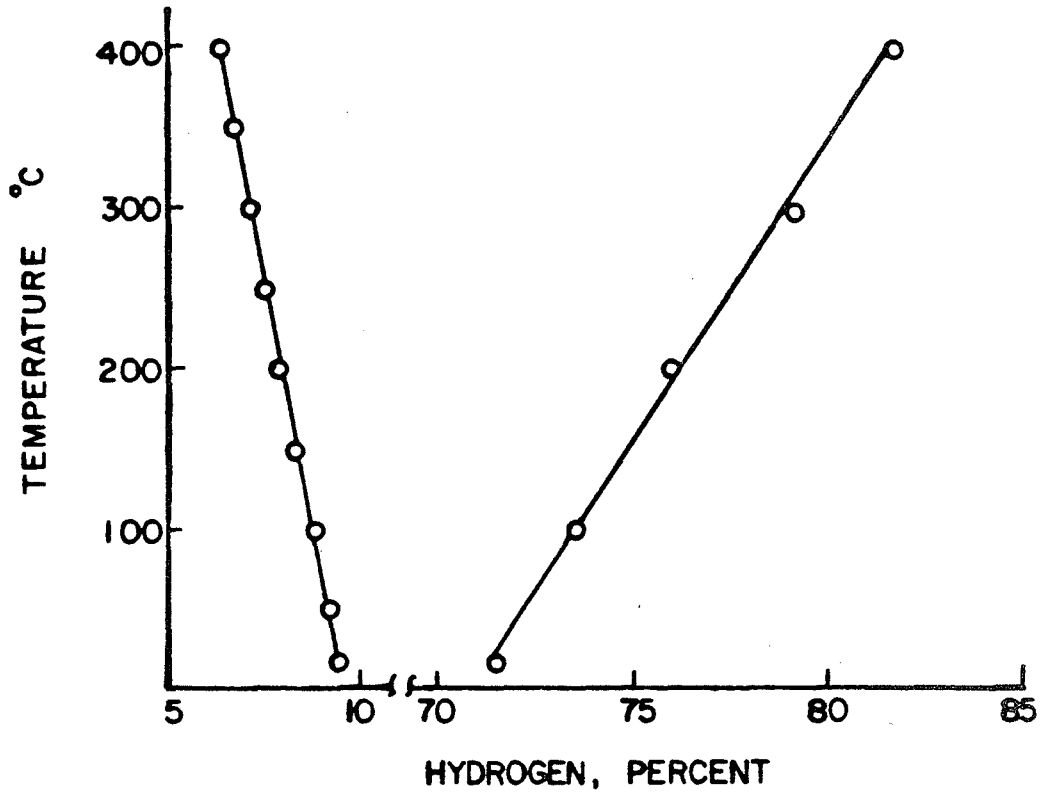

Figure 1. FLAMMABILITY LIMITS FOR HYDROGEN AS A FUNCTION OF TEMPERATURE

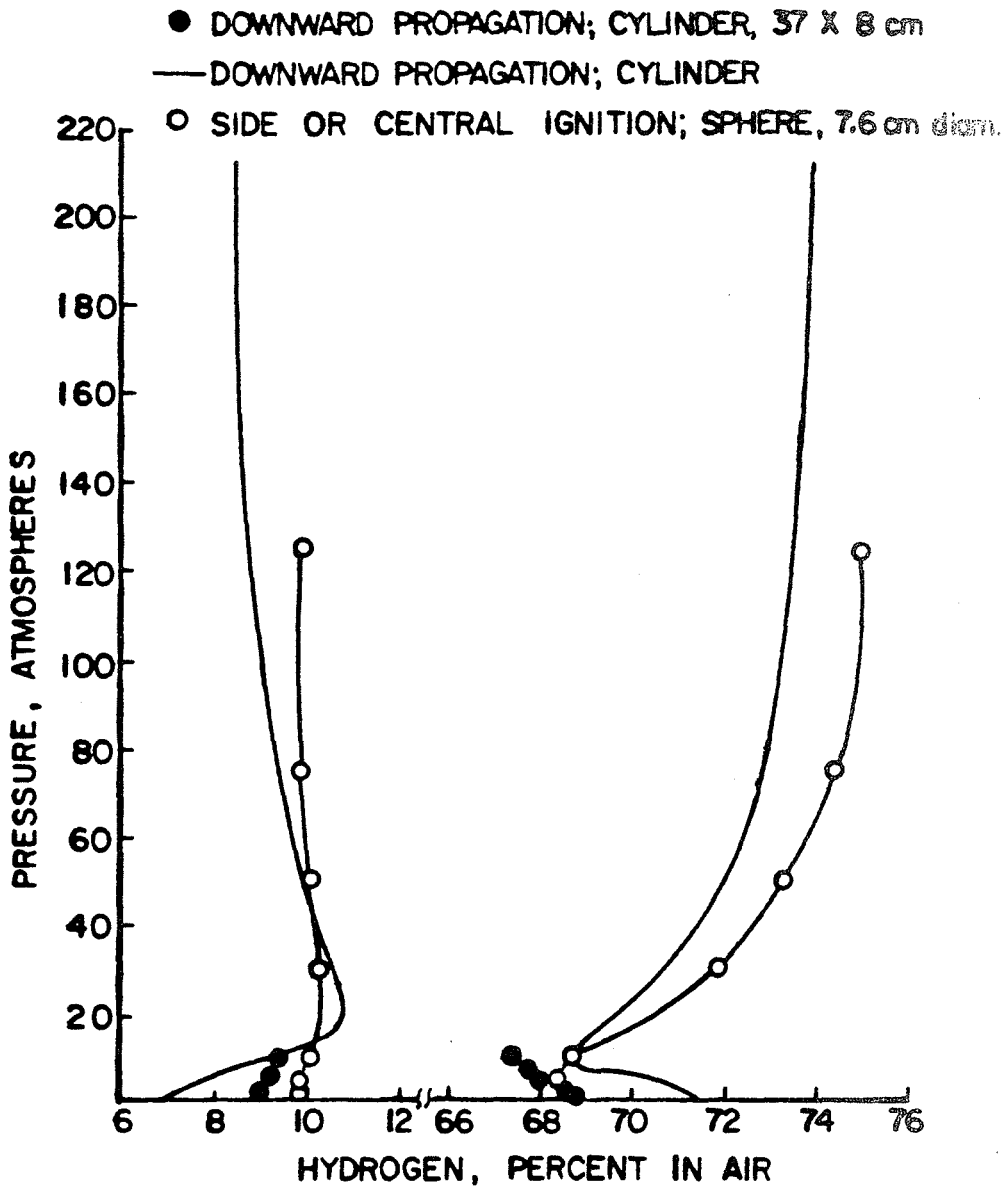

Figure 2. FLAMMABILITY LIMITS FOR HYDROGEN AS A FUNCTION OF PRESSURE

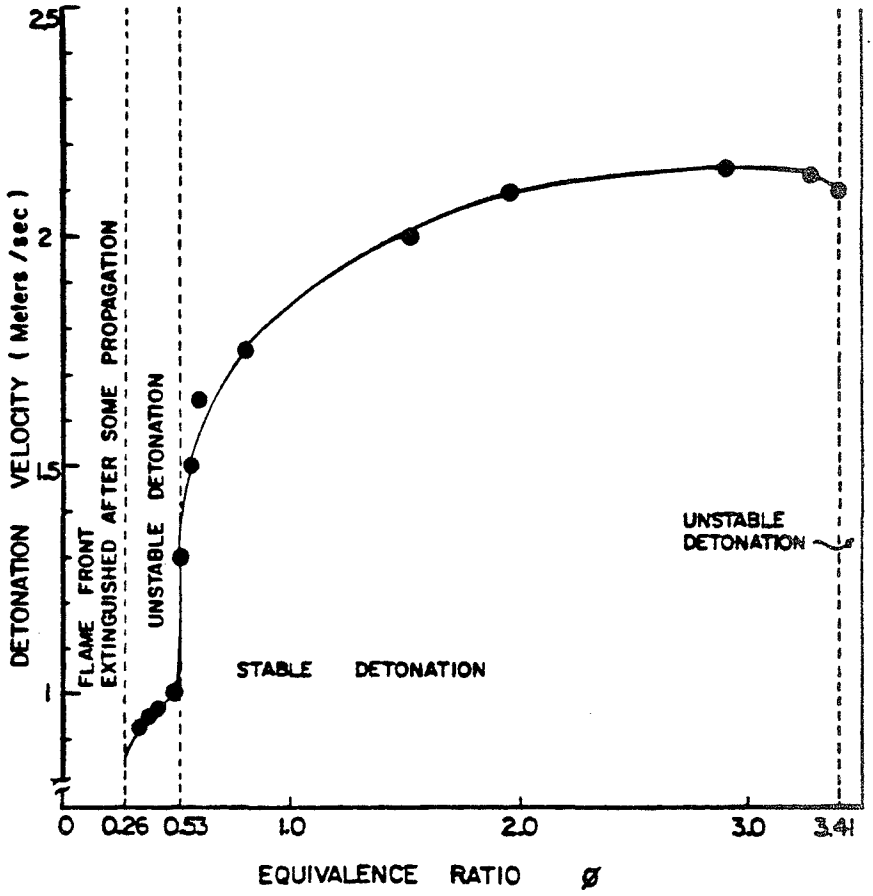

Figure 3. DETONATION VELOCITY OF H_2 - AIR MIXTURES (P = 1 ATM, DETONATION IN CLOSED END GLASS TUBE. DATA IS COMPOSITE OF WORKS BY BRETON [4] AND WENDLANDT [5], FROM [6])

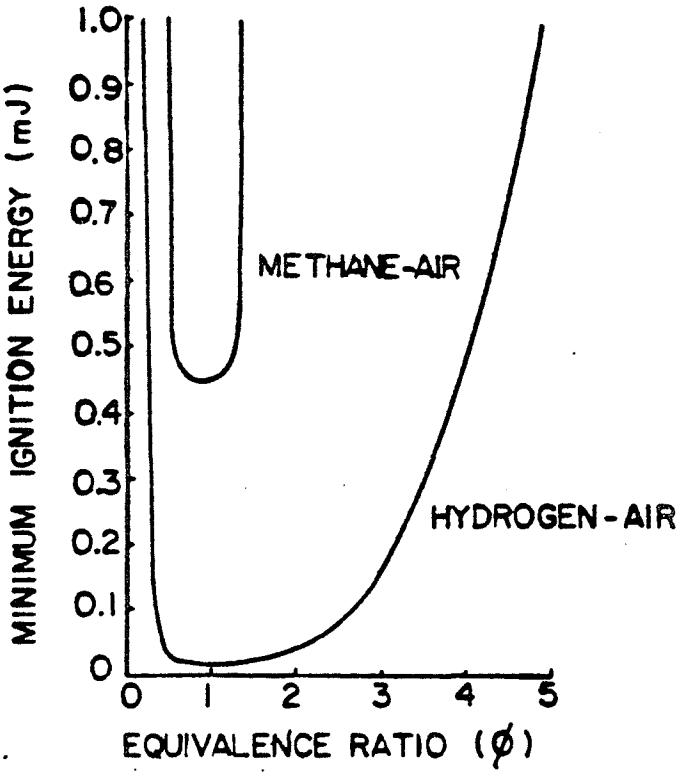

Figure 4.

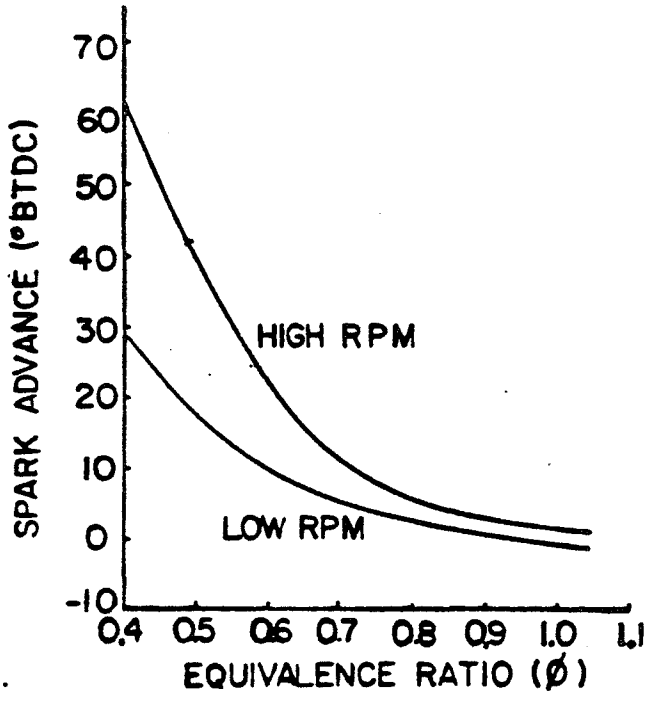

Figure 5.

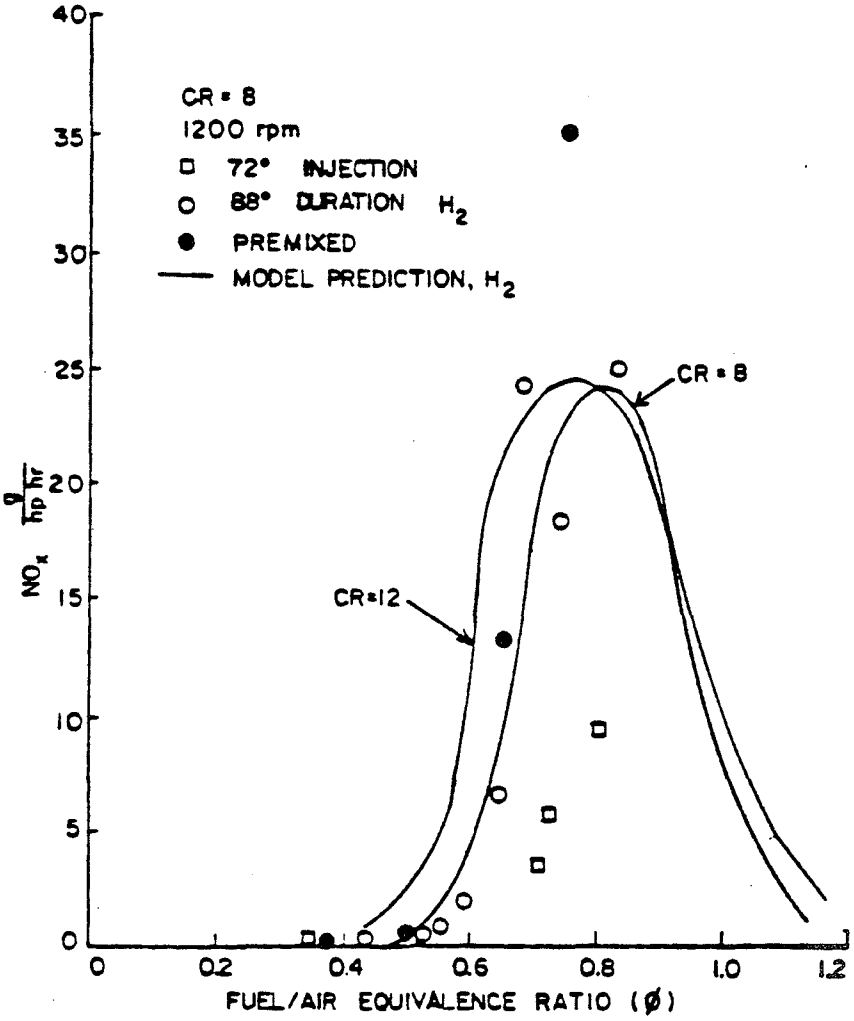

Figure 6. MODEL PREDICTIONS FOR NO_x PRODUCTION (DATA OF de BOER et al) [3]

Figure 7. Fuel Combustion Properties (From [7])

	H_2	CH_4	C_3H_8	Gasoline
Minimum Ignition Energy (mJ)	0.02	0.28	0.25	(0.25)[a]
Ignition Temperature (^oK)[b]	858	810	783	530
Adiabatic Flame Temperature (^oK)[b]	2384	2227	2268	(2270)
Flammability Limits (% in air)	4.0-75	5.3-15	2.2-9.5	1.5-7.6
Laminar Flame Velocity (cm/sec)[b]	190	38	40	($\leq$30)
Diffusivity (cm^2/sec)	0.63	0.20	--	(0.08)
Minimum Quenching Distance (cm)	0.06	0.25	0.19	--
Normalized Flame Emissivity[b]	1.00	1.7	1.7	1.7

[a]Quantities in parentheses are estimates.

[b]Data for stoichiometric air-fuel mixtures.

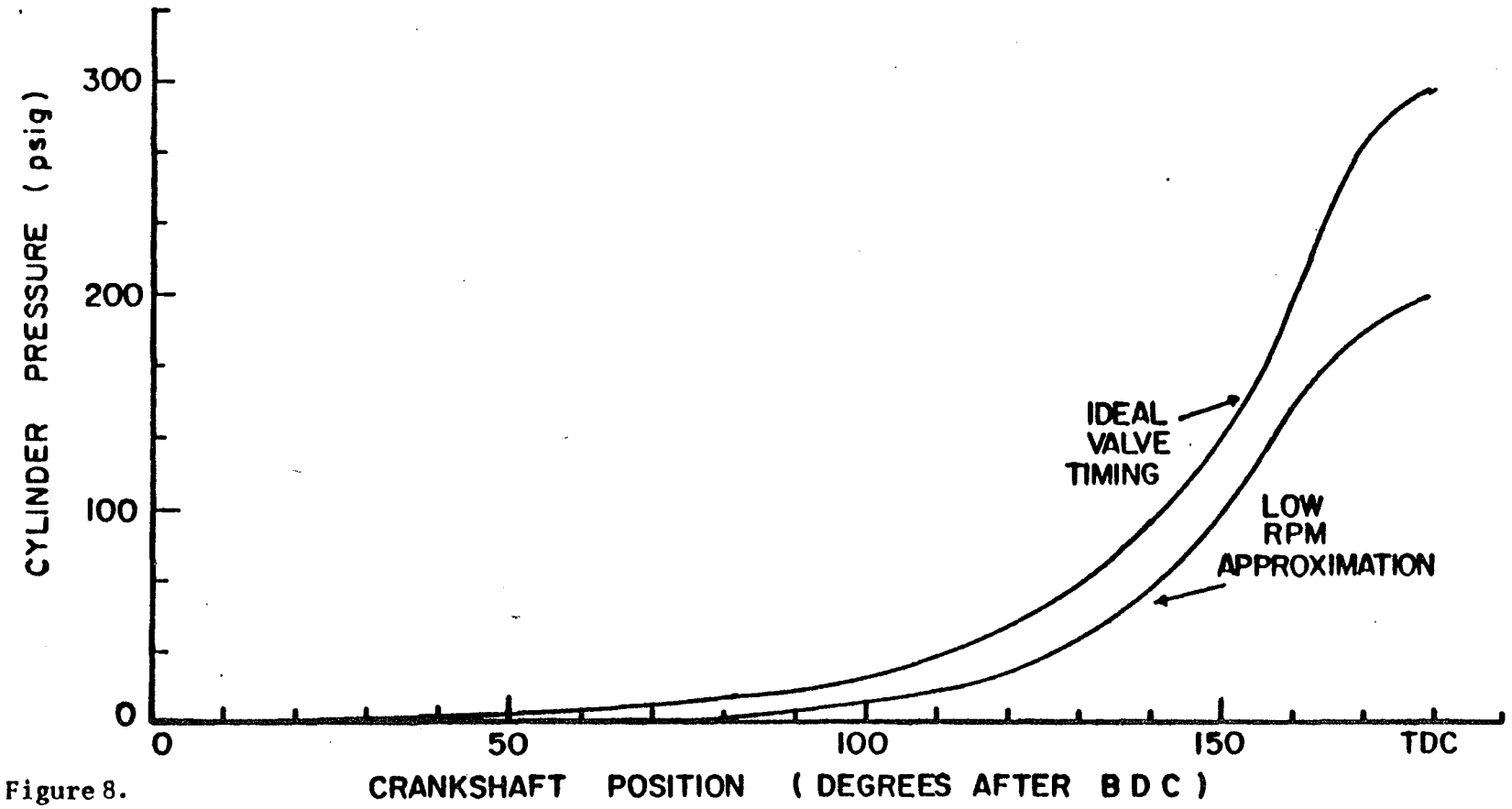
CYLINDER PRESSURE (psig)
300
200
100
0
0
50
100
150
TDC
CRANKSHAFT POSITION (DEGREES AFTER B D C)
IDEAL
VALVE
TIMING
LOW
RPM
APPROXIMATION

Figure 8.

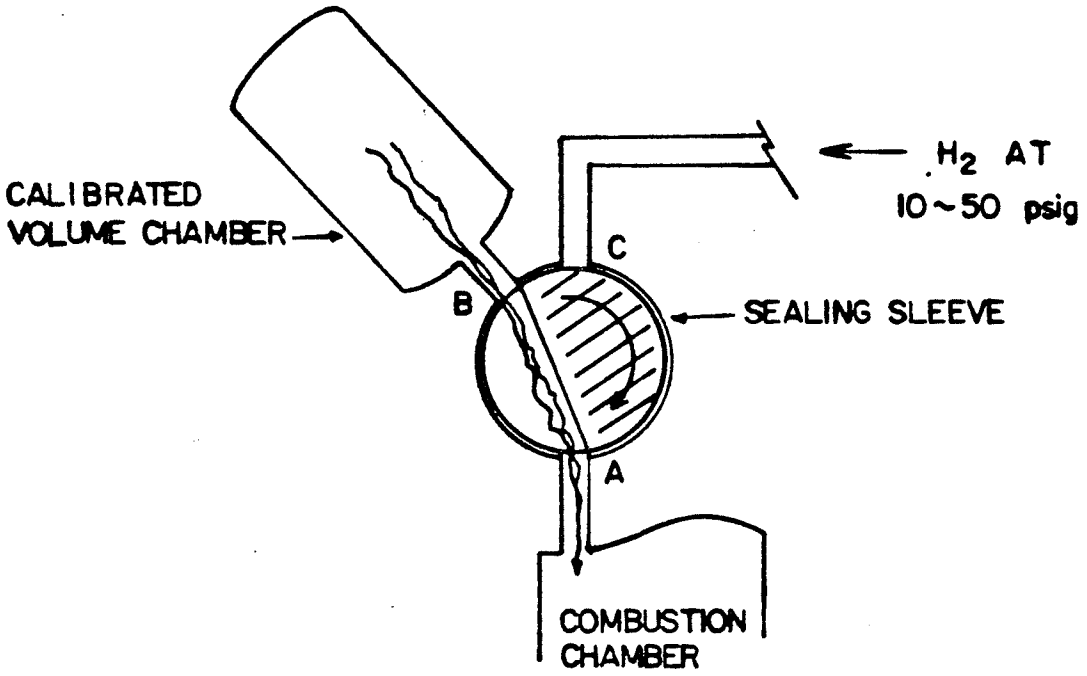

Figure 9. ROTARY-VALVE APPARATUS

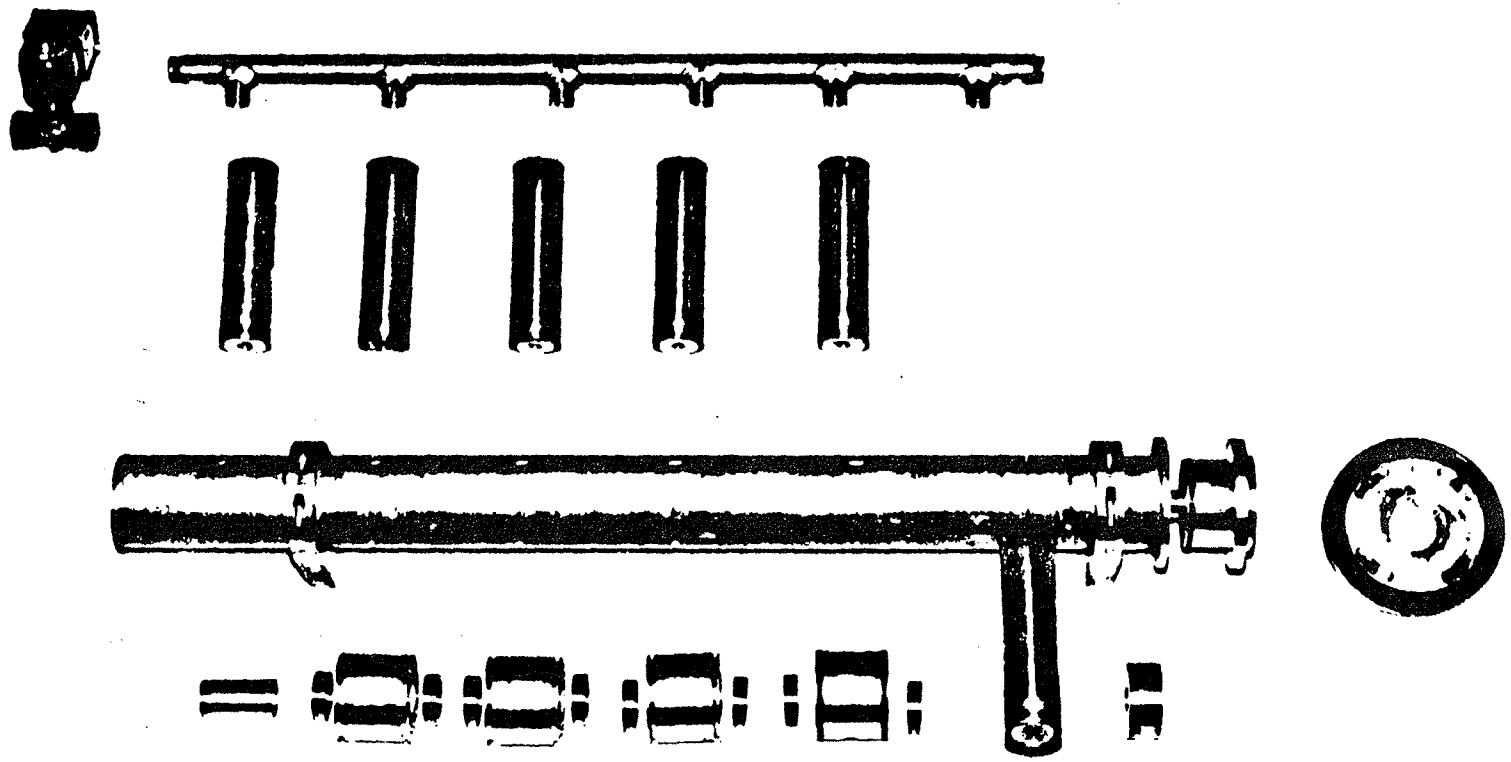

Figure 10. Rotary Valve Injection Apparatus, Disassembled

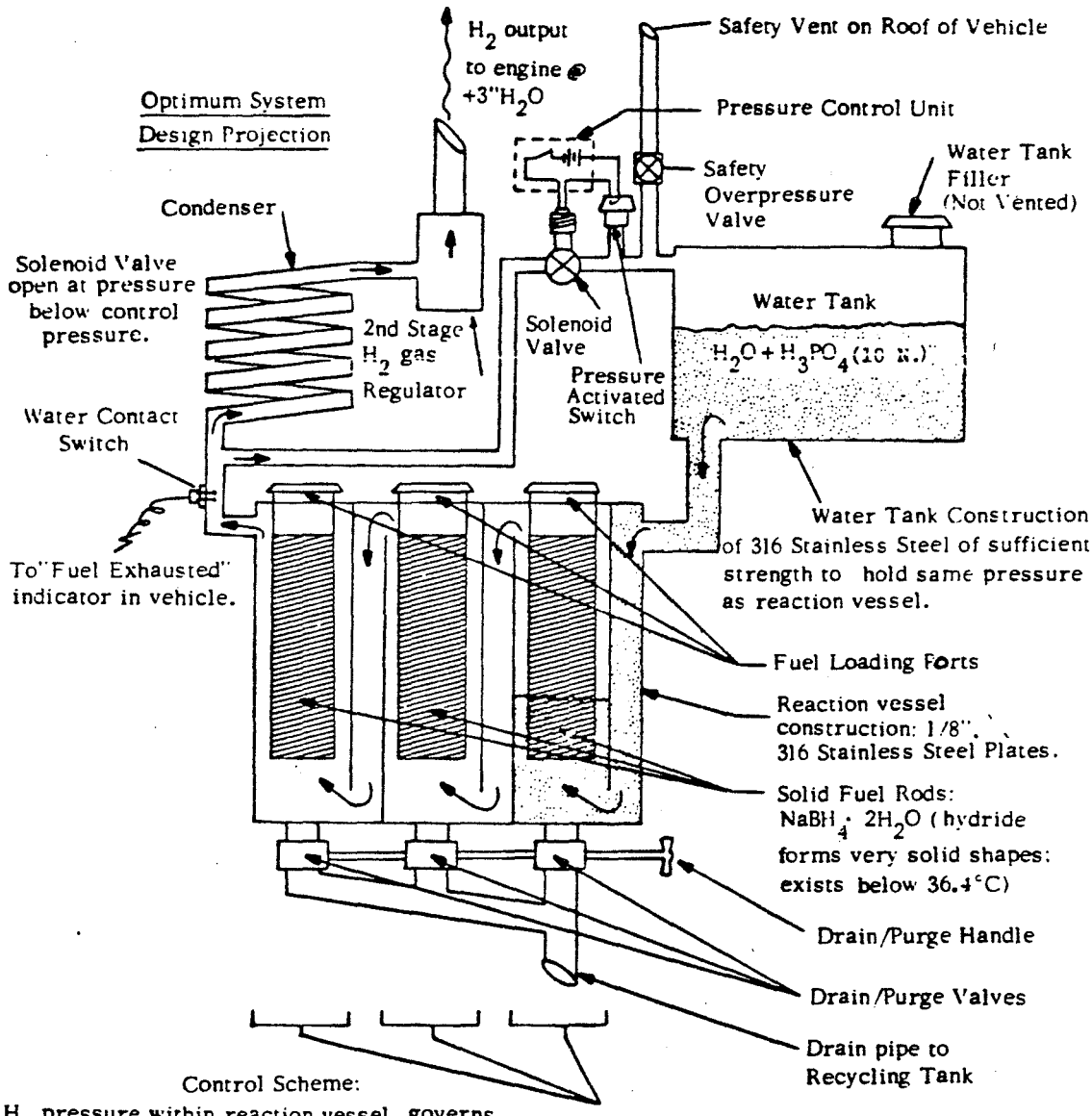

Figure 11. Sodium Borohydride Hydrogen Fuel Storage System

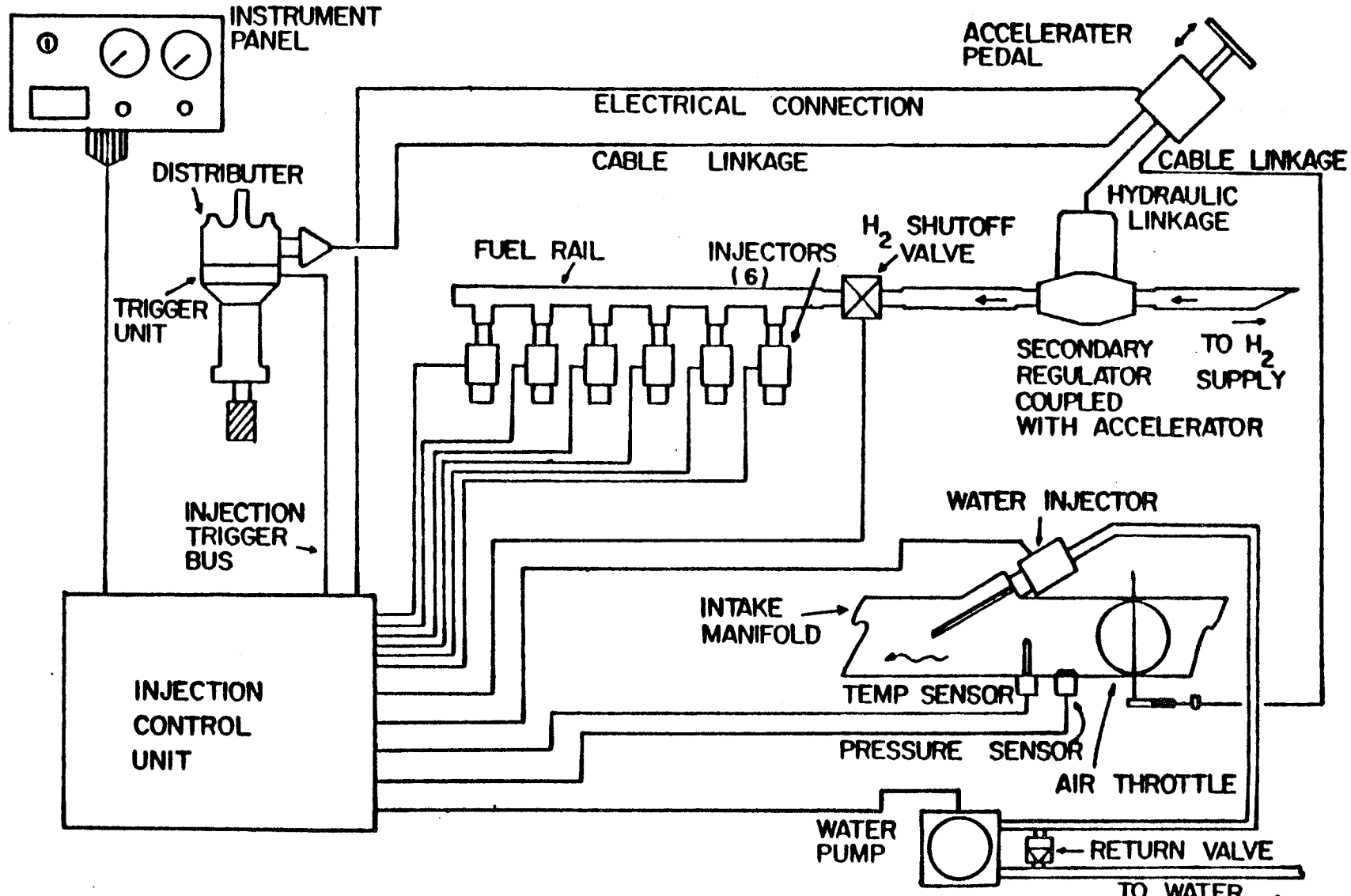

Figure 12. GENERAL LAYOUT OF ELECTRONIC HYDROGEN INJECTION SYSTEM

Figure 13. BLOCK DIAGRAM OF INJECTION ELECTRONICS

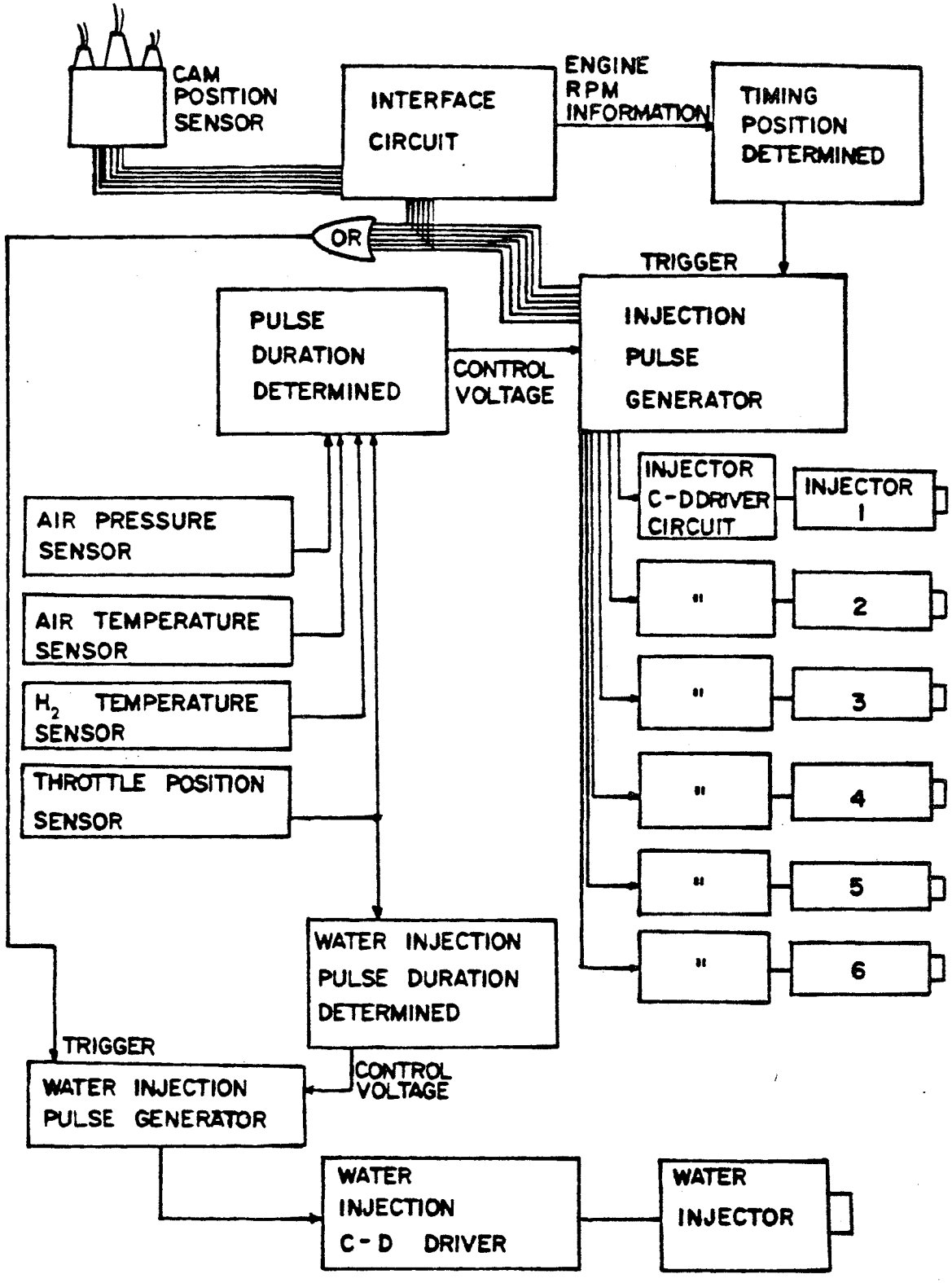

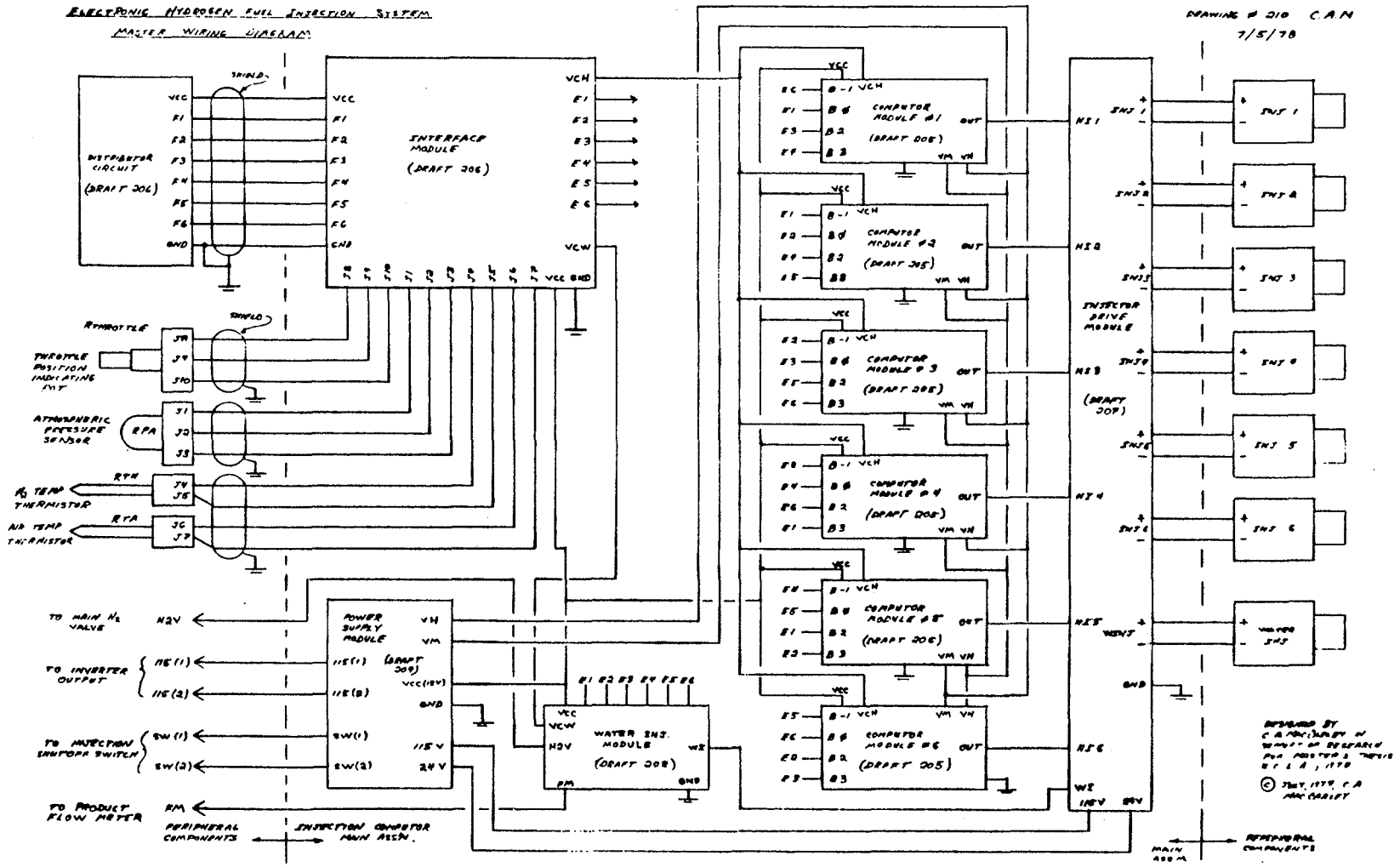

Figure 14. Injection Control Unit, Mainframe Wiring Diagram

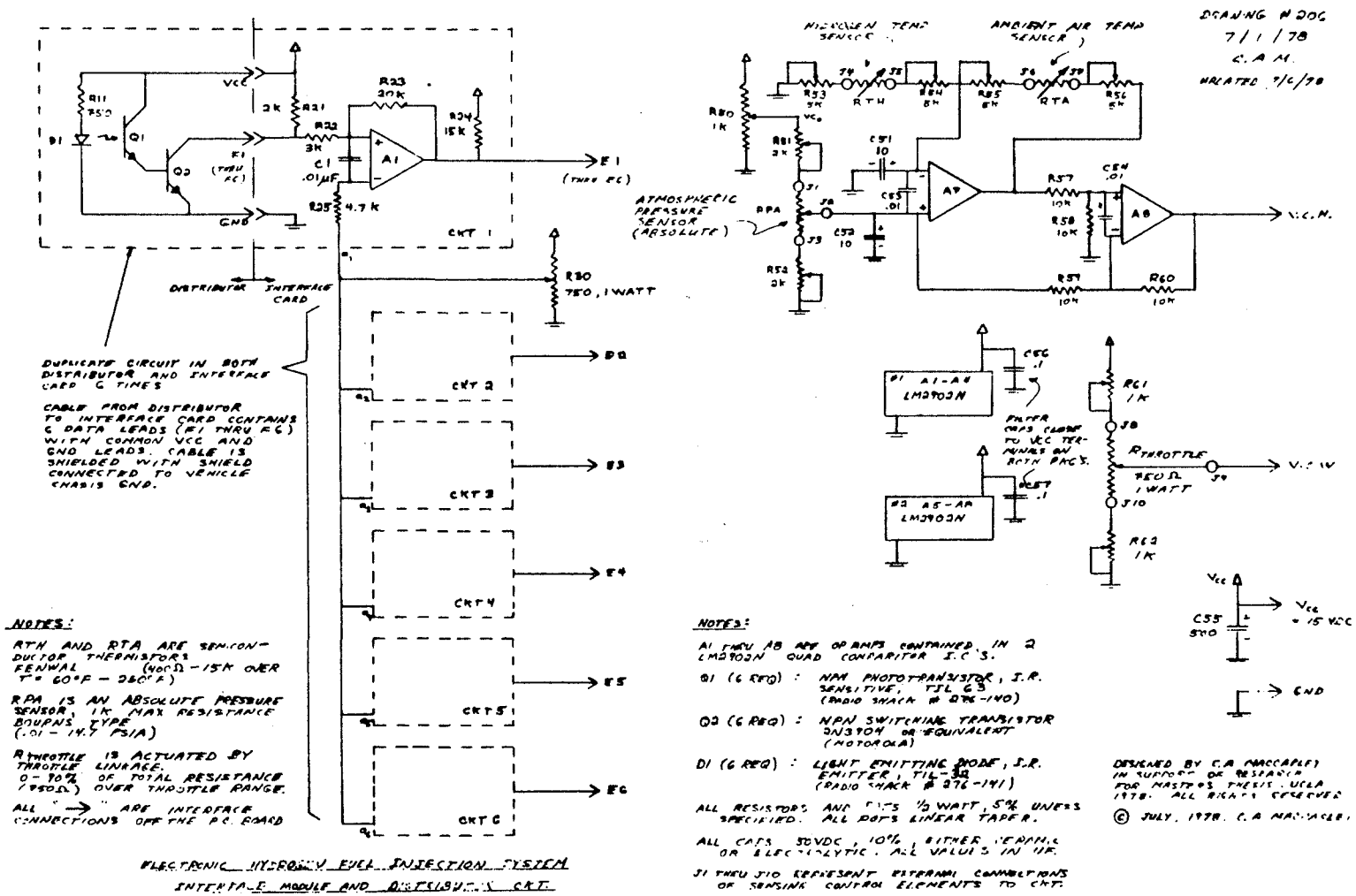

Figure 15. Injection Control Unit, Interface Module and Trigger Circuit Schematics

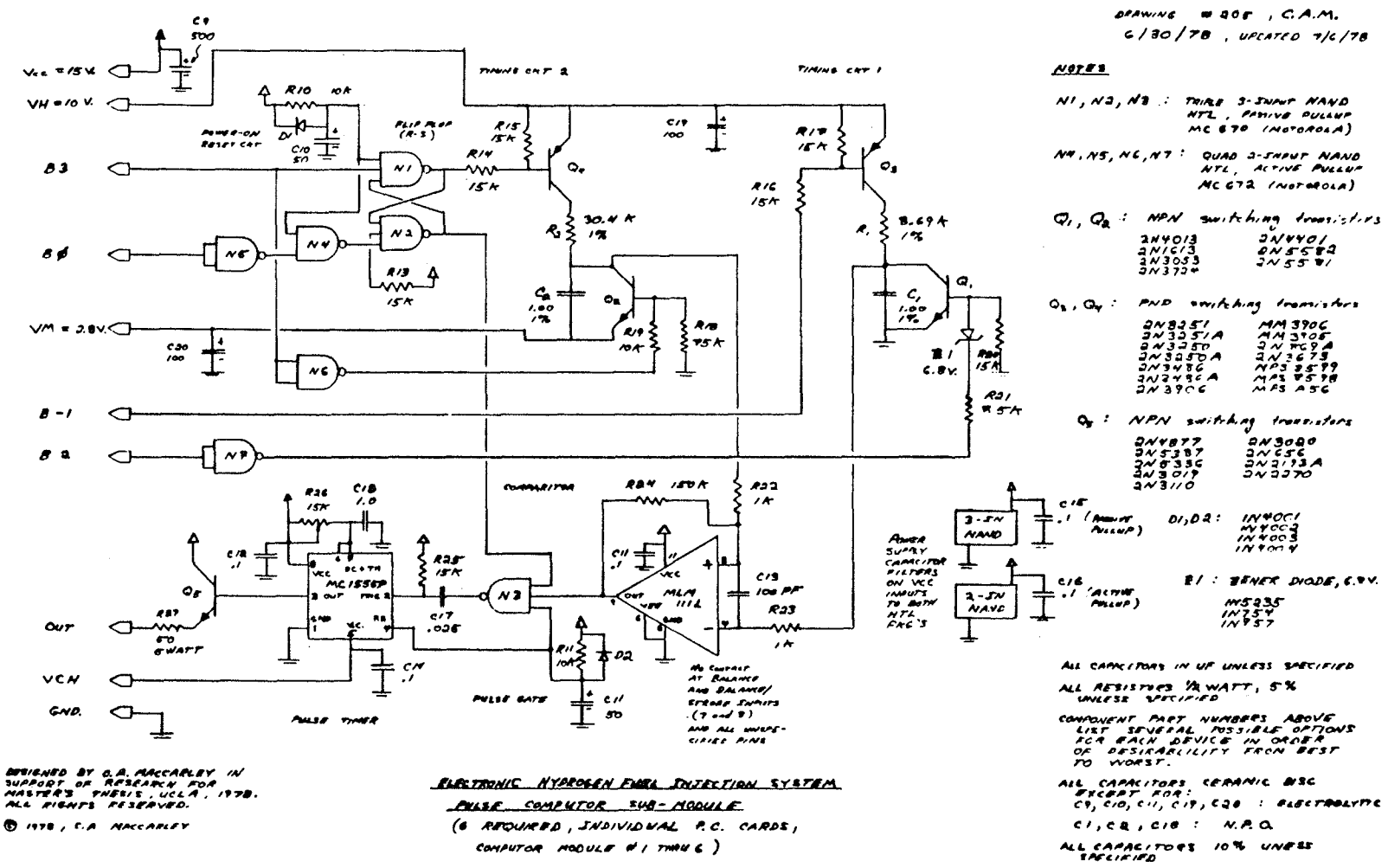

Figure 16. Injection Control Unit, Pulse Computer Module Schematic

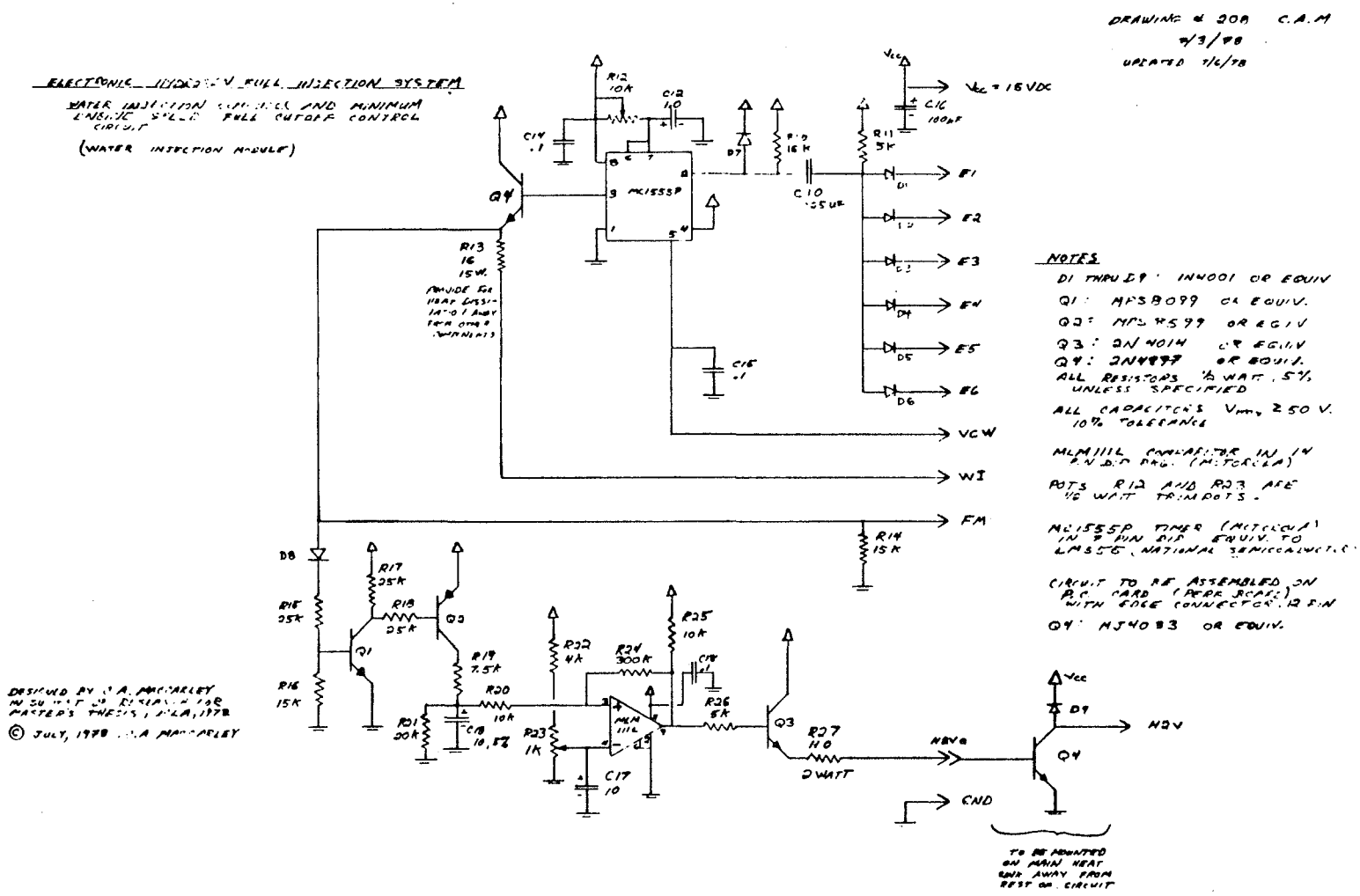

Figure 17. Injection Control Unit, Water Injection Module Schematic

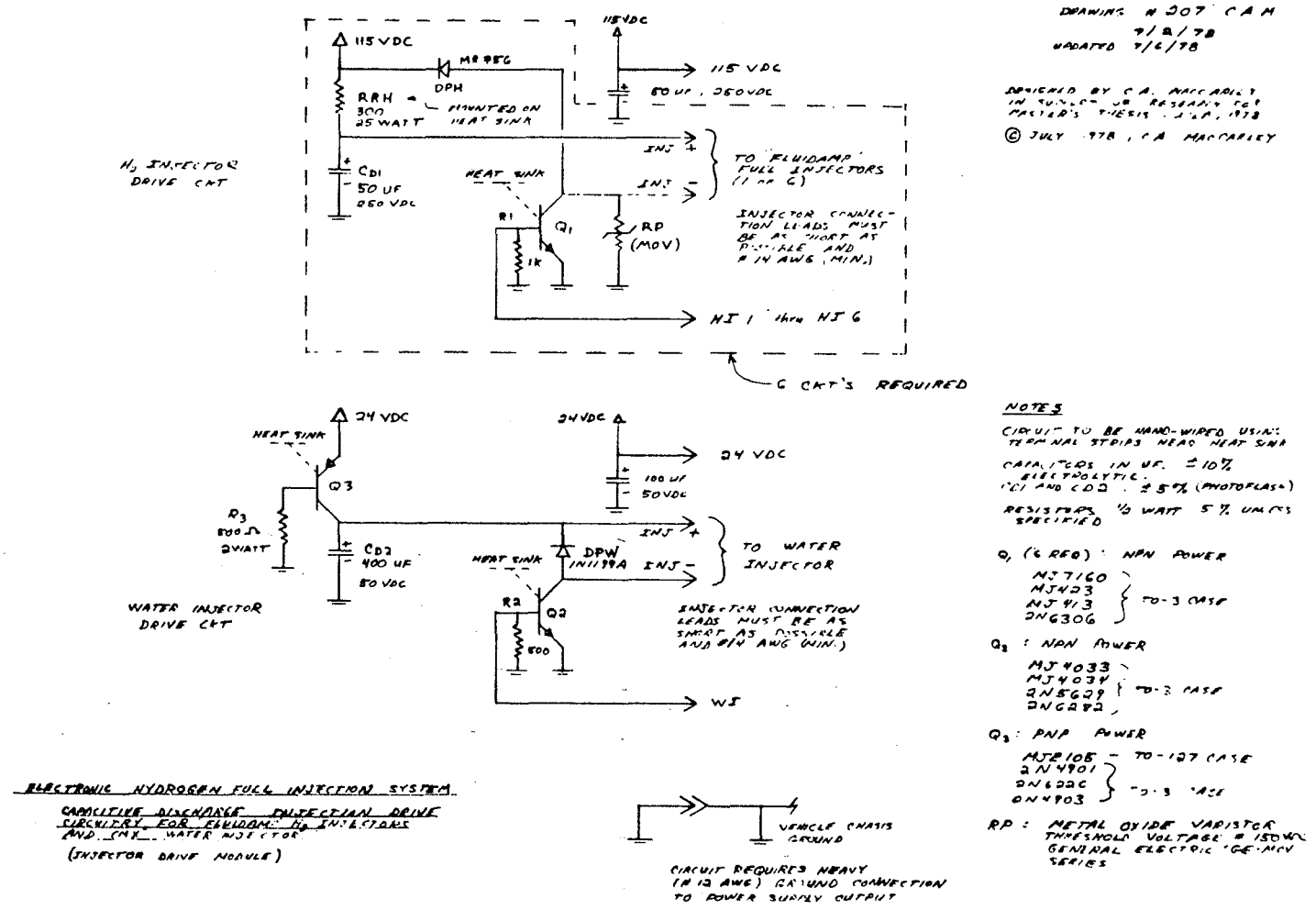

Figure 18. Injection Control Unit, C-D Injector Drive Module Schematic

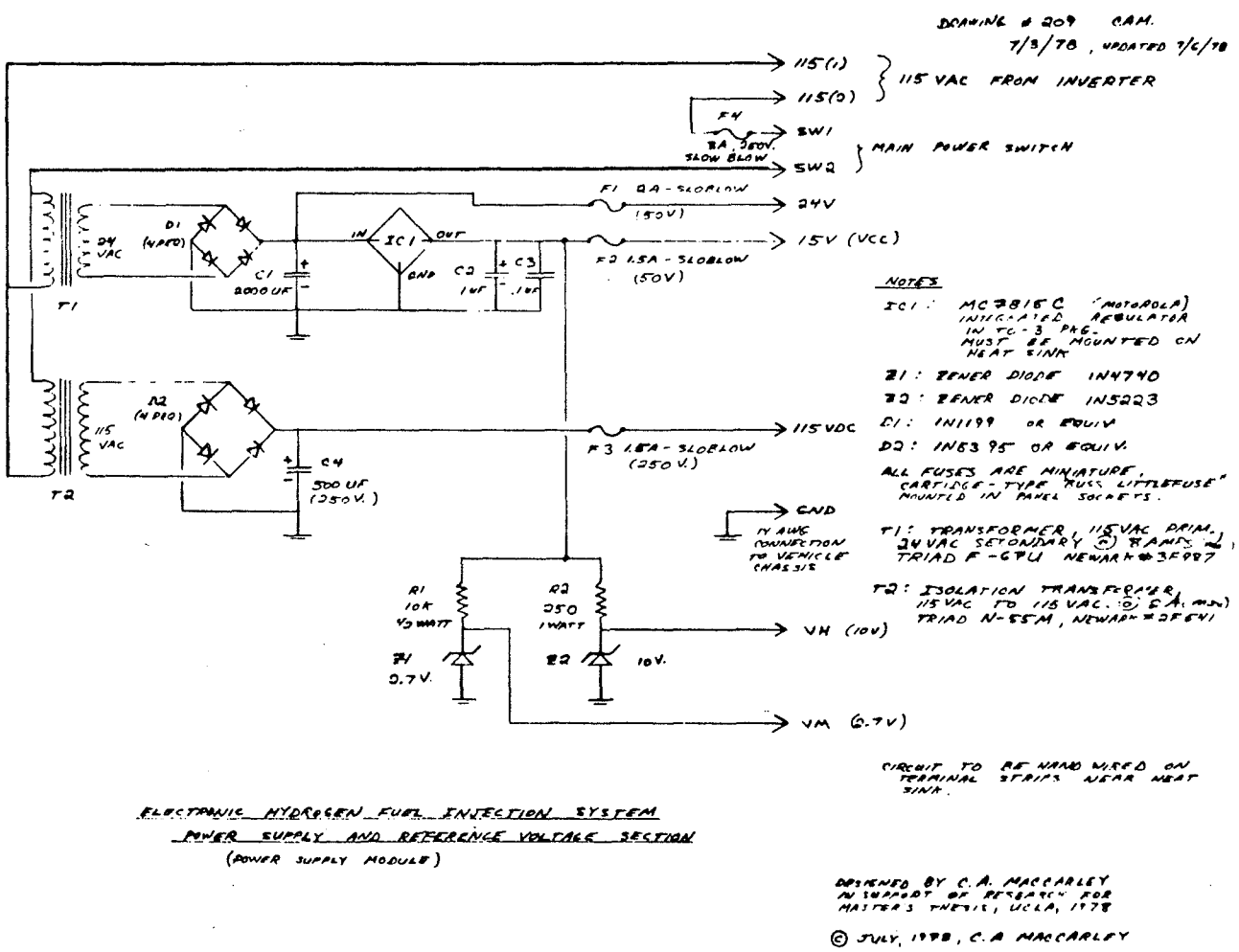

Figure 19. Injection Control Unit, Power Supply Schematic

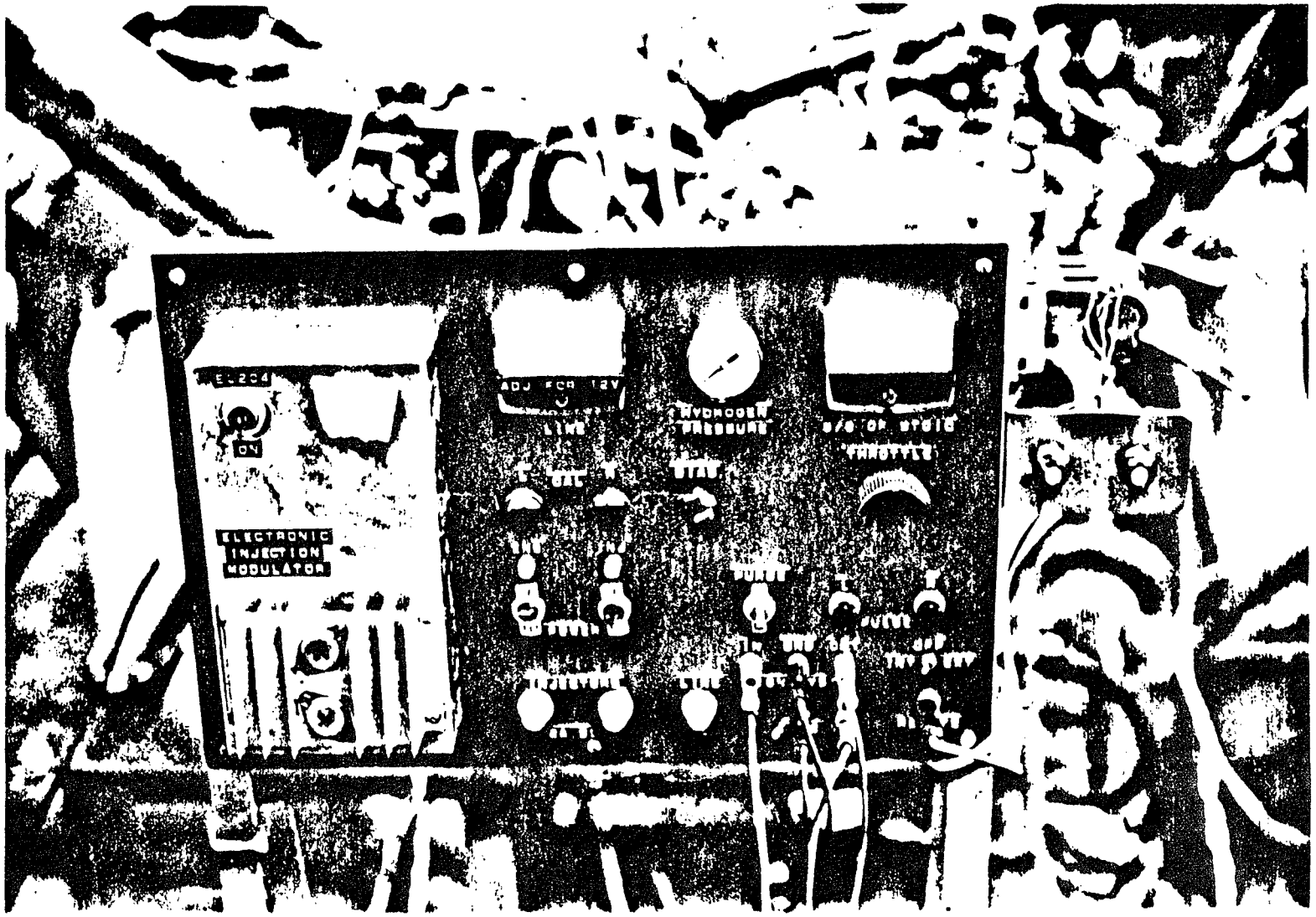

Figure 20. Electronic Injection Control Console for TX-650 Test Engine

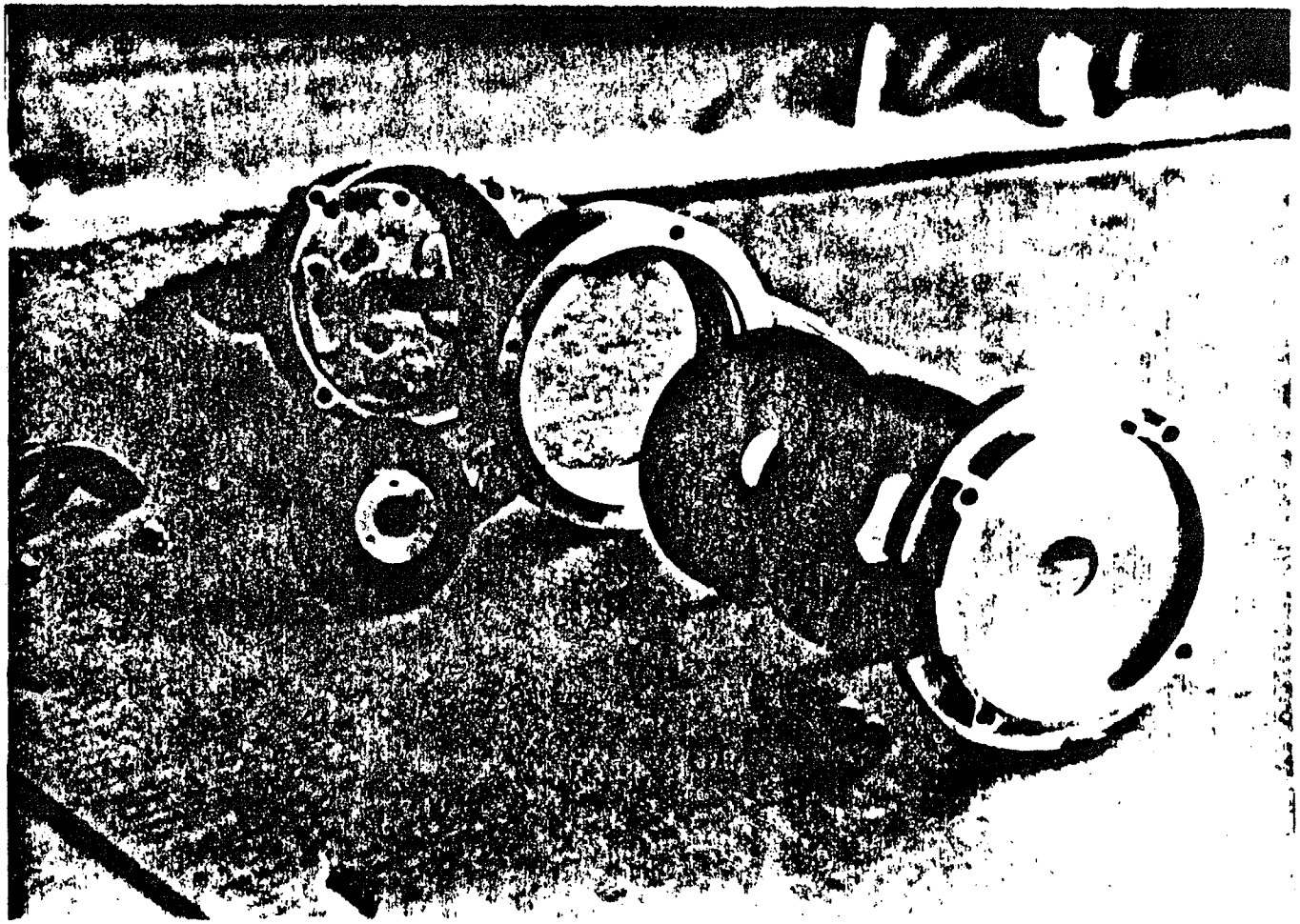

Figure 21. Distributor/Trigger Unit for Vehicle Injection System

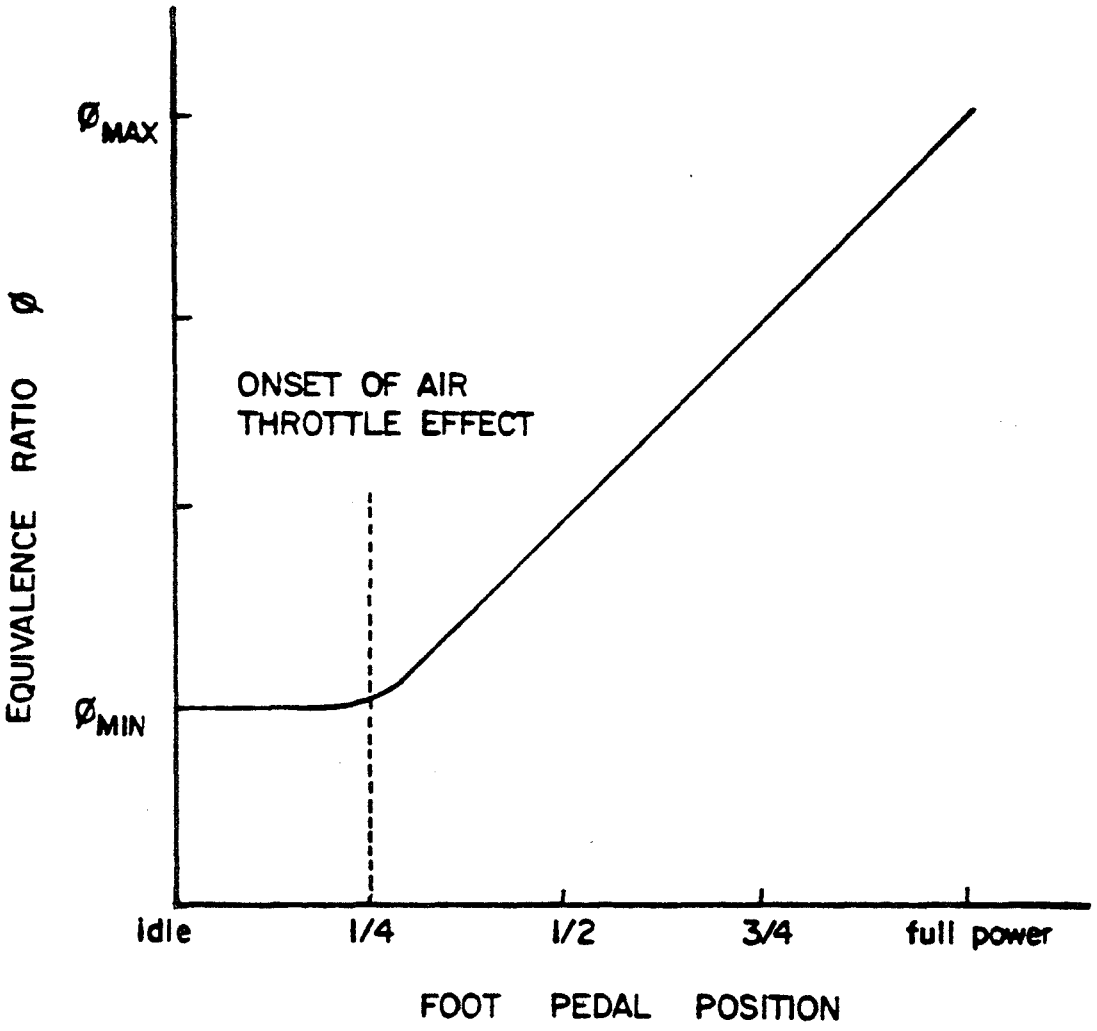

Figure 22. EQUIVALENCE RATIO vs PEDAL POSITION FOR THE AMC-232 SYSTEM

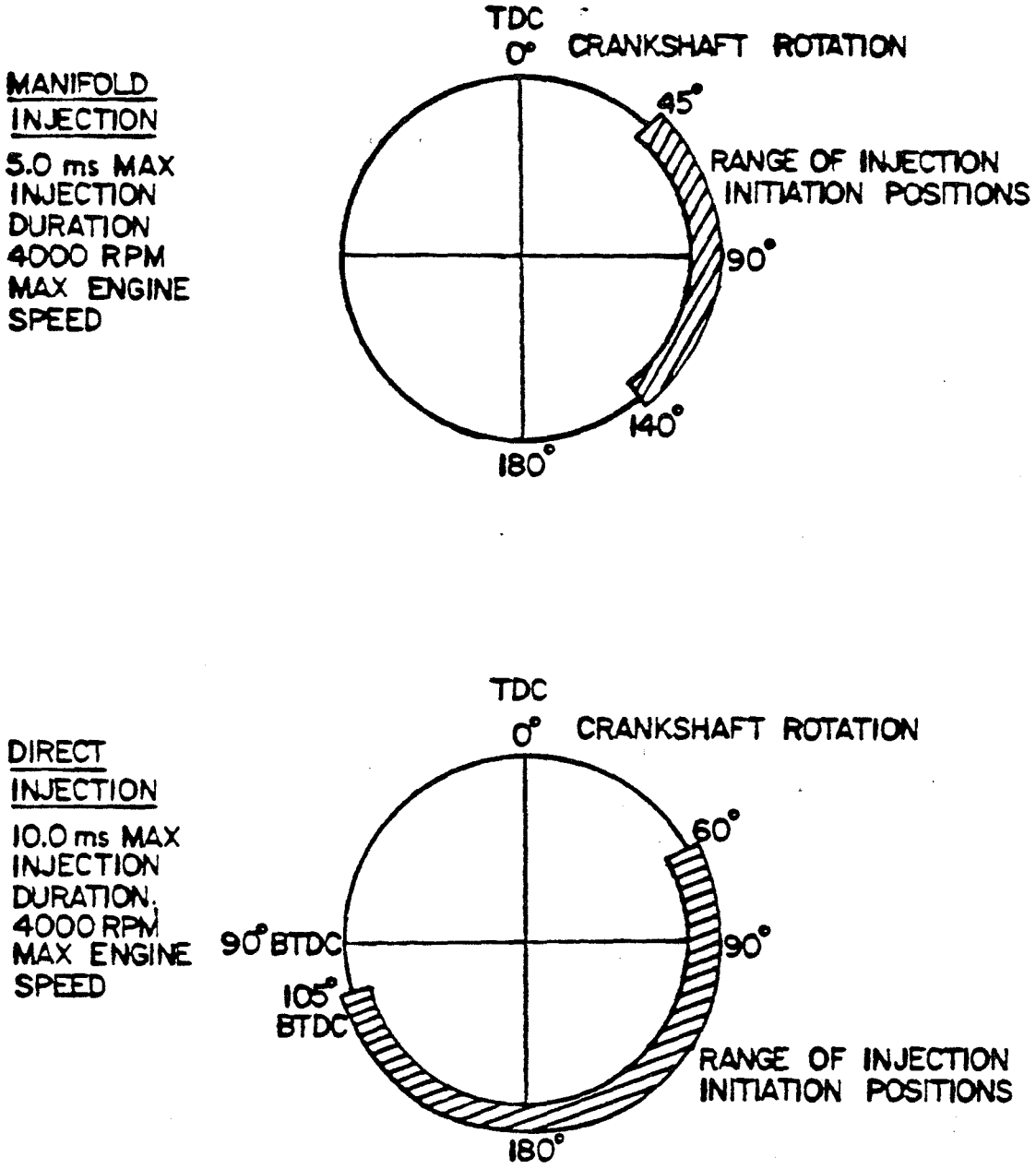

Figure 23. INJECTION TIMING POSITION RANGE FOR MANIFOLD OR DIRECT INJECTION, AMC 232 C.I.D. POWERPLANT

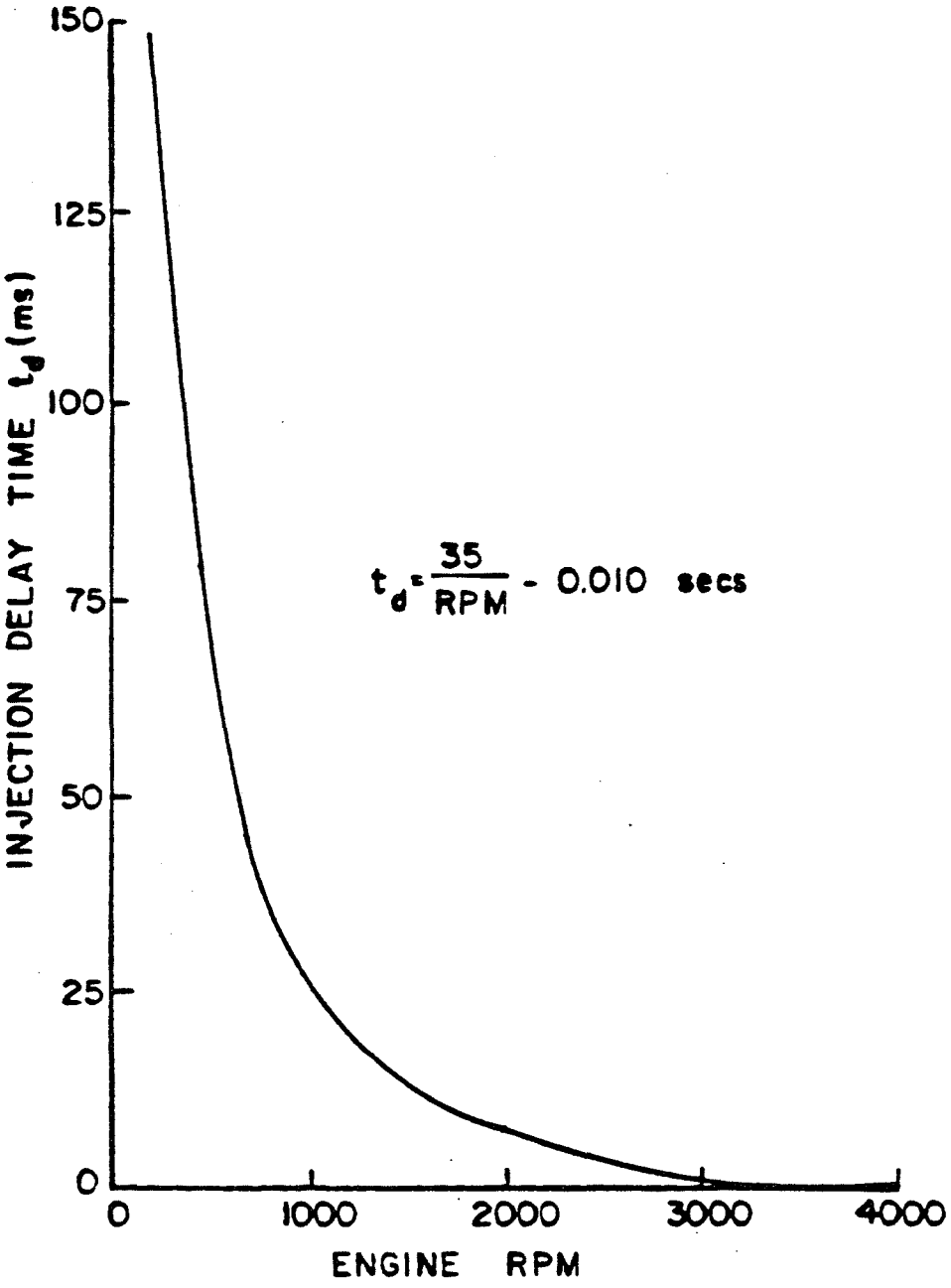

Figure 24. INJECTION TIME DELAY FUNCTION FOR DIRECT INJECTION APPLIED TO AMC 232 CID POWERPLANT

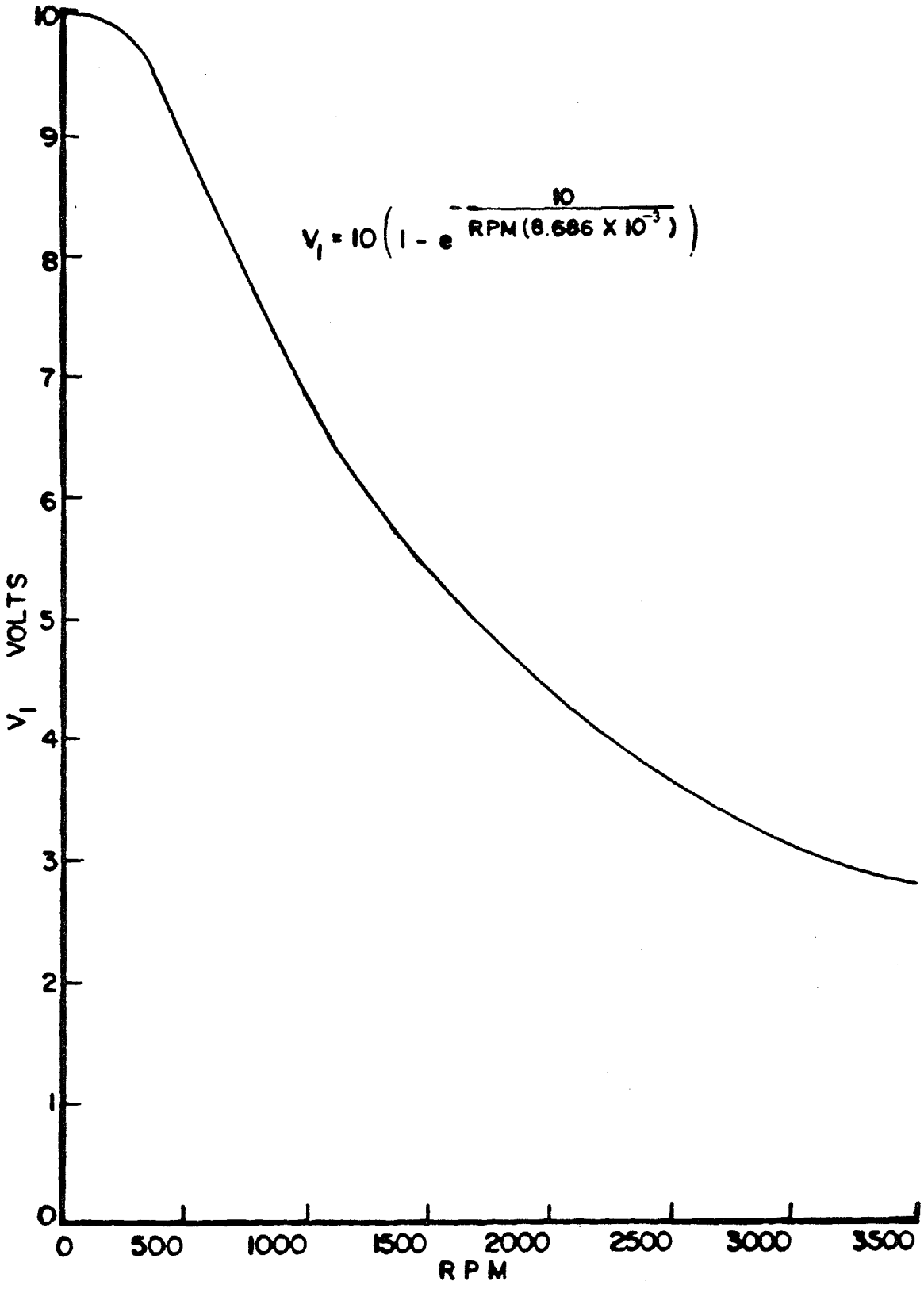

Figure 25. V_1 vs RPM

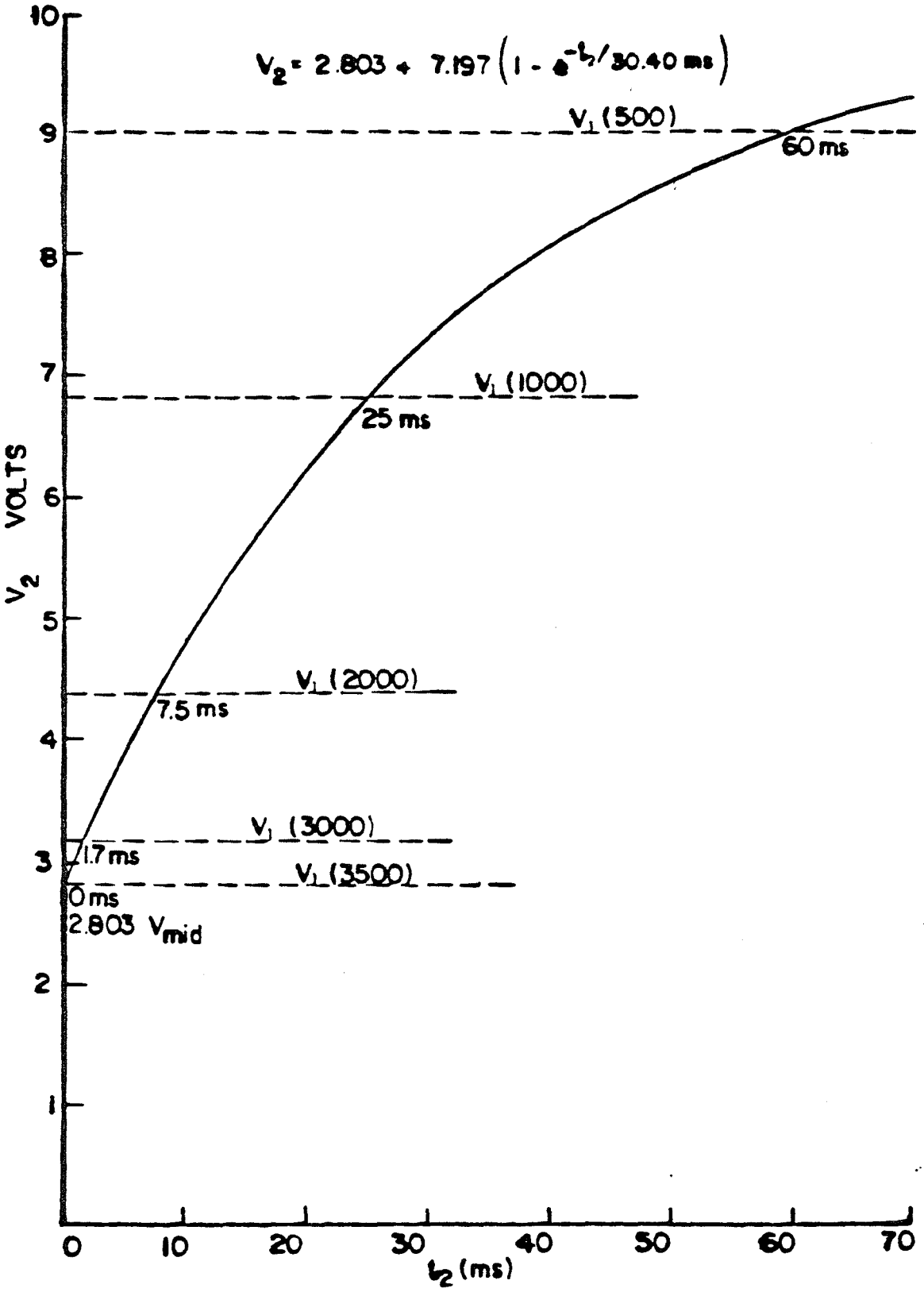

Figure 26. V_2 vs t_2 (with V_1 superimposed)

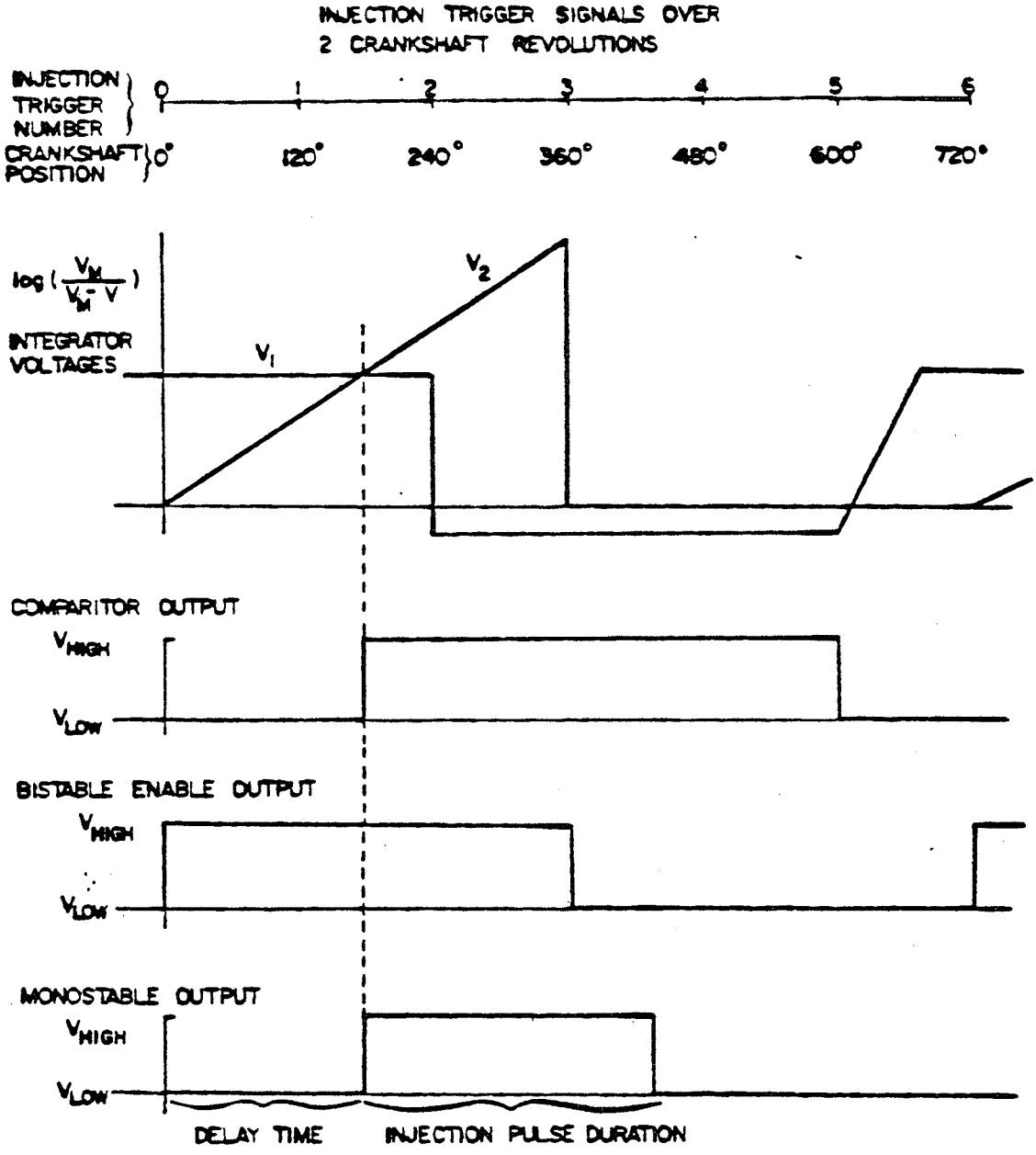

Figure 27. INJECTION TIMING AND PULSE DURATION COMPUTOR – DYNAMIC CIRCUIT VOLTAGES

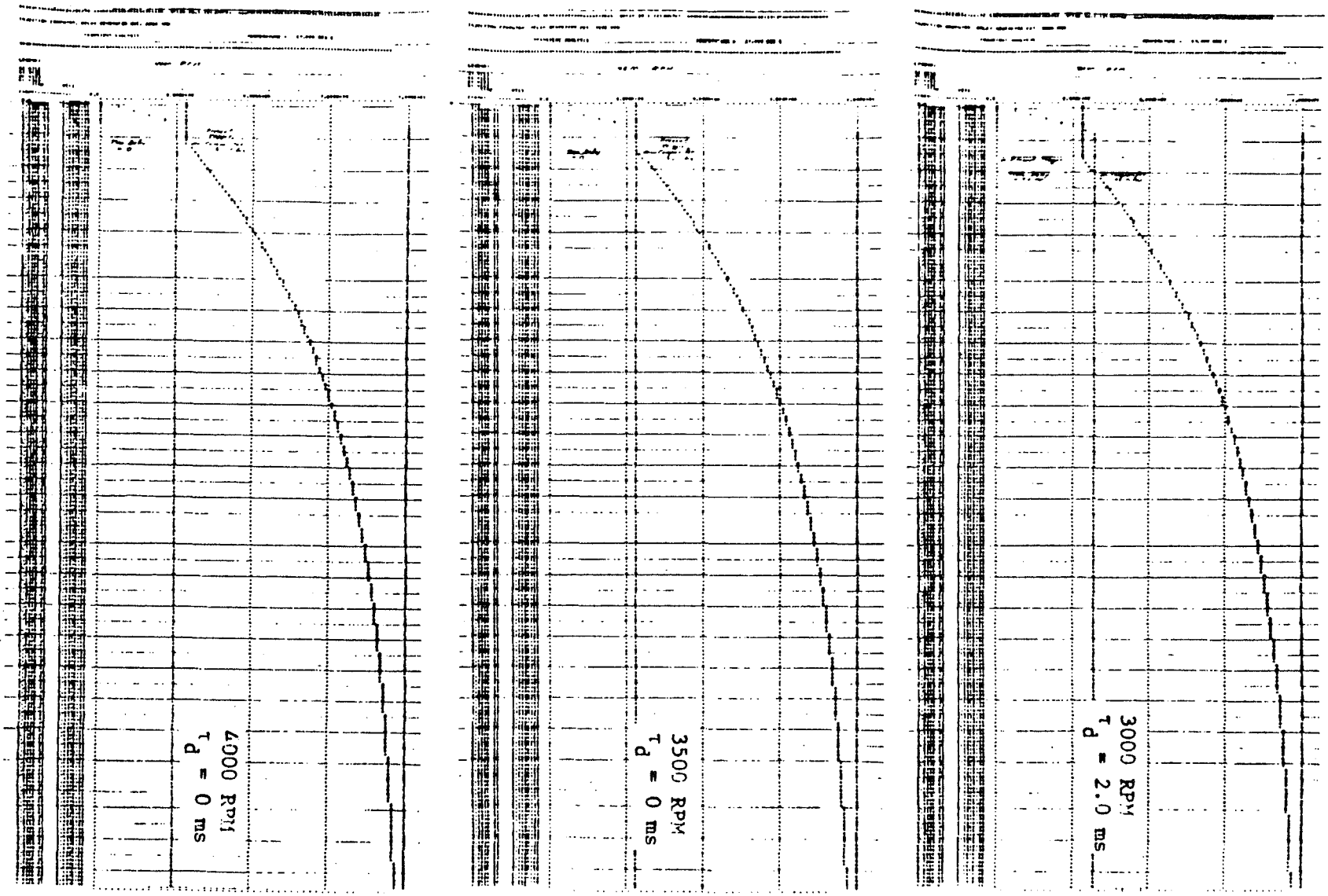

Figure 28b. Computer Simulation of Timing Function Generation Circuit (3000, 3500, 4000 RPM)

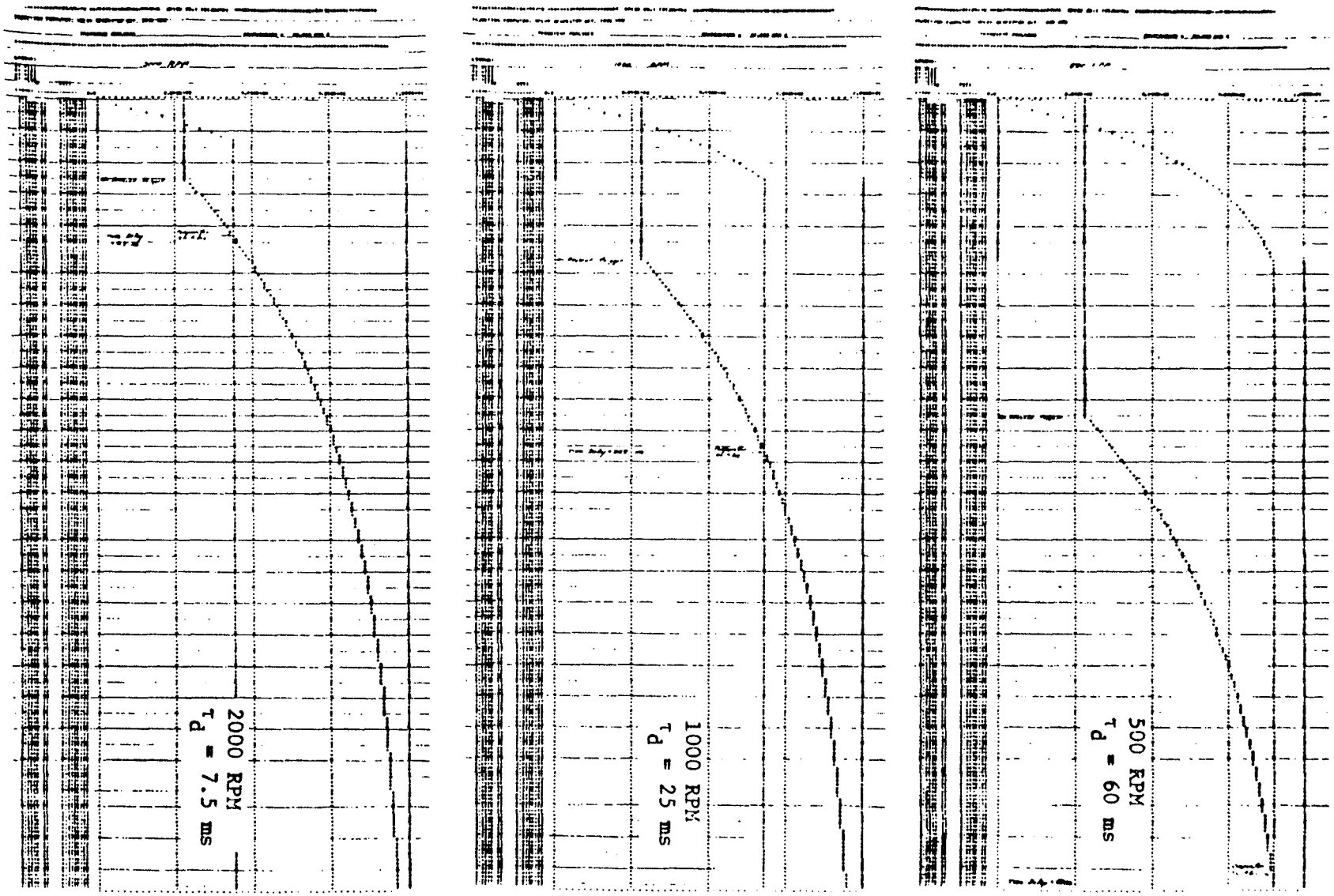

Figure 28a. Computer Simulation of Timing Function Generation Circuit (500, 1000, 2000 RPM)

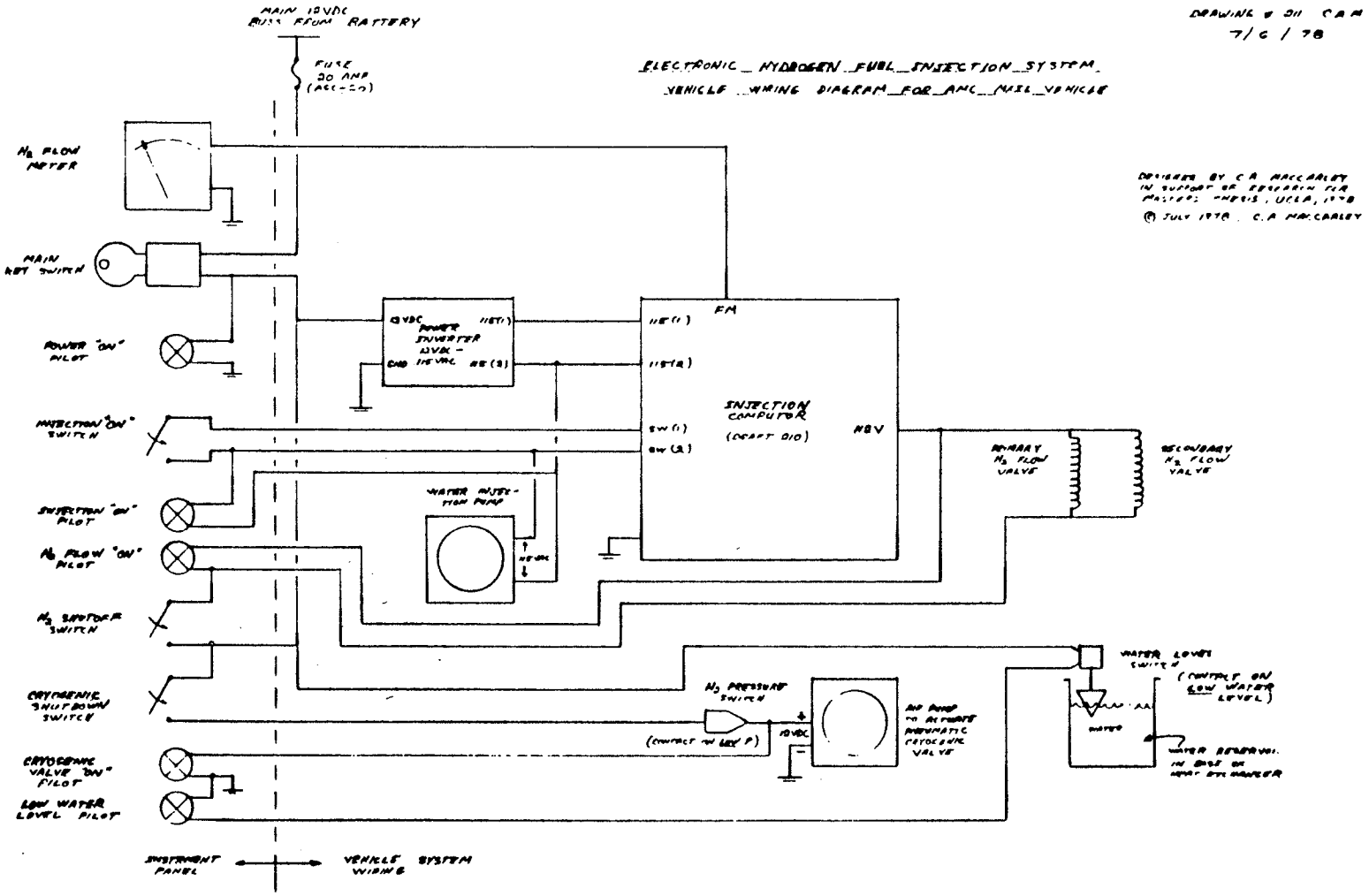

Figure 29. AMC Test Vehicle, Main Wiring Diagram

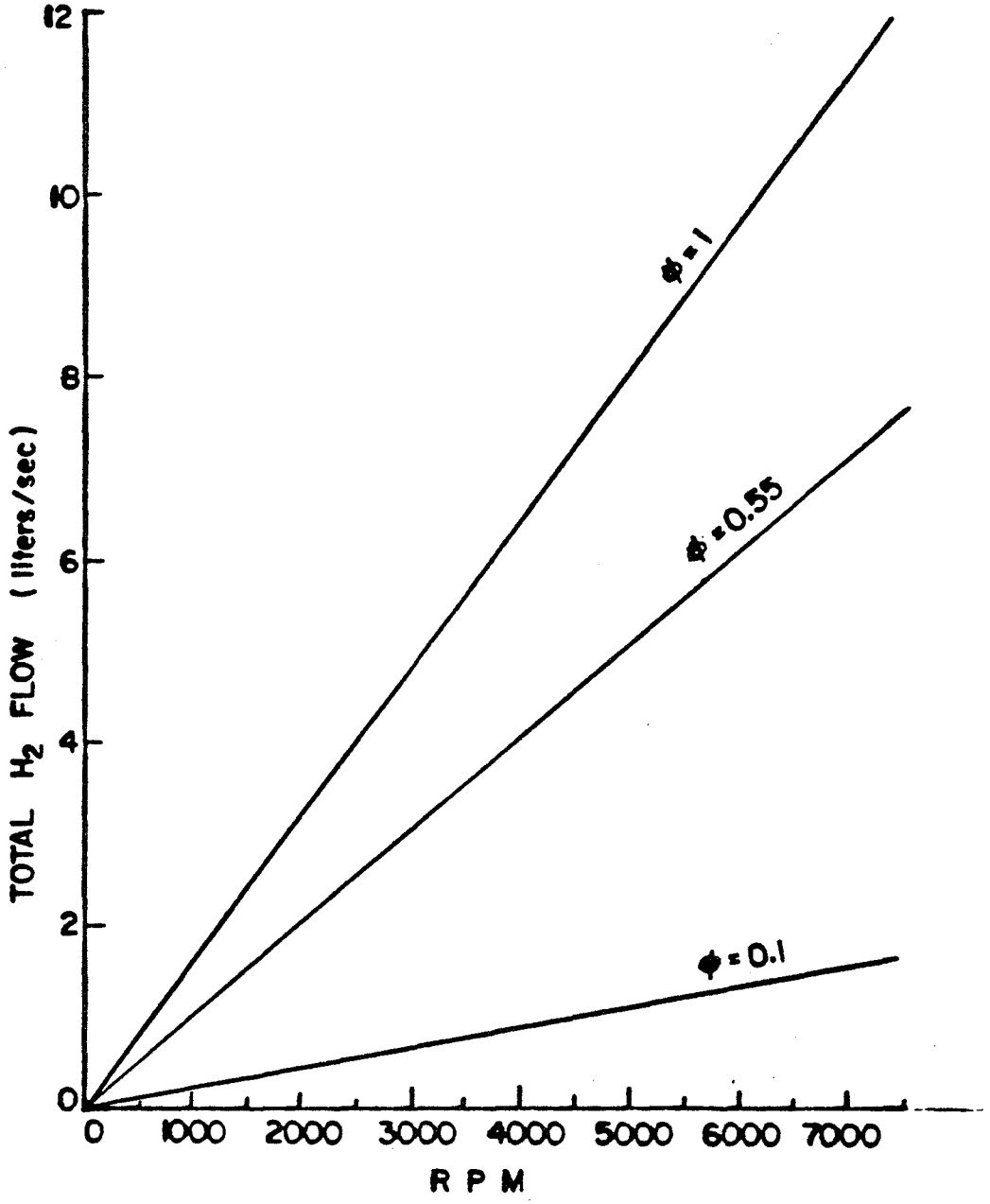

Figure 30. H_2 FLOW REQUIRED vs R P M
(653cc 2 cylinder engine, quality governing used; volumetic efficiency assumed 100%)

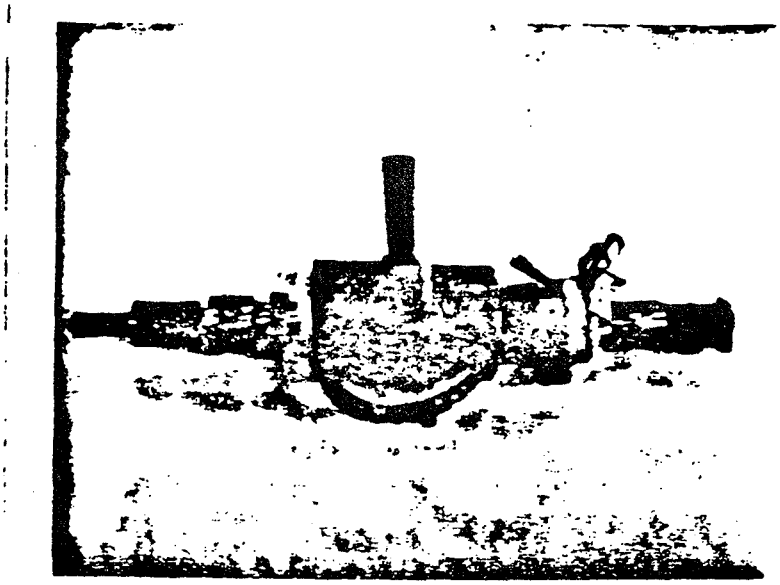

Figure 31. Fluidamp Injector

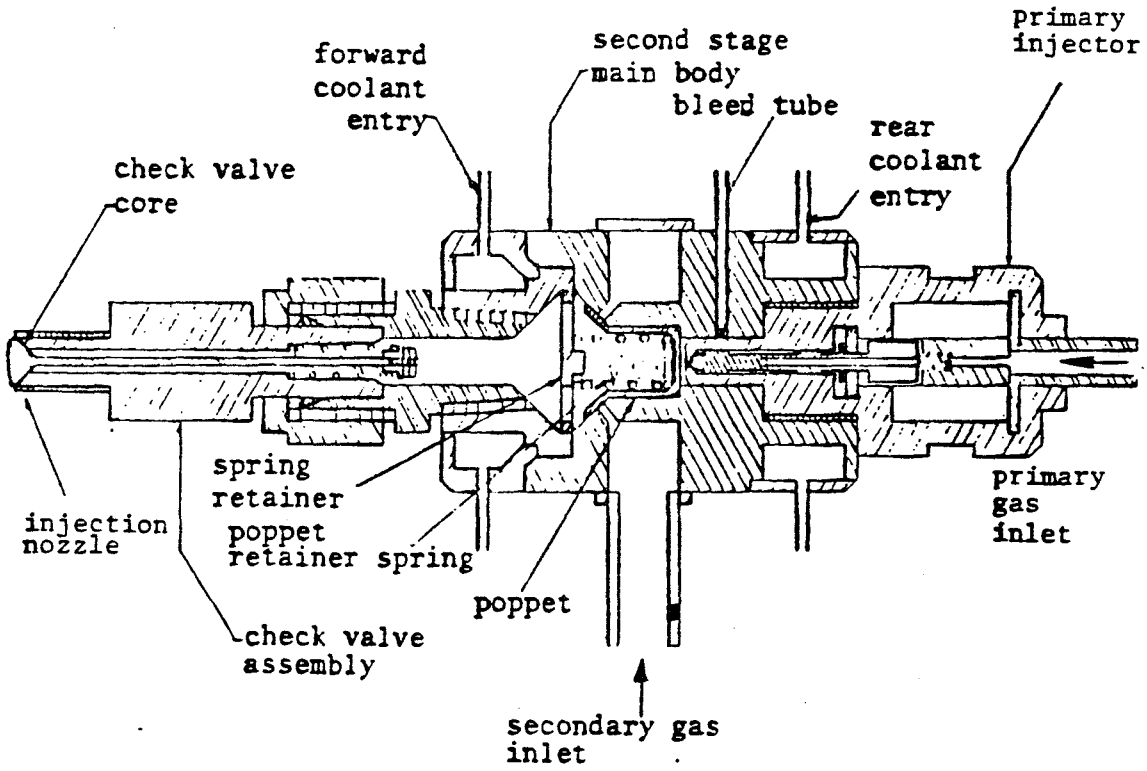

Figure 32. Comparative Flow Responses of Fluidamp Injector
Pulse Duration = 5 ms, p = 30 psig

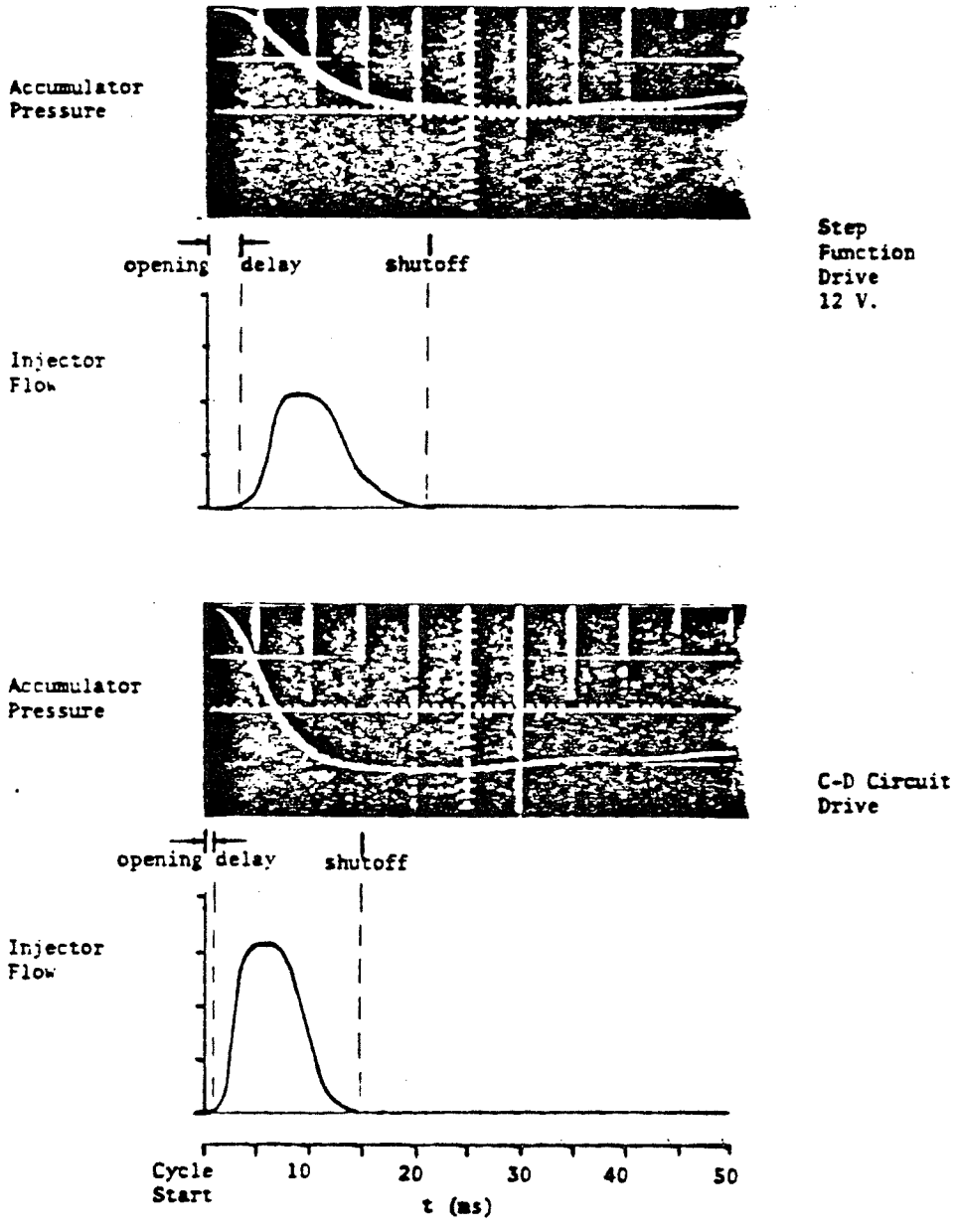

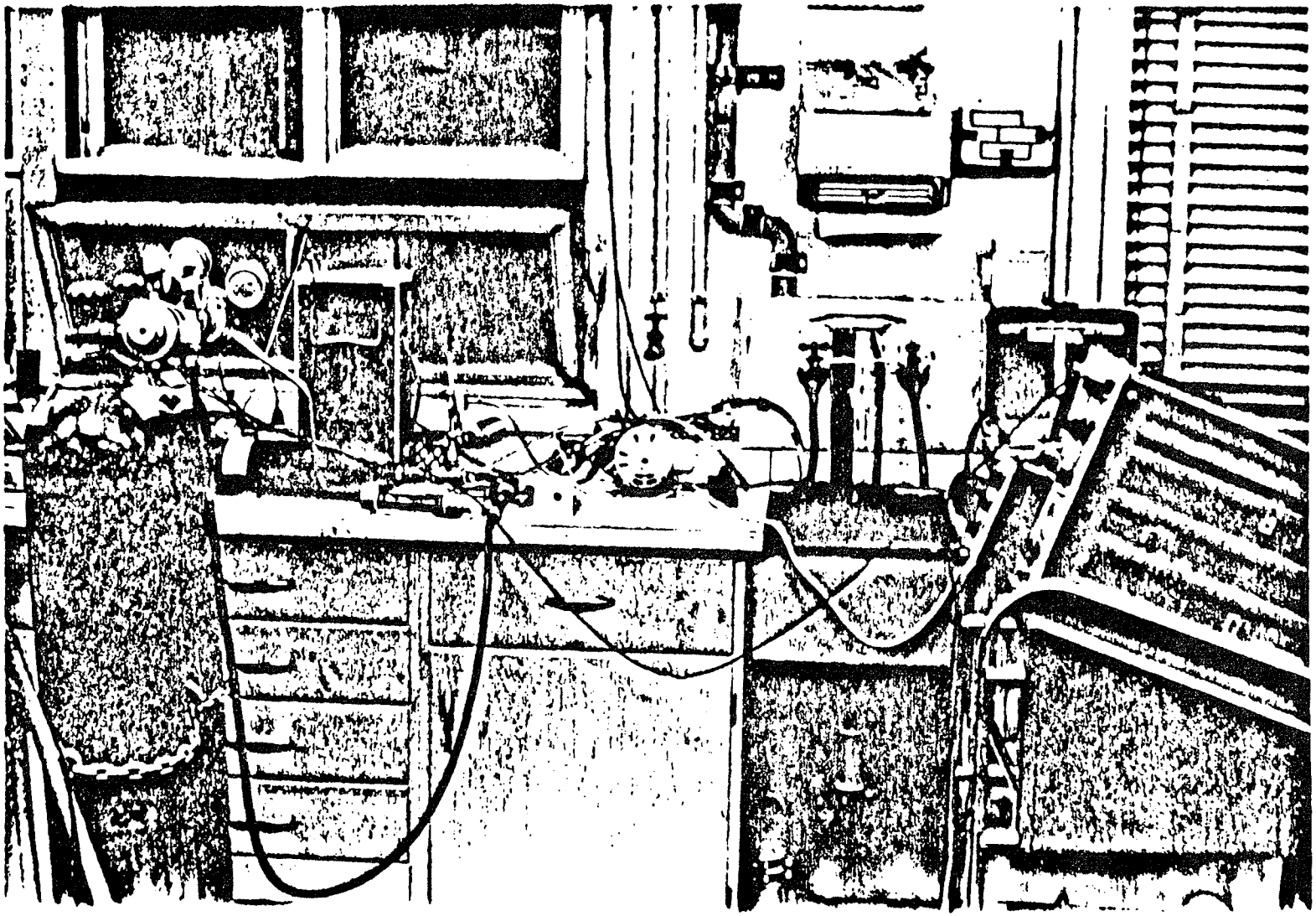

Figure 33. Experimental Apparatus for Injector Testing and Calibration

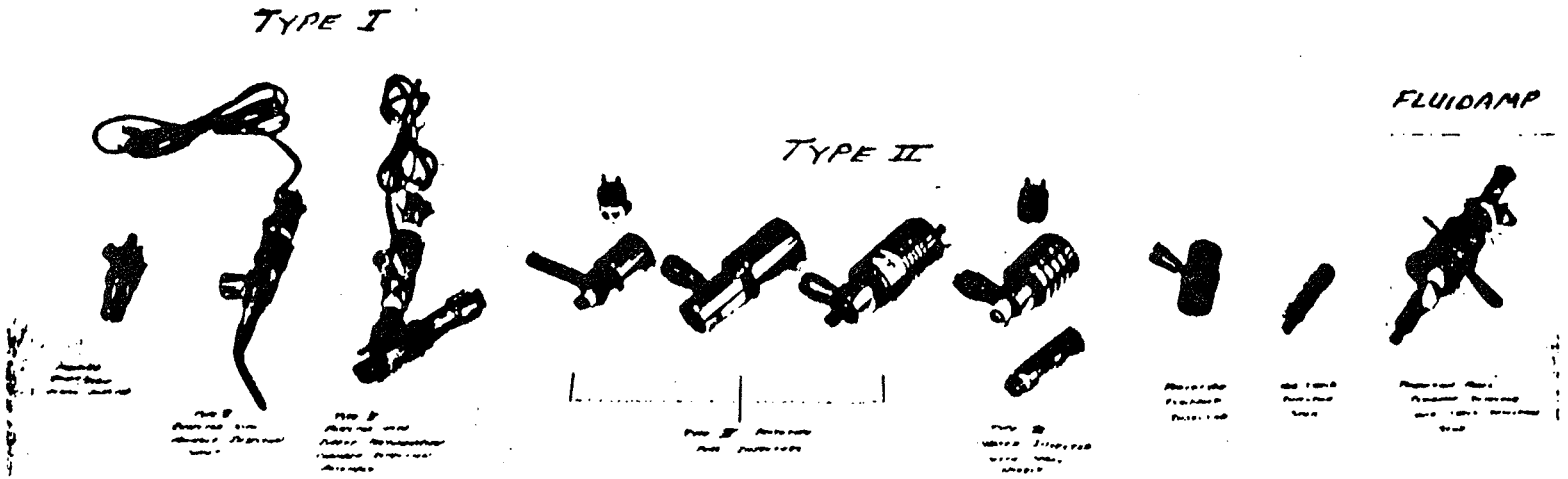

Figure 34. Electronic Fuel Injectors, Type I, Type II, and Fluidamp

Valve	t_{act} t_{open} (ms)	t_{act} t_{close} (ms)	C_v	Maximum Usable ΔP (psig)	Minimum Usable Pulse Duration (ms)	Volume Delivery, 5 ms pulse @ 30 psig cm^3, (Room T and P)
Solenoid Valve (Fluid Logic Type)	100	25	~1.5	~150	-	-
Bosch Petrol Injector Flowing Hydrogen, (ΔP=75 psig)	1.5	2.0	.011	95	1.5	2.6
Type I Hydrogen Injector	2.0	2.0	.280	45	2.0	70
Type II Hydrogen Injector	1.0	1.5	.466	50	1.0	110
Type II Water Injector (Hydrogen Flow)	0.5	0.8	.148	75	0.5	35
Fluidamp Hydrogen Injector (Stock electronics)	3.0	5.0	1.02	35*	1.0	380
Fluidamp Hydrogen Injector (CD electronics)	1.5	3.0	1.02	35*	0.3	240

*Primary pressure = 60 psig; can be increased by use of higher primary pressure.

Figure 35. Hydrogen Injection Valve Comparative Data

Figure 36. Ideal Coil Force Function and Coil Current Response of Injector Using Step Function Vs. C-D Drive

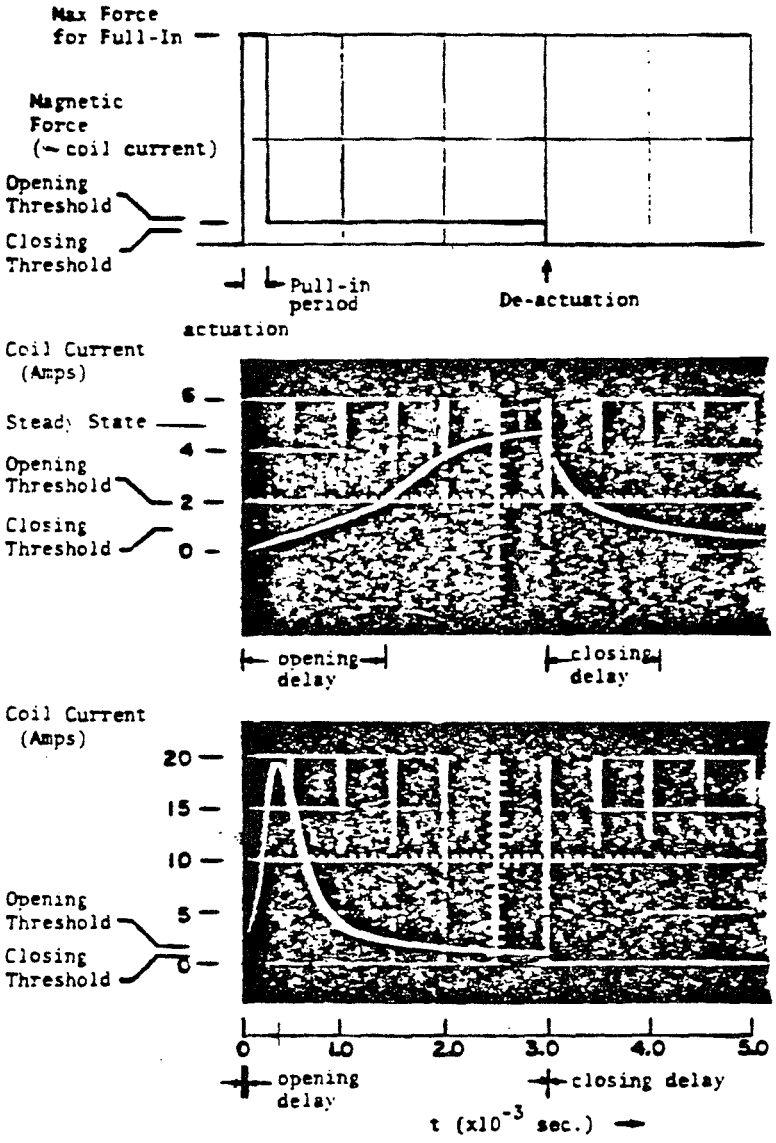

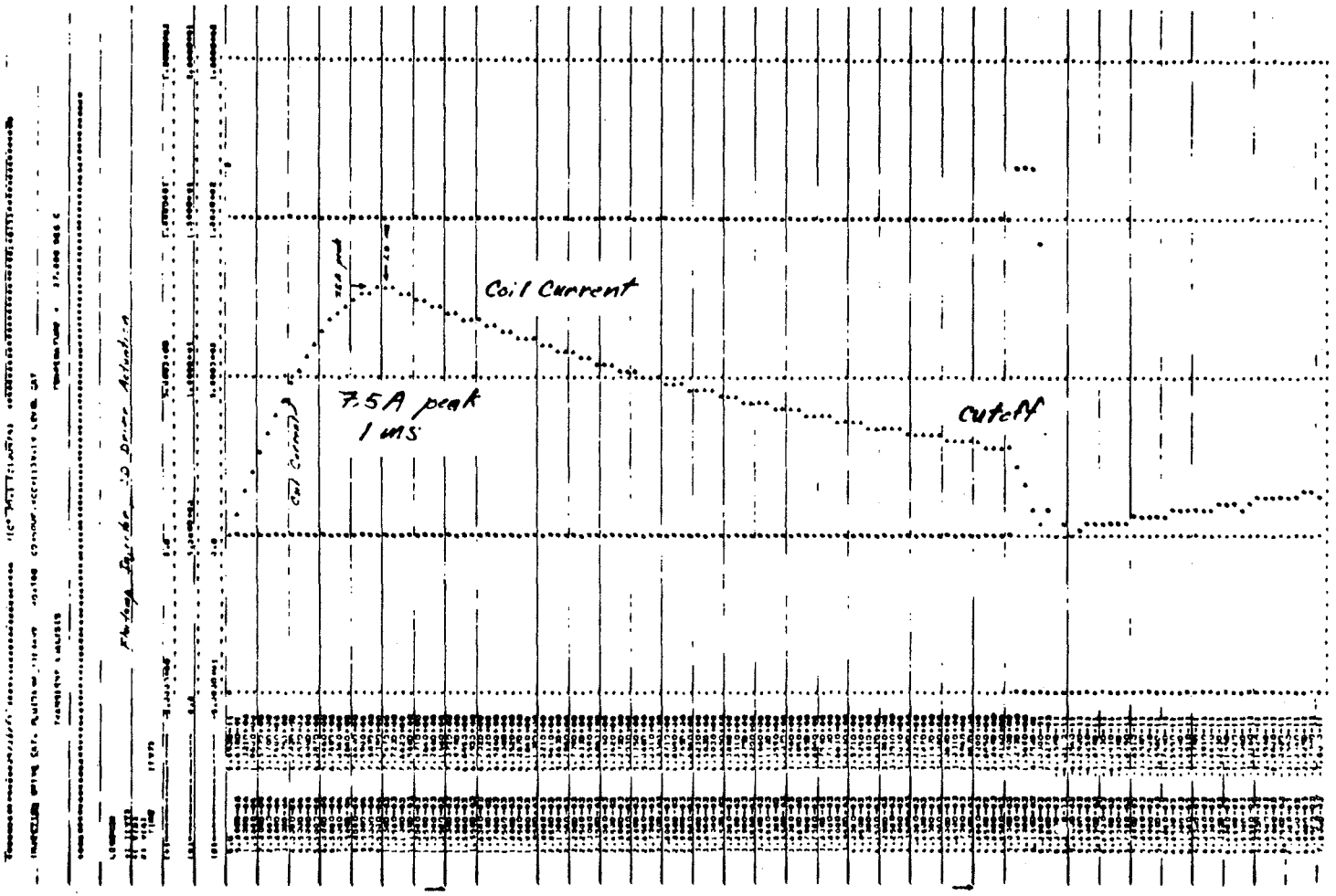

Figure 37. Computer Simulation of Type I Injector Coil Current Response to Actuation by C-D Drive Circuit

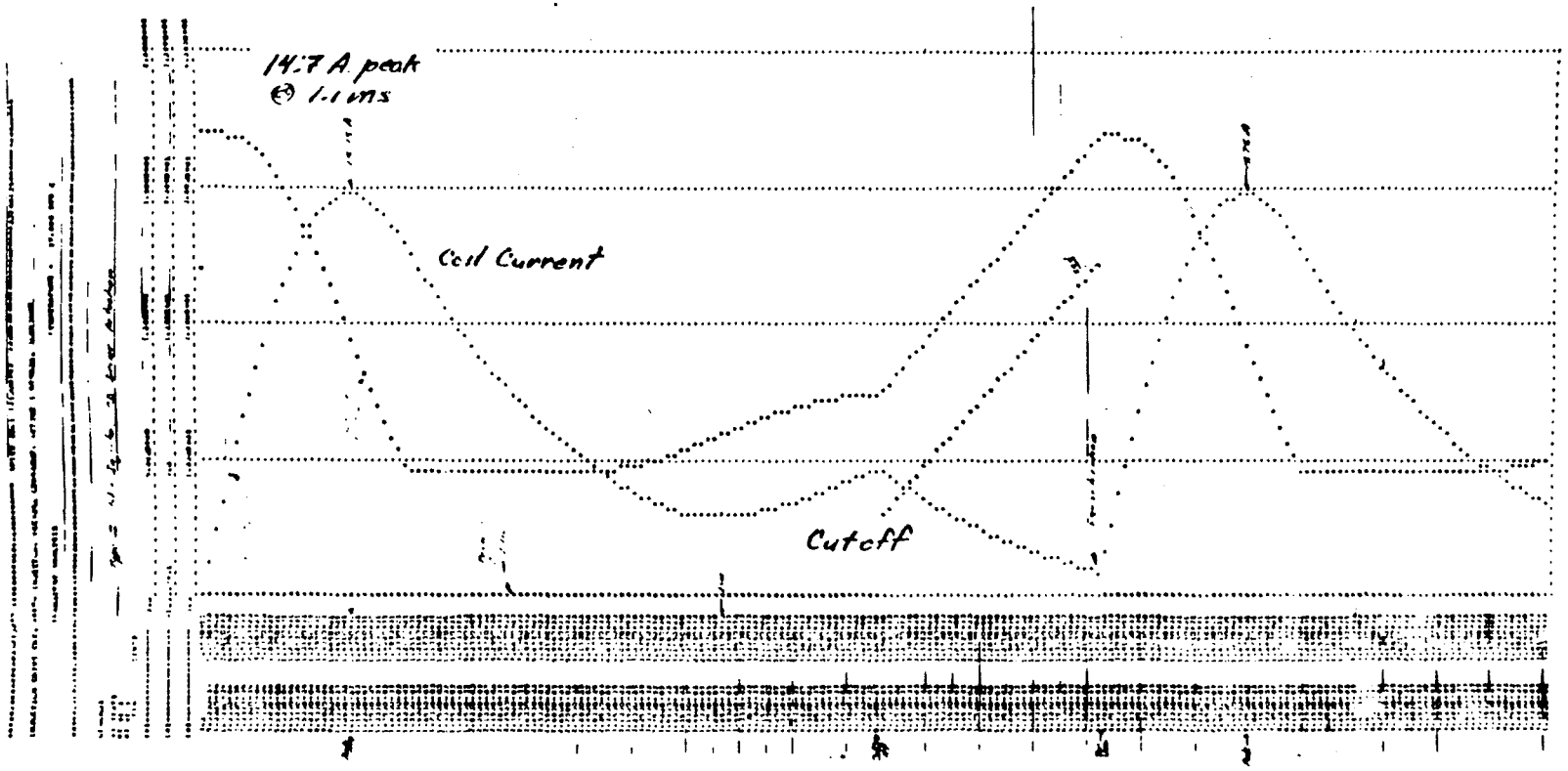

Figure 38. Computer Simulation of Type II Water Injector Coil Current Response to Actuation by C-D Drive Circuit

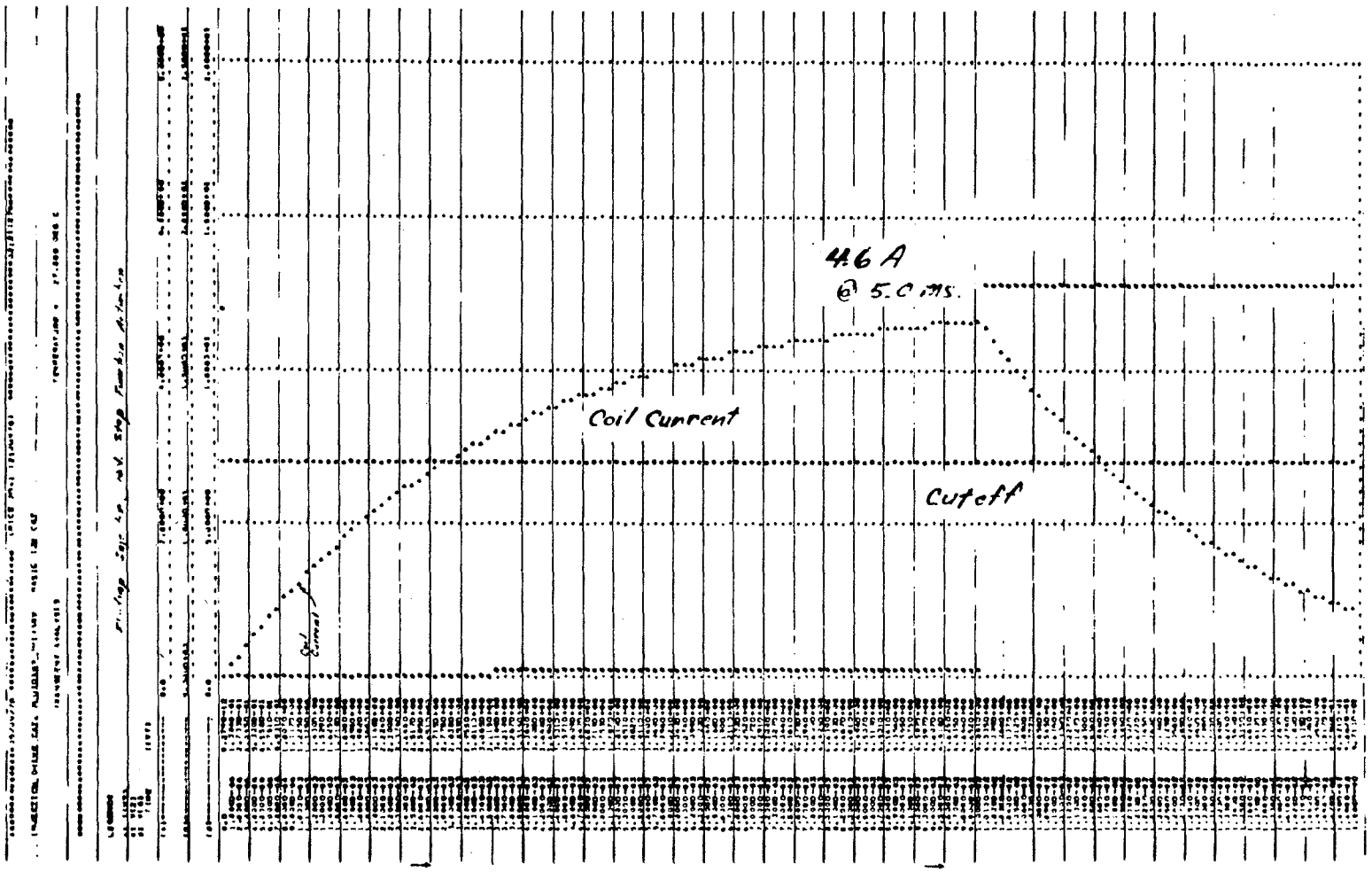

Figure 39. Computer Simulation of Type I Injector Coil Current Response to 12 Volt Step Function Actuation

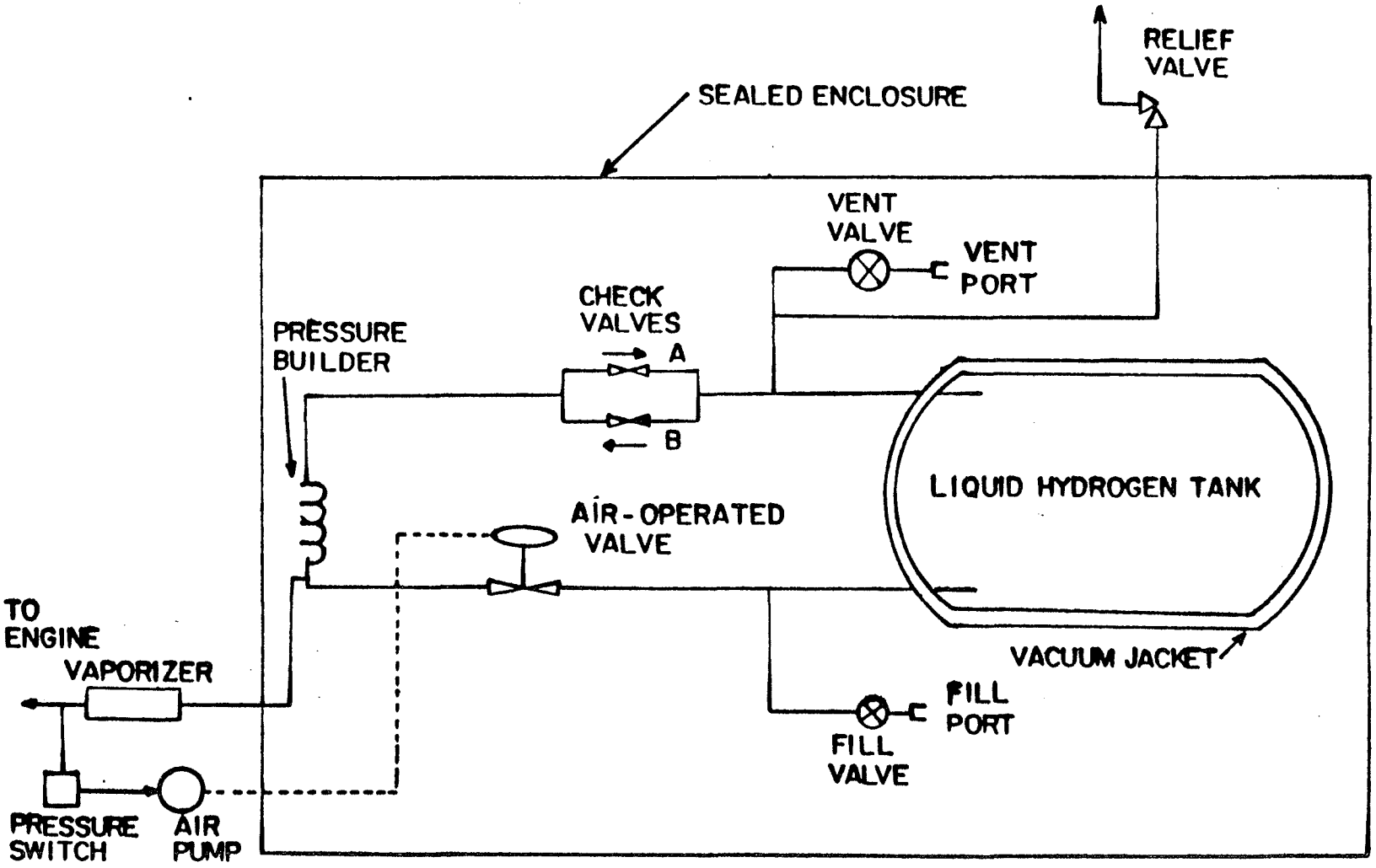

Figure 40. LH_2 FUEL-FLOW SYSTEM (DESIGNED BY N. BAKER, UCLA, 1977)

HYDROGEN CARBURETION DIAGRAM

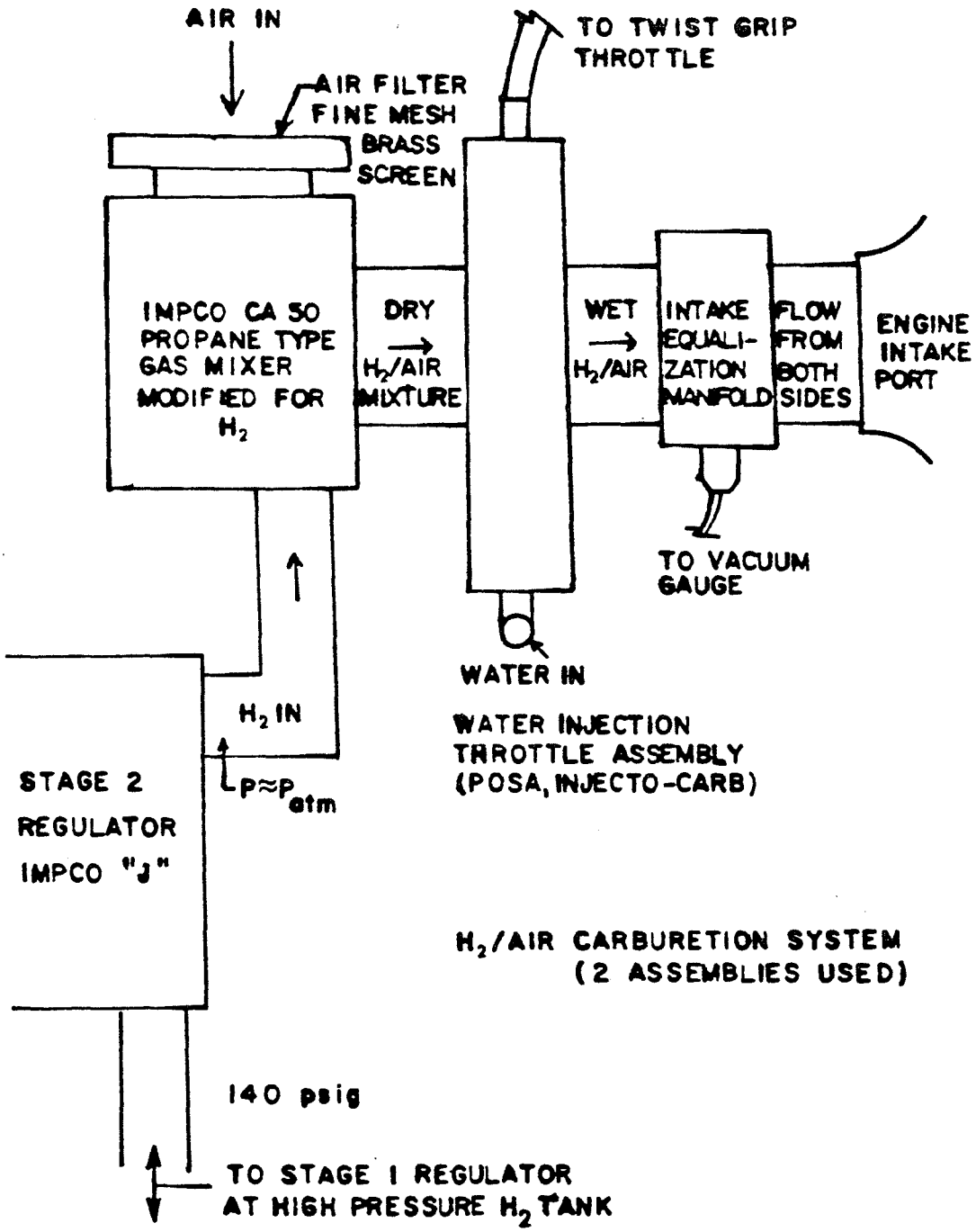

Figure 41.

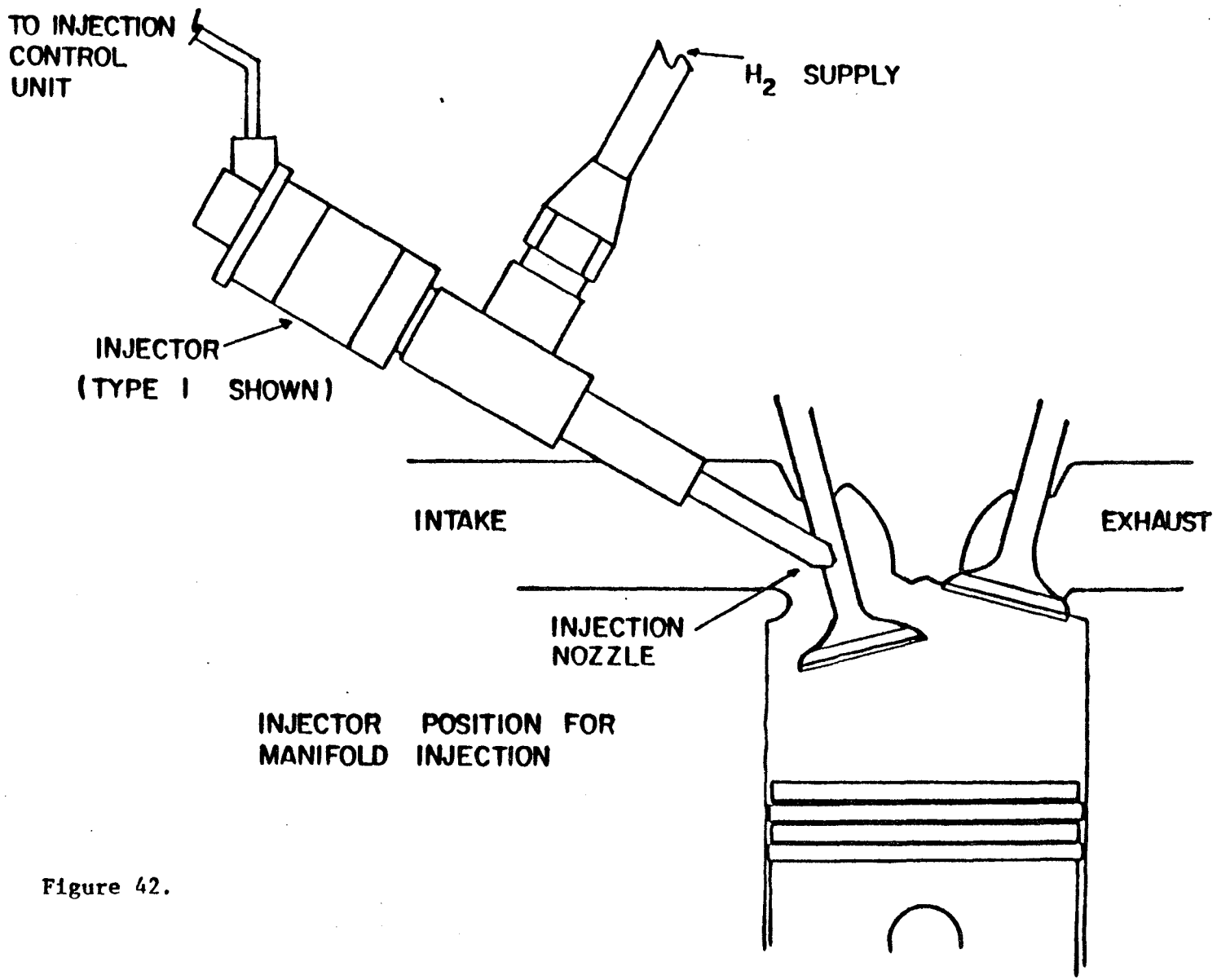
TO INJECTION CONTROL UNIT
H_2 SUPPLY
INJECTOR
(TYPE I SHOWN)
INTAKE
EXHAUST
INJECTION NOZZLE
INJECTOR POSITION FOR MANIFOLD INJECTION

Figure 42.

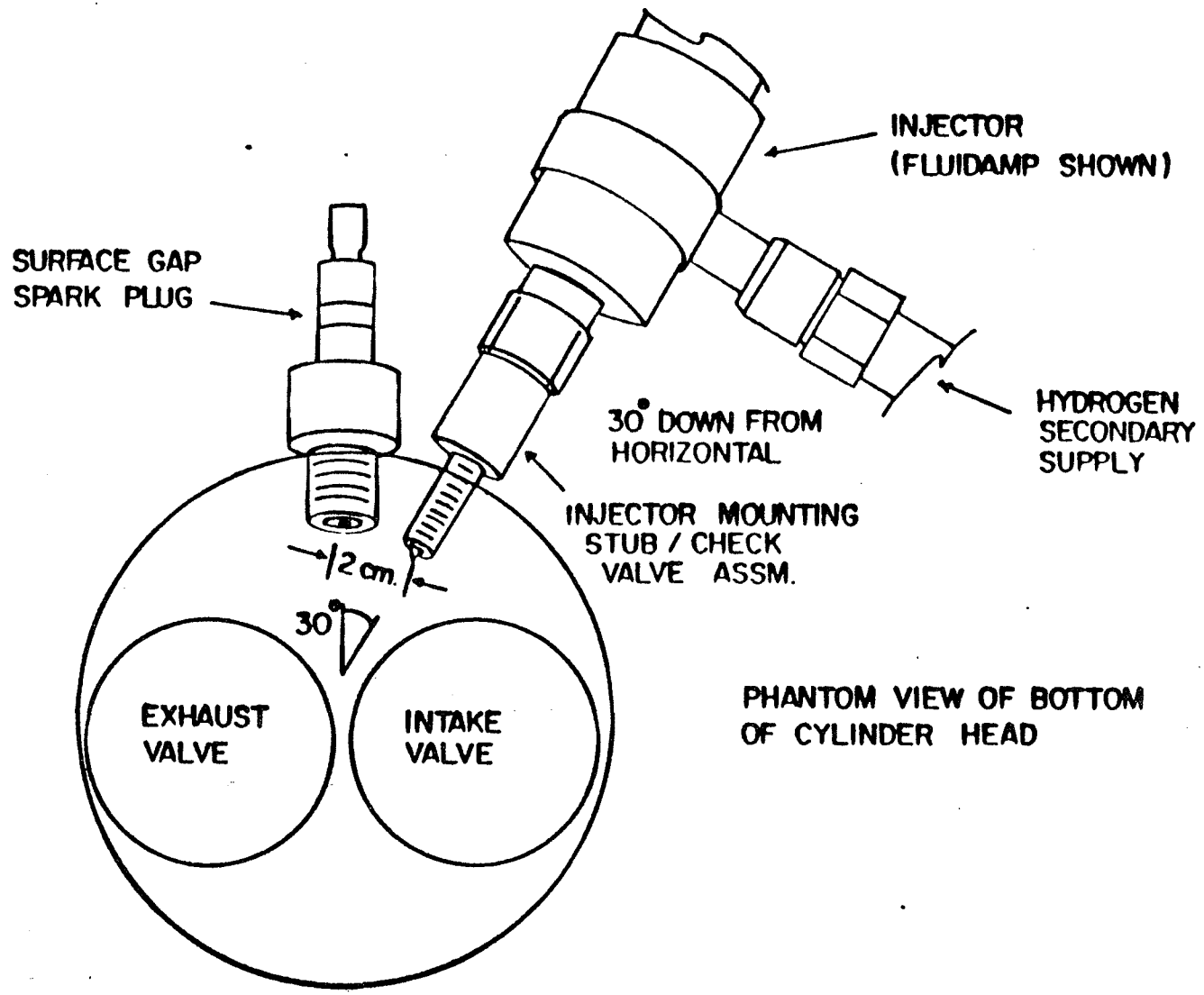

Figure 45a. INJECTOR POSITION FOR DIRECT INJECTION

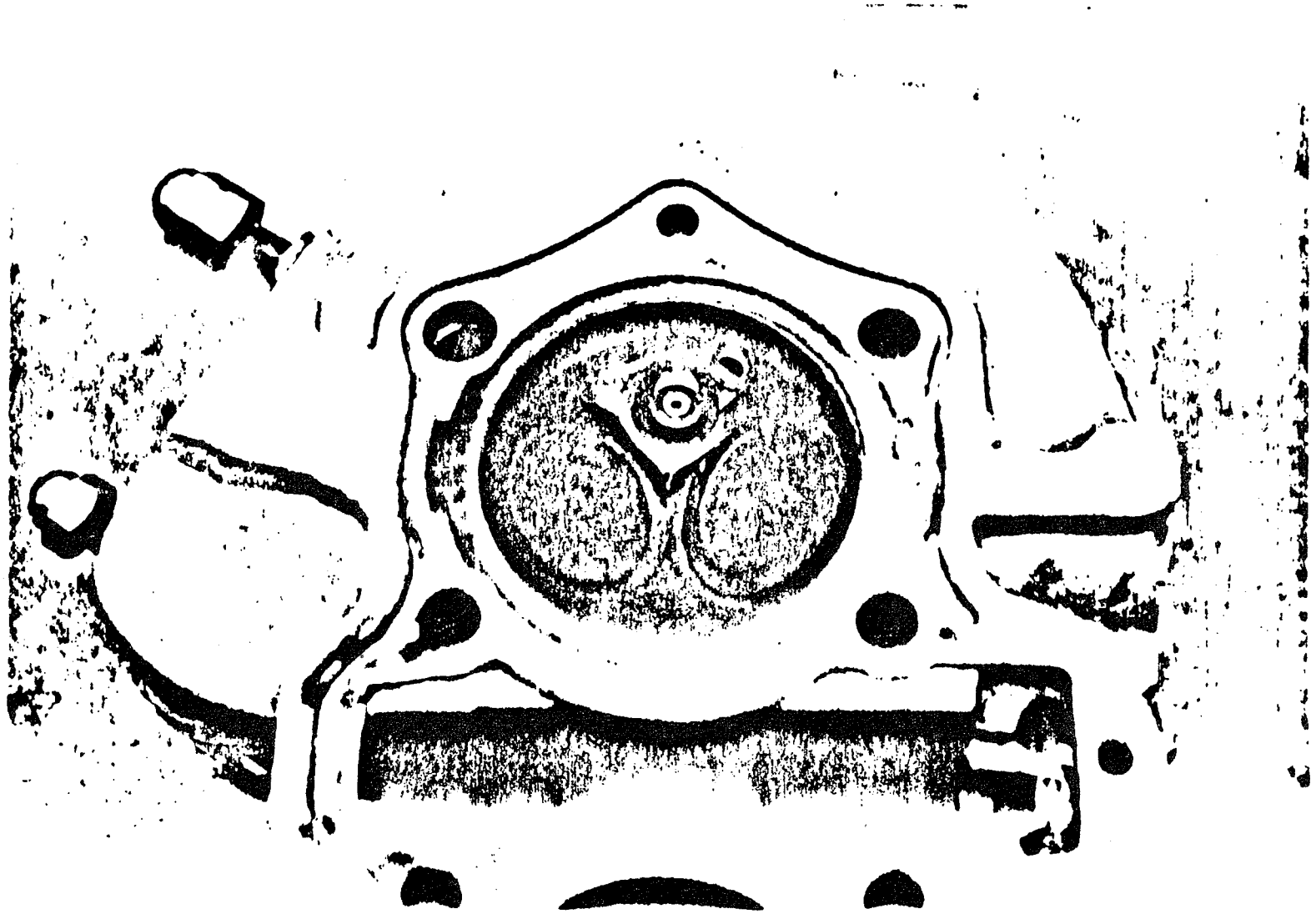

Figure 45b. Detail of Cylinder Head of TX-650 Test Engine Fitted for Direct Injection

Figure 46. Detail of Fluidamp Injector Position for Direct Injection Experiments

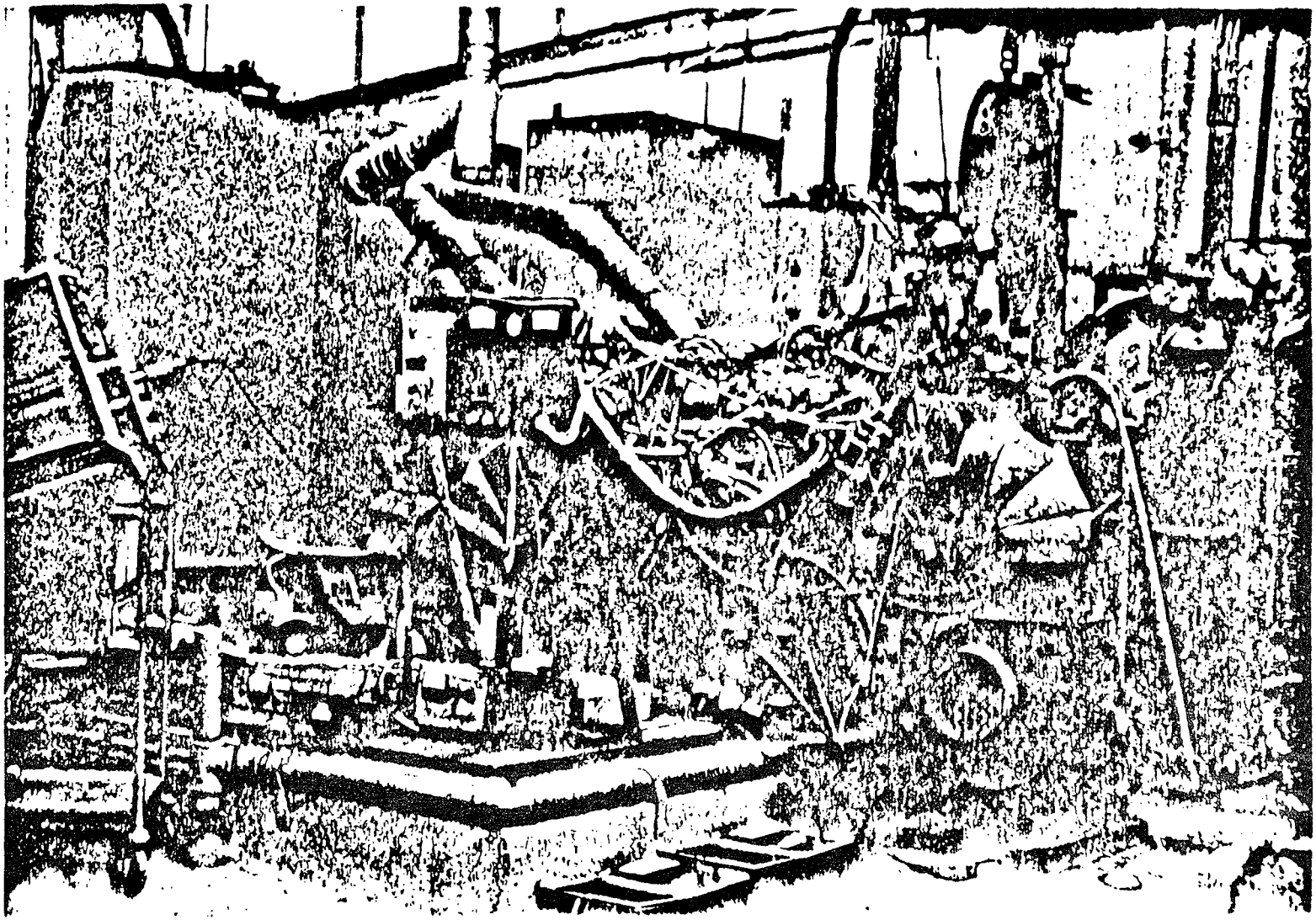

Figure 47. Experimental Apparatus: TX-650 Test Engine with Support Equipment

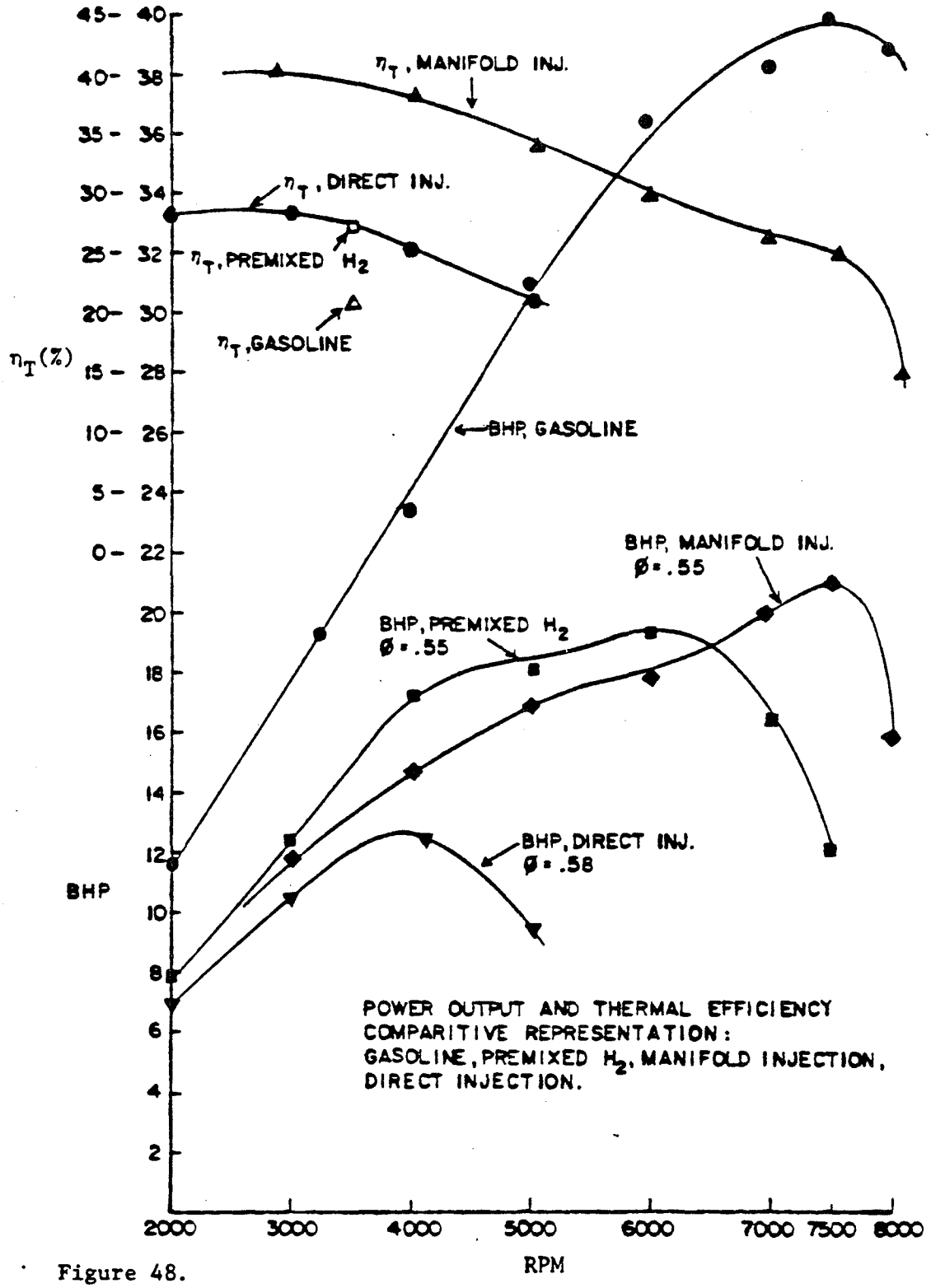
η_T, MANIFOLD INJ.
η_T, DIRECT INJ.
η_T, PREMIXED H_2
η_T, GASOLINE
η_T(%)
BHP, GASOLINE
BHP, MANIFOLD INJ.
Ø = .55
BHP, PREMIXED H_2
Ø = .55
BHP, DIRECT INJ.
Ø = .58
BHP
POWER OUTPUT AND THERMAL EFFICIENCY
COMPARITIVE REPRESENTATION:
GASOLINE, PREMIXED H_2, MANIFOLD INJECTION,
DIRECT INJECTION.
RPM

Figure 48.

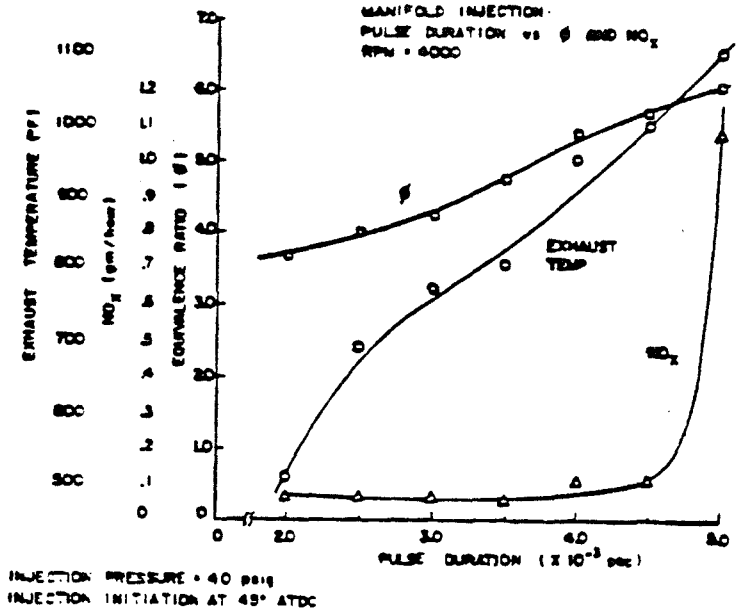

Figure 49.

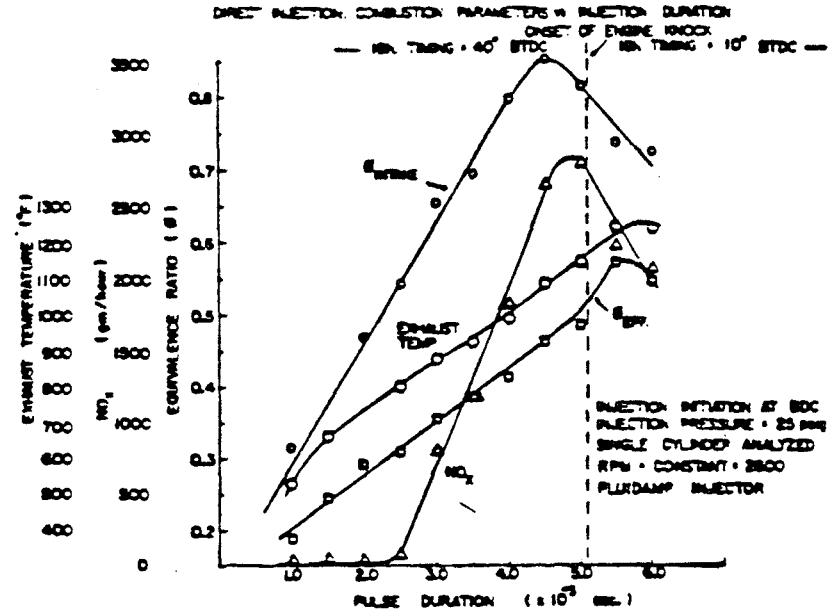

Figure 50.

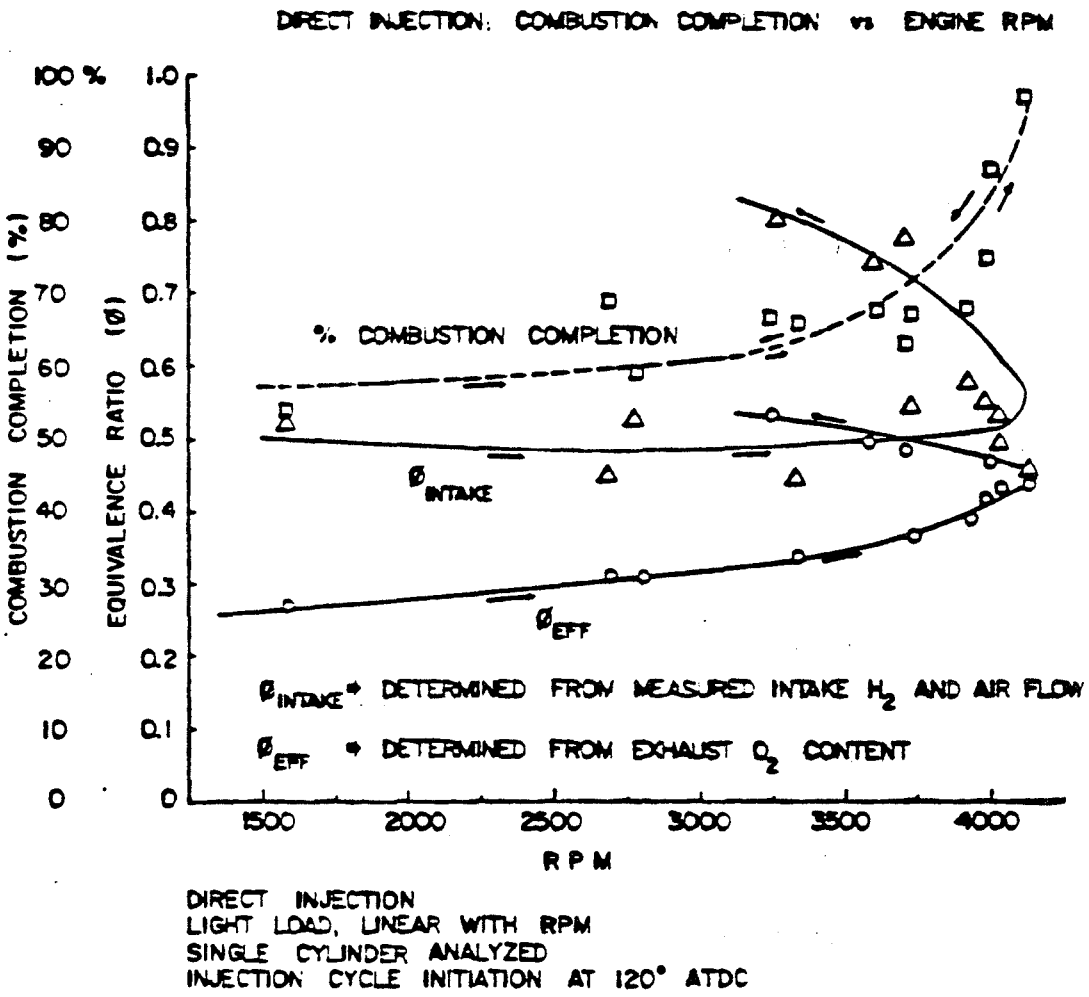
DIRECT INJECTION: COMBUSTION COMPLETION vs ENGINE RPM
COMBUSTION COMPLETION (%)
EQUIVALENCE RATIO (Ø)
100 %
90
80
70
60
50
40
30
20
10
0
1.0
0.9
0.8
0.7
0.6
0.5
0.4
0.3
0.2
0.1
0
% COMBUSTION COMPLETION
Ø INTAKE
Ø EFF
Ø INTAKE = DETERMINED FROM MEASURED INTAKE H2 AND AIR FLOW
Ø EFF = DETERMINED FROM EXHAUST O2 CONTENT
1500
2000
2500
3000
3500
4000
RPM
DIRECT INJECTION
LIGHT LOAD, LINEAR WITH RPM
SINGLE CYLINDER ANALYZED
INJECTION CYCLE INITIATION AT 120° ATDC

Figure 51.

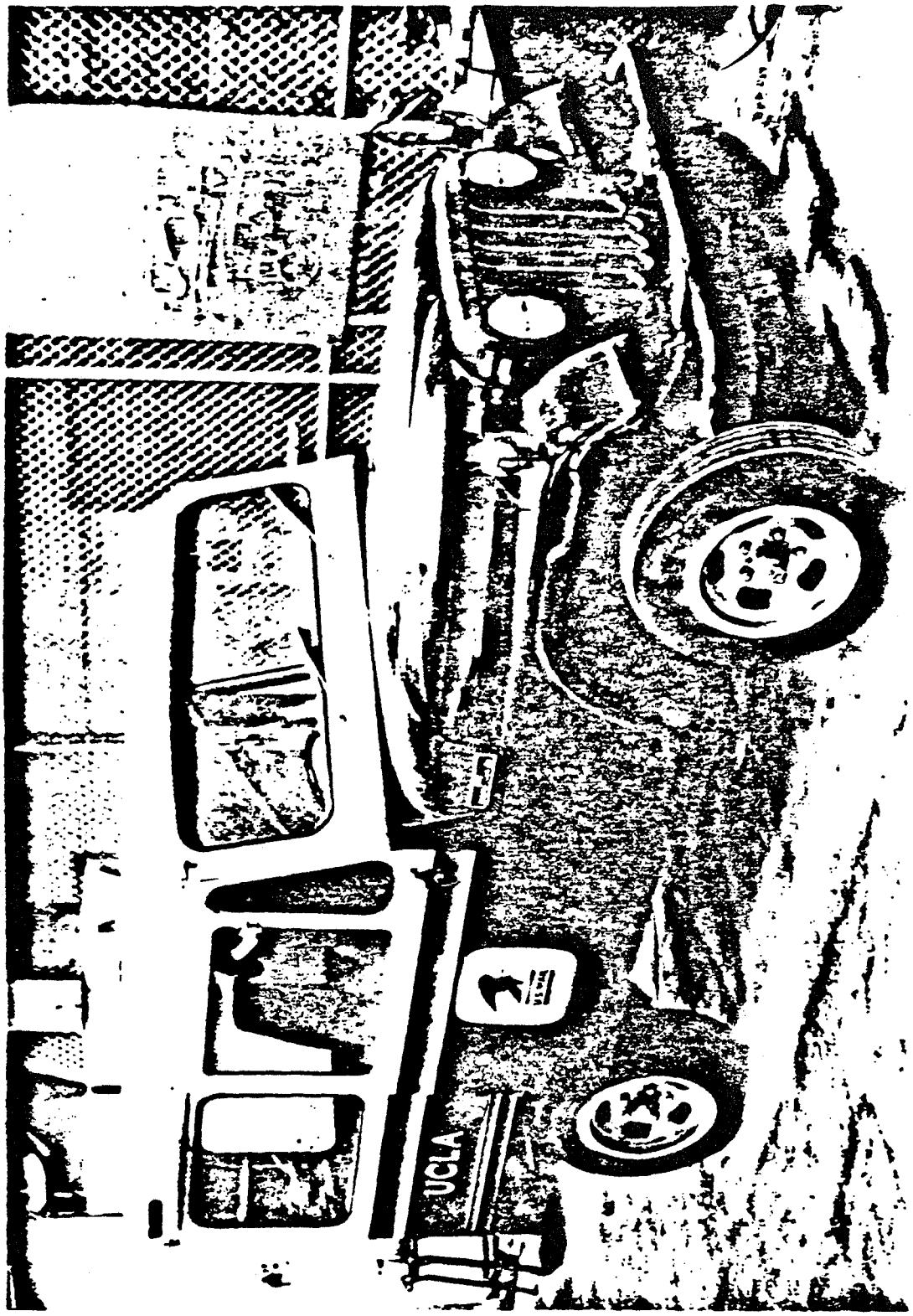

Figure 52. AMC Mail Service Vehicle

APPENDIX I

Mechanical Drawings of the Fluidamp Injector

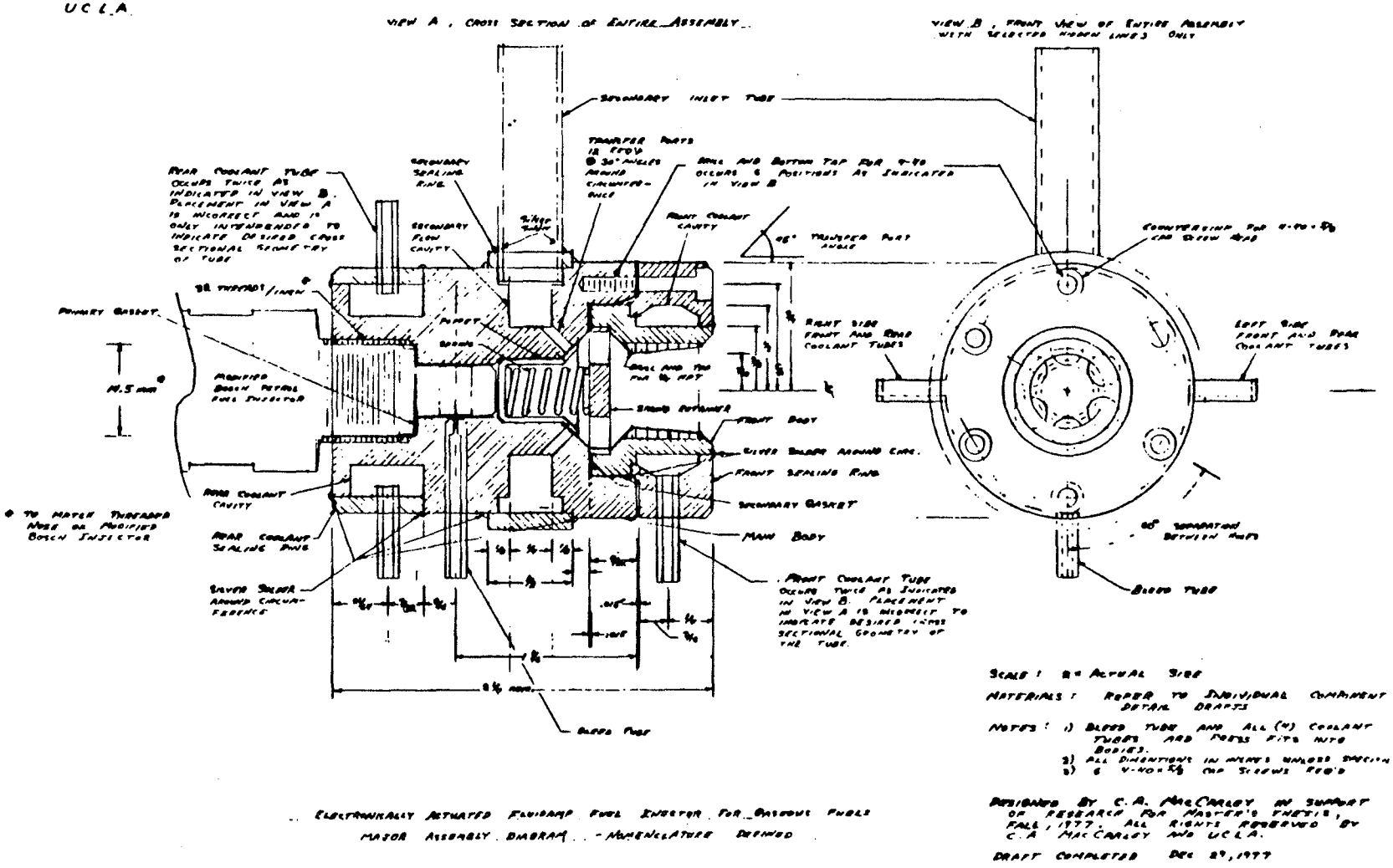

Appendix I.1 Fluidamp Injector, Cross-Sectional Drawing

DRAWING #: 0011, C A M. 12/29/77
UCLA

MAIN BODY, ELECTRONIC FLUIDAMP INJECTOR

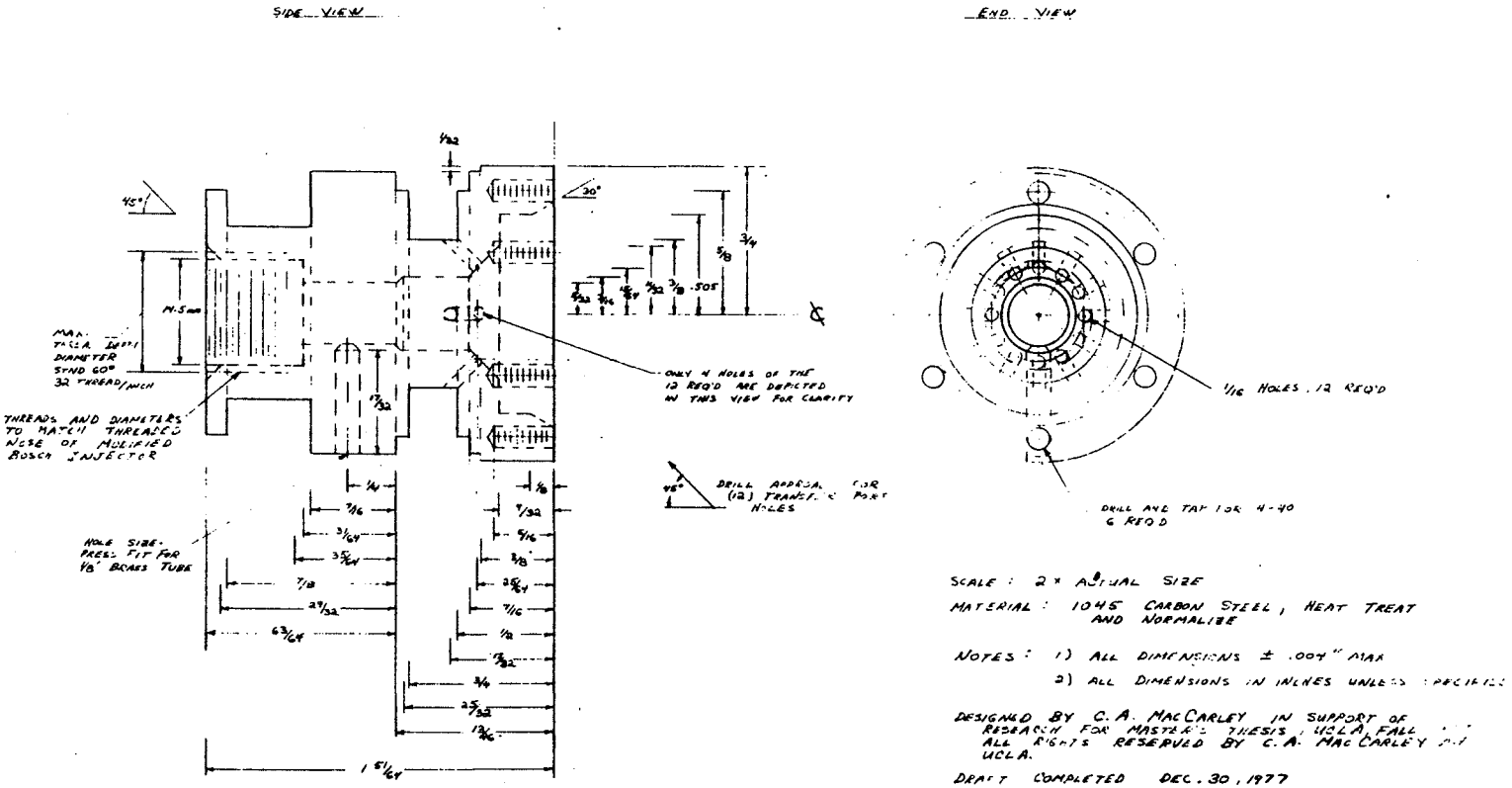

Appendix I.2 Fluidamp Injector, Main Body Drawing

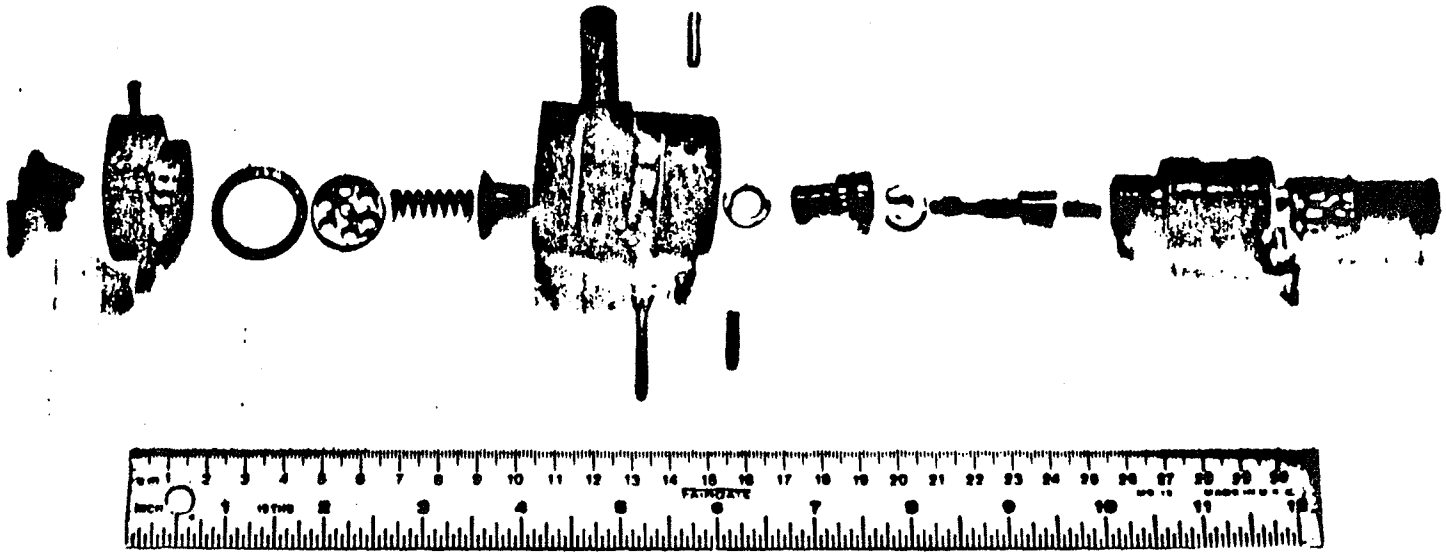

Appendix I.3 Fluidamp Injector, Disassembled

APPENDIX II

Mechanical Drawings of the Rotary Valve Injection Apparatus

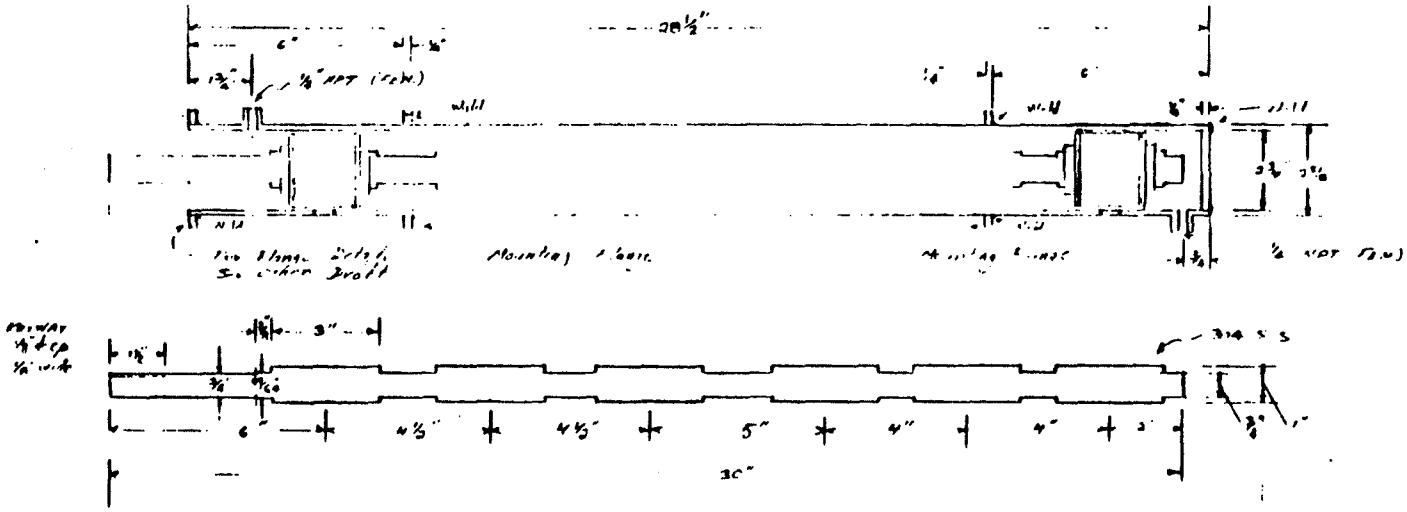

No Injection Apparatus
Shaft and Housing Detail
Scale - ½ of ... size

(Dimensions)

Appendix II.1

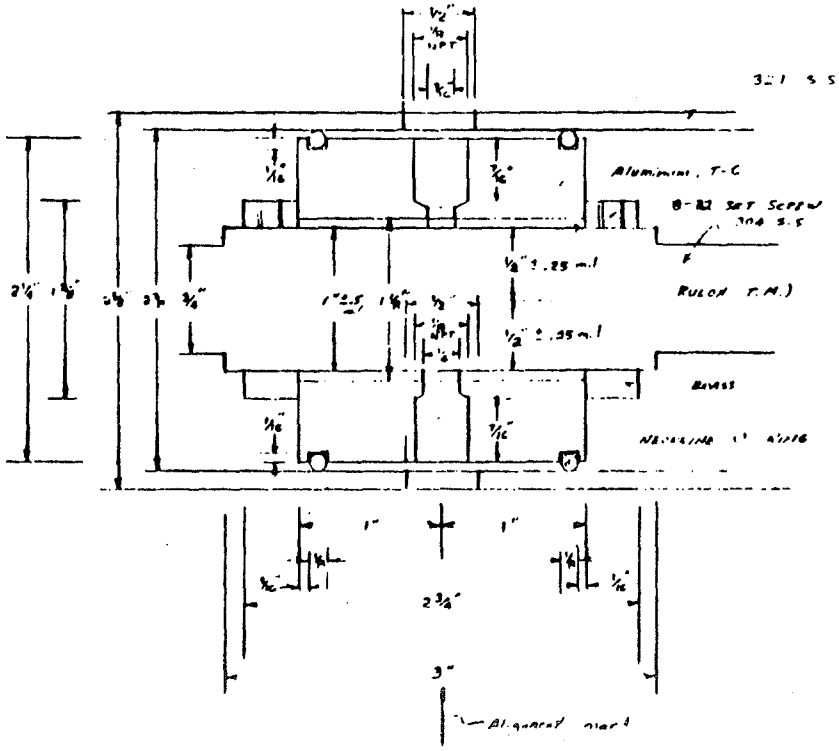

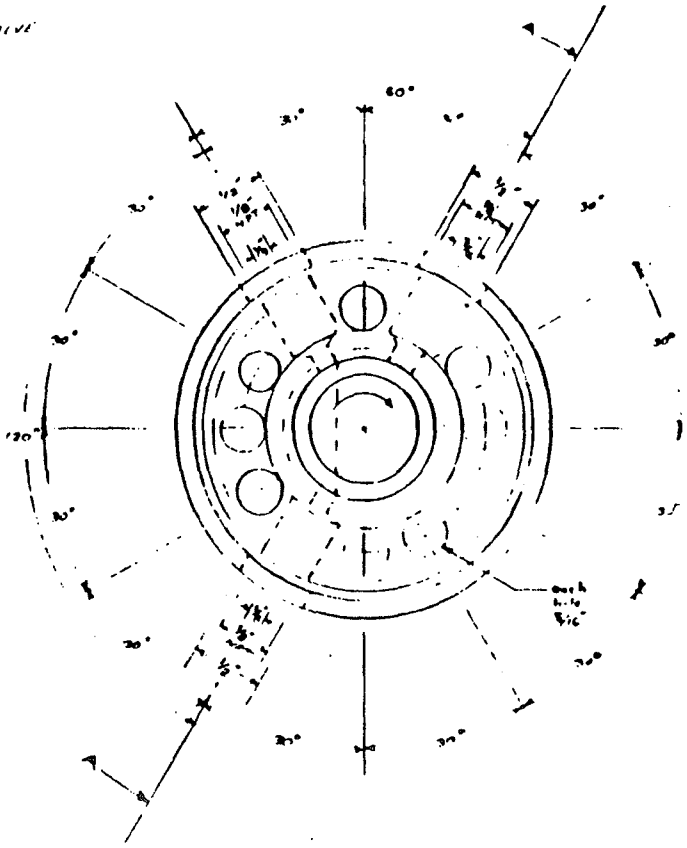

Appendix II 2

ROTARY VALVE INJECTION
BEARING HOUSE DETAIL
SCALE 1:1

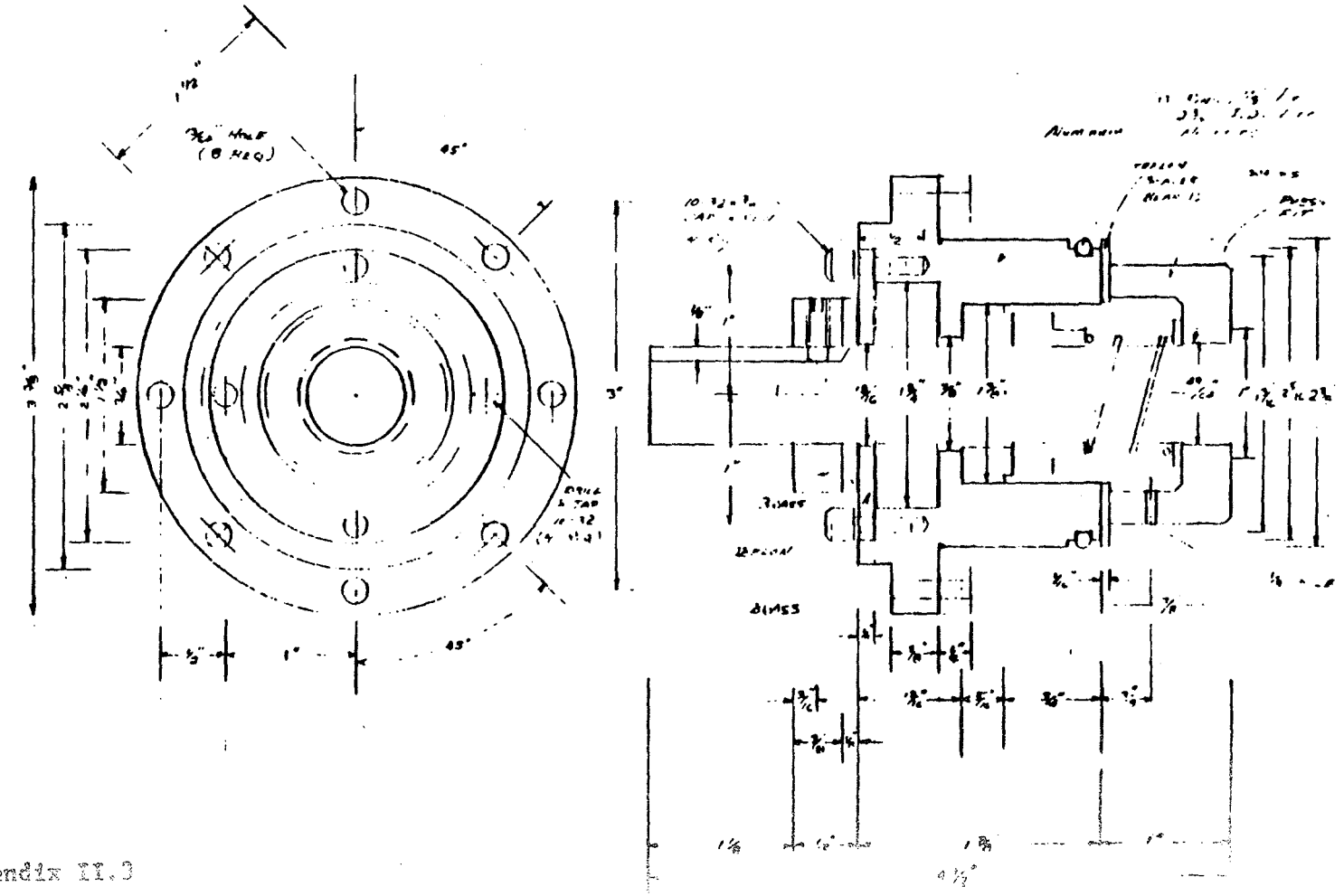

Appendix II.3

CAM
7/3/77

ROTARY VALVE INJECTION
MAIN SHAFT CROSS SECT.
SCALE: 2x Actual size

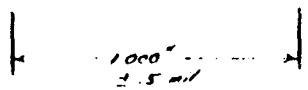

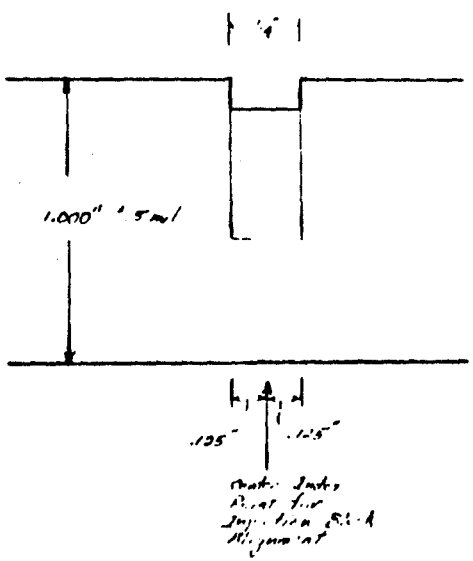

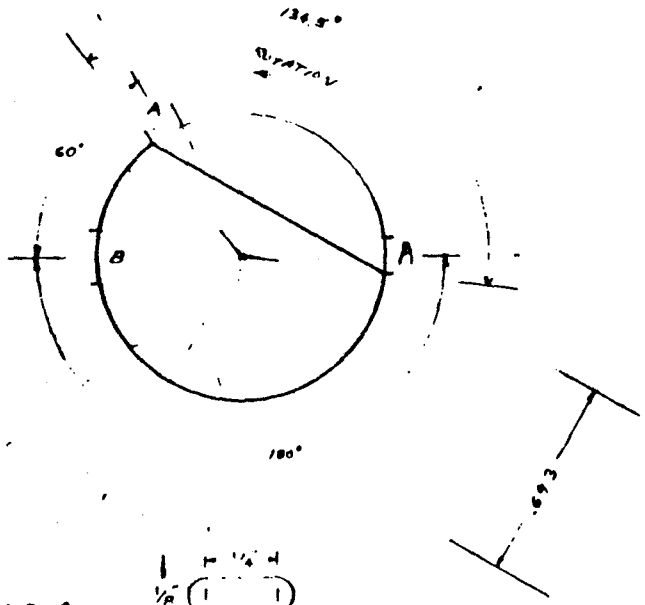

ORIFICE A DETAIL

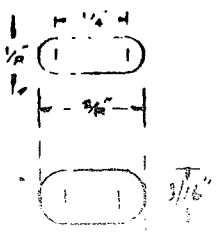

ORIFICE B DETAIL

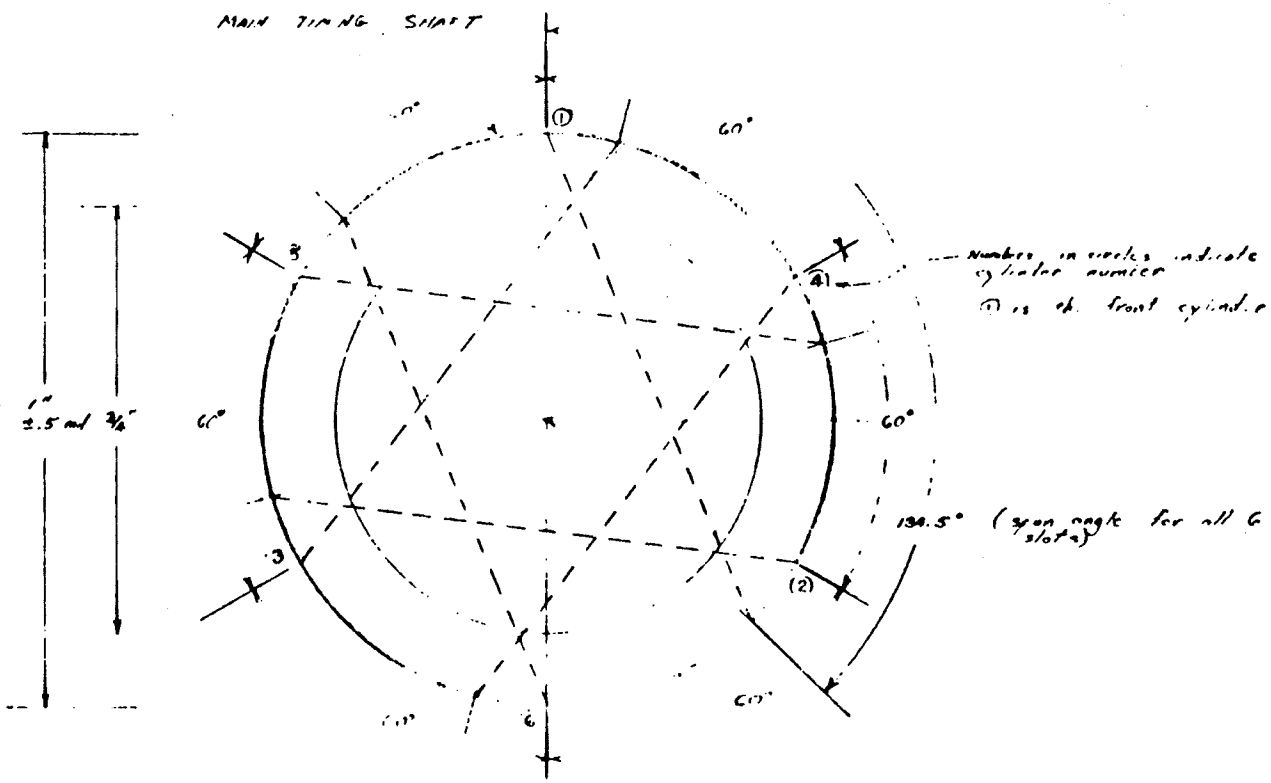

ROTARY VALVE TIMING DIAGRAM
FOR PLACEMENT OF MACHINED
TIMING SLOTS. (FRONT VIEW)
SCALE: 4 = Actual Size

Appendix II.5

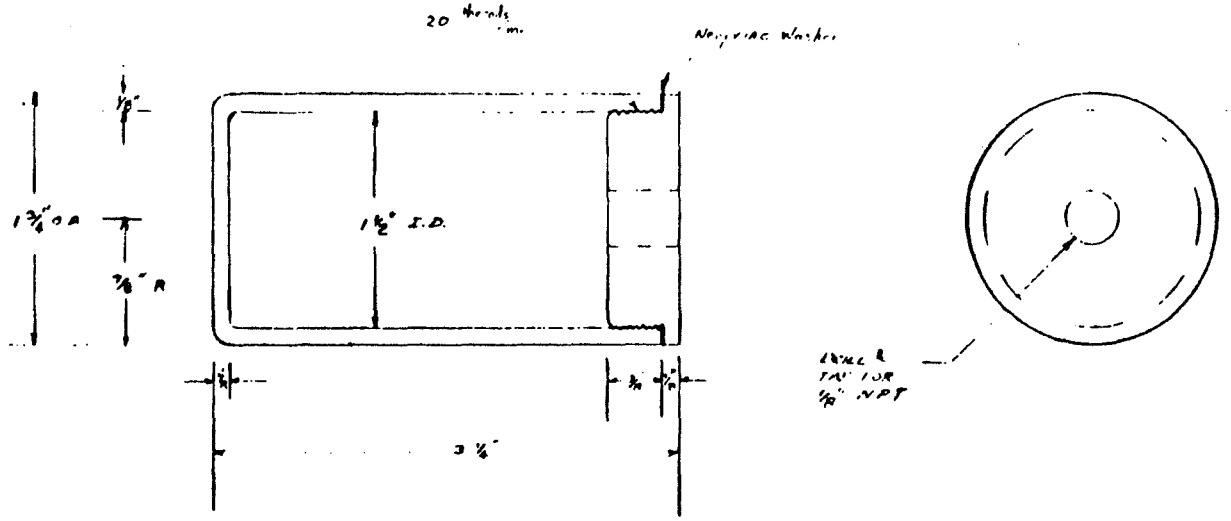

ROTARY VALVE INJECTION
DETAIL OF VOLUME CHAMBER
(6 PORT)

SCALE : 1/1

MATERIAL : 303 S.S. (except where noted)

Appendix II.6

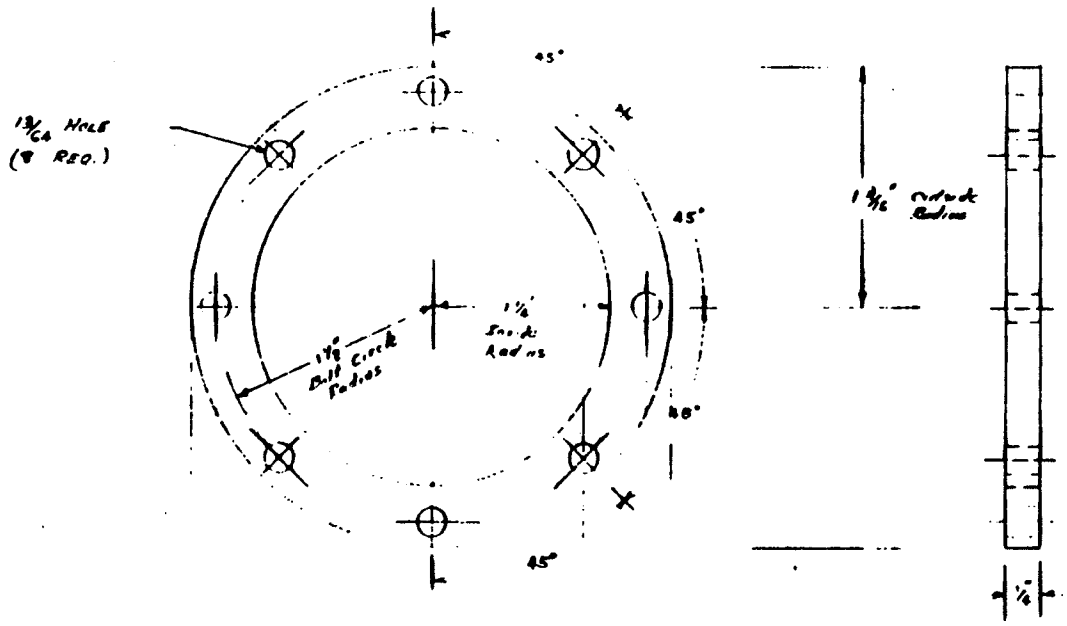

FRONT FLANGE & (2) MOUNTING FLANGES
FOR ROTARY VALVE ACTUATOR
MAIN HOUSING ASSEMBLY

SCALE : 1 : 1

MATERIAL : ALUMINUM

Appendix II.7